STANNIC OXIDE

CRYSTAL GROWTH AND ELECTRICAL PROPERTIES

by

CLIFTON GILBERT FONSTAD, JR.

B.S., University of Wisconsin
(1965)

M.S., Massachusetts Institute of Technology
(1966)

SUBMITTED IN PARTIAL FULFILLMENT OF THE
REQUIREMENTS FOR THE DEGREE OF
DOCTOR OF PHILOSOPHY
at the
MASSACHUSETTS INSTITUTE OF TECHNOLOGY
September, 1970

Signature of Author ____________________
Department of Electrical Engineering, August 24, 1970

Certified by ____________________
Thesis Supervisor

Accepted by ____________________
Chairman, Departmental Committee on Graduate Students

Archives

MASS. INST. TECH.
NOV 17 1970
LIBRARIES

STANNIC OXIDE
CRYSTAL GROWTH AND ELECTRICAL PROPERTIES

by

CLIFTON GILBERT FONSTAD, Jr.

Submitted to the Department of Electrical Engineering on September 24, 1970 in partial fulfillment of the requirements for the Degree of Doctor of Philosophy.

ABSTRACT

Single crystals of the wide bandgap semiconductor, stannic oxide, have been grown and studied electrically with the objective of considering SnO_2 as a potentially useful material for active device applications. A chemical vapor deposition crystal growth technique using chlorine transport, no inert carrier gases, and low pressure has been used to grow stannic oxide crystals of higher purity and with almost an order of magnitude higher low temperature Hall mobility, over 8500 cm^2/V-sec at 80°K, than have previously been available. The system offers distinct advantages over conventional vapor phase systems in the control available over the reactants and the growth reaction, in the purity of the crystals, and in the ease of introducing electronic dopants. Undoped, antimony doped, and seeded crystals have been grown.

Measurements of Hall mobility, carrier concentration, and resistivity have been made on samples between 20°K and 625°K. The conductivity anisotropy in SnO_2 is found to be small, $\rho_c/\rho_a \leq 1.2$ at 77°K and 300°K. All results reported are for the a-direction. From measurements on crystals with room temperature carrier concentration between 8×10^{15} and 2×10^{18} cm^{-3}, a donor level due to antimony at ~35 meV deep and another level ascribed to oxygen vacancies at ~140 meV have been observed. A polaron effective mass of 0.39 m_e has been found consistently in the analyses of the data. Polar optical mode scattering with a dominant characteristic temperature of 1080°C is the main scattering mechanism above 250°K. Below 250°K acoustic deformation potential scattering dominates. Ionized impurity scattering is eventually important in all samples as the temperature is lowered. Excellent agreement was found between theory and experiment.

A technique of fabricating good Schottky barriers on SnO_2 has also been developed and used to measure the net donor concentration in samples. The agreement found between these measurements and N_d from Hall measurements indicate that shallow trapping is not a problem in these crystals.

THESIS SUPERVISOR: R.H. Rediker
TITLE: Professor of Electrical Engineering

ACKNOWLEDGEMENT

I wish to first and foremost express my indebtedness to my thesis advisor, Prof. R.H. Rediker, for his continued guidance, assistance, and interest in all phases of this work. The guidance of Dr. A. Linz in the design and construction of the crystal growth system was invaluable and is also gratefully acknowledged. Of great value also were many discussions with Dr. R.C. Folweiler; the assistance of Dr. T.B. Reed and Dr. J.A. Marley, too, is acknowledged.

The technical assistance and untiring helpfulness of Mr. A Colozzi should not go unthanked. In fact, the friendliness and willingness to assist when problems arose of all of the members of the Solid State Device Research Group and of the Crystal Physics Group has been exceptional. The bulk electrical measurements could not have been made without the cooperation of Dr. M. Lichtenstieger in the use of his Hall measurement facility and other equipment. The efforts of Mrs. Pauline Alldred, who typed the manuscript, are very much appreciated.

A most important factor in the success of this entire project has been the understanding and confidence of my wife, Carmenza. Her encouragement when I felt down and joy when I was up, and her many sacrifices for me, will be impossible to ever repay.

Finally the support of the National Science Foundation is acknowledged with gratitude.

TABLE OF CONTENTS

	Page
Title Page	1
Abstract	2
Acknowledgment	3
Table of Contents	4
List of Figures	6
List of Tables	7
Chapter 1 - Introduction	8
Chapter 2 - Growth of Stannic Oxide Crystals	14
2.1 Material Requirements	14
2.2 Methods of Crystal Growth	14
2.3 Present Growth Method	17
2.4 The Growth System	18
2.5 Conditions for Crystal Growth	22
2.6 Crystals Grown - General	26
2.7 Specific Growth Runs	30
2.8 Summary of Technique	35
Chapter 3 - Electrical Studies	38
3.1 Schottky Barrier Program	38
3.1.1 Nature of Program	38
3.1.2 Fabrication Procedure	40
3.1.3 Electrical Characteristics	45
3.2 Bulk Electrical Properties	55
3.2.1 Crystal Anisotropy and Experimental Considerations	55
3.2.2 Sample Preparation	58
3.2.3 Measurement Technique	59
3.2.4 Experimental Results	62
3.3 Analysis of Electrical Measurements Data	74
3.3.1 Review of Anisotropy Considerations	74

	Page
3.3.2 Carrier Concentration vs. Temperature	75
3.3.3 Net Donor Concentrations - Hall vs. Schottky	81
3.3.4 Analysis of Hall Mobility Data	82
3.4 Implications of Results for Device Applications of SnO_2	94
Chapter 4 - Summary of Results and Proposals for Future Work	96
Appendix A - Stannic Oxide Parameters	100
Appendix B - Crystal Growth System Details, Drawings, and Photographs	105
B.1 Gas Flow and Metering Controls	105
B.2 Furnace Tube Endcaps	109
B.3 Injection Nozzles	112
B.4 Cold Traps, P-control, and Vacuum Pump	114
B.5 Furnace Construction, Controls, and Characteristics	118
Appendix C - Detailed Procedures for Growth Runs	120
C.1 Pre-run Preparations	120
C.2 Start-up Procedure	121
C.3 Shut-down Procedures	122
Appendix D - Measurement of Resistivity Anisotropy	127
References	129
Biographical Note	132

LIST OF FIGURES

	Page
Figure 1 - Stannic Oxide Crystal Structure	9
Figure 2 - Crystal Growing System	19
Figure 3 - Crystal Growth Habit	27
Figure 4 - Photograph of Typical Crystals	28
Figure 5 - Seed Growth from Run 012	34
Figure 6 - Schottky Barrier I-V Characteristics	46
Figure 7 - Schottky Barrier C-V Characteristics	50
Figure 8 - n, μ_H, and σ for Sample 008-8-b1, 80^oK to 300^oK	64
Figure 9 - n, μ_H, and σ for Sample 008-9-b, 80^oK to 300^oK	65
Figure 10 - n, μ_H, and σ for Sample 016-1-b, 80^oK to 300^oK	66
Figure 11 - n, μ_H, and σ for Sample 016-1-b, 20^oK to 80^oK	67
Figure 12 - n, μ_H, and σ for Sample 009-9-c, 300^oK to 625^oK	69
Figure 13 - Log-log Composite of Hall Mobility Data	72
Figure 14 - Theoretical Polar Optical Mode Scattering Mobility	88
Figure 15 - Total Theoretical Mobility	90
Figure A-1 - Gas Flow and Metering Controls	106
Figure A-2 - Photographs of Gas Flow and Metering Controls	107
Figure A-3 - Input Endcap	110
Figure A-4 - Output Endcap	111
Figure A-5 - Injector Nozzles	113
Figure A-6 - Output Gas Handling System	115
Figure A-7 - Photograph of Output Gas Handling System	116

LIST OF TABLES

Page

Table 1 - Summary of n, μ_H, and σ at 80^oK and 300^oK. 71

Table 2 - Net Donor Concentrations 82

Table 3 - Parameters in Polar Optical Mode Scattering Theory 85

I - Introduction

Stannic oxide - also known as tin oxide or tin dioxide - SnO_2, has been known for many years as a transparent conductor. It is in fact much more; it is a wide bandgap semiconductor with very exciting potential for application in high temperature active electronic devices.

A great deal of effort has been expended in the past twenty years in the development of gallium arsenide and silicon carbide with the goal of producing active devices that can operate above 300°C for industrial, space, and military applications. The success of this work has been modest however and the need for high temperature active semiconductor devices remains very real. Some general properties of stannic oxide indicate that it may be useful as such a high temperature semiconductor. It is a transparent material indicating that it has a wide bandgap (optical measurements indicate a minimum bandgap of about 3.5 eV). It has a very high melting point (over 2000°C). In its main applications as a transparent conducting coating on glass in which form it is used to defrost aircraft windows and as a high temperature electrode, it has shown good physical stability at elevated temperatures. And finally, it is a semiconductor that can be doped to reasonable n-type conductivities and has room temperature mobilities of several hundred cm^2/V-sec.

Stannic oxide crystallizes in the rutile crystal structure[1] (tetragonal, D_{4h} symmetry) illustrated in Figure 1. The semiconducting nature of naturally occurring stannic oxide crystals[2] - cassiterite - and the electrical and optical properties of stannic oxide films[3] - Nesa and similar commercial transparent conductive coatings on glass - have been studied by a large number of researchers. The pertinence of this work to the

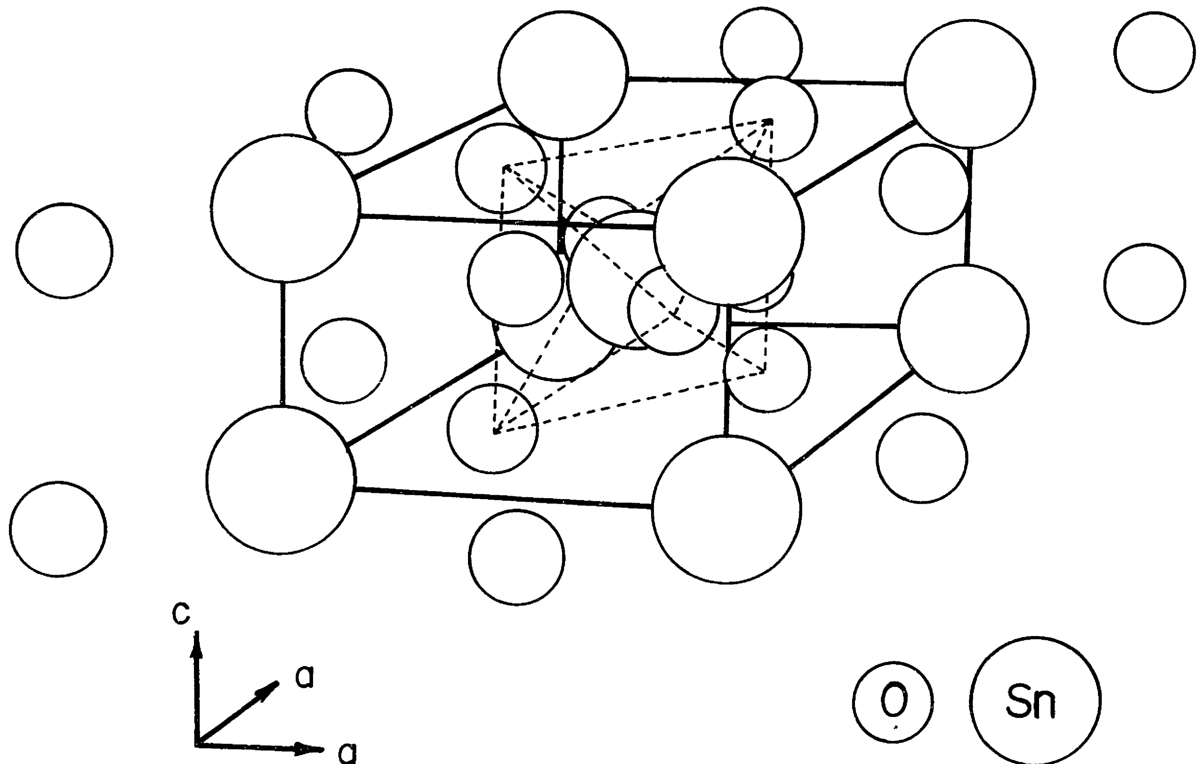

(a) Perspective view showing tin atoms arranged in a body-centered tetragonal lattice, each tin atom being surrounded by an octahedron of oxygen atoms.

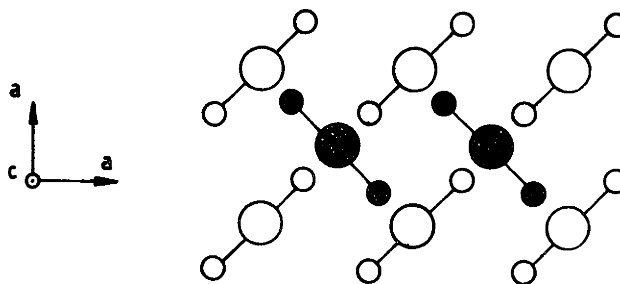

(b) A "top" view along c-axis. The atoms shown by blackened circles lie one-half a lattice spacing in the c-direction below and above the atoms shown by open circles. Note the 90° rotation of the O-Sn-O "dumbbells" in alternate layers.

Figure 1 - Stannic oxide crystal structure, the "rutile" structure which has tetragonal D_{4h} symetry.

use of stannic oxide as a useful electronic semiconductor is limited, however, because of the presence of many impurities in natural crystals, and because of the polycrystallinity and high doping levels of the films. It has only been within the last ten years that single crystals of stannic oxide have been grown in the laboratory and that meaningful attempts have been made at measuring properties of good single crystals of SnO_2. Still, as many of the results reported in this paper will show, even with laboratory grown single crystals, measurements have often been dominated by the influence of impurities and/or defects. This is particularly true of electrical studies. Tables of stannic oxide parameters can be accumulated to be sure - see Appendix A - but they must be carefully interpreted. Very few measurements have been made on good quality crystals, and many parameters have not been measured at all.

The first group to successfully grow stannic oxide crystals was Marley, et. al.[4] at the Corning Glass Works Laboratory in 1961. Before their interest in this material waned they made extensive electrical,[5] optical,[6-8] and etching[9] studies on their crystals. The electrical studies were made on undoped samples annealed in oxygen atmospheres and on several crystals degenerately doped with antimony. They measured Hall mobilities up to 200 $cm^2/V\text{-}sec$ at 300^oK and found that the mobility fell at higher temperatures due, they said, to polar optical mode scattering with a characteristic temperature of ~ 500^oK. At lower temperatures the mobility also decreased in most crystals and was below 250 $cm^2/V\text{-}sec$ - most commonly under 100 $cm^2/V\text{-}sec$ - at 80^oK. They found an electron effective mass of 0.22 m_e and placed the donor level due to the oxygen vacancies at $150 - 8.7 \times 10^{-5} N_d^{1/3}$ MeV below the band edge [N_d is in cm^{-3}].

Reed, et. al.[10] at Lincoln Laboratories grew crystals of stannic oxide soon after Marley but did not make many electrical measurements on their samples. Wright, et. al.[11] in Great Britain have also grown crystals of SnO_2 and made numerous electrical[11,12] and optical[12-14] studies of their crystals. Their electrical measurement results were similar to Marley's although they did not anneal their samples. They measured an effective mass of 0.17 m_e and in one sample measured a Hall mobility as high as 700 cm^2/V-sec at low temperatures. More recently, Nagasawa, et. al.[15] in Japan have grown crystals which appear to be of better quality than those of the other studies and they have reported a series of electrical[16,17] and optical[18-20] studies directed primarily at shedding light on the nature of the stannic oxide bandgap minimum. From magneto-resistance data,[17] symmetry and magnetic field splitting of the excitonic absorption spectrum,[18,19] and Urbach's rule analysis of the absorption edge[20] they conclude that stannic oxide has a direct gap. Electrically they have measured antimony doped crystals and have found Hall mobilities as high as 250 and 1000 cm^2/V-sec at 300^oK and 80^oK respectively with, they stated, acoustic deformation potential scattering being dominant. They placed the antimony donor level at 24 $\pm$ 4 MeV and found an effective mass of 0.35 m_e. A final important body work on grown stannic oxide crystals has been done by vanDaal[21] at Philips Research Laboratories in the Netherlands. From infrared reflection studies and direct measurements[22] he has found the static dielectric constants to be 9.0 $\pm$ 0.5 and 14 $\pm$ 2 parallel and perpendicular to the c-axis respectively rather than 24.0 and 23.4 as was previously thought. He also has determined the optical phonon frequencies and indicated that the pertinent characteristic temperature for polar

optical mode scattering is $1050^{o}K$. He used this value to analyze his Hall mobility measurements which are similar to Nagasawa's. He also used an electron effective mass of 0.25 m_e with four minima, a possibility not considered by either Marley or Wright in spite of the fact that they both concluded from their optical studies[6,13] that stannic oxide is an indirect semiconductor.

The results of these studies showed that stannic oxide merited attention as a possibly useful semiconductor but none had been directed towards consideration of stannic oxide as a useful electronic device material. As became evident during the course of this study none had in fact studied crystals of sufficient purity and quality to truly examine the details of stannic oxide's conduction properties.

Described in this thesis, first, is a low pressure, chlorine transport chemical vapor deposition stannic oxide crystal growing system. This system is designed to grow high quality stannic oxide crystals under conditions giving enough control over crystal growth, electronic dopants, and sample quality to be of potential use in making electronic devices and in studying fundamental parameters of stannic oxide. The crystals grown have proven to be superior to previously grown crystals in purity and quality. Also, controlled doping has been achieved and detailed measurements of carrier concentration, Hall mobility, and conductivity between $20^{o}K$ and $600^{o}K$ on samples ranging in room temperature carrier concentration from 7×10^{15} to 2×10^{18} cm^{-3} have been made and analyzed. Our experiments, on the purest samples, indicate an anisotropy in the conductivity of about 1.2. The mobility and conductivity reported are for the a-direction (see Figure 1 which shows the crystal directions) and

values for the c-direction would be lower. The Hall mobility is found to be limited by polar optical mode scattering above $250^{o}K$ while below this temperature acoustic deformation potential scattering and ionized impurity scattering play important roles. The $80^{o}K$ mobility in the purest samples of 8800 cm^2/V-sec is significantly higher than the highest value reported by others[15] of 1100 cm^2/V-sec. The highest mobility ever reported in stannic oxide, over 13,000 cm^2/V-sec, was measured at $40^{o}K$ in these samples. Donor levels at 37 meV and 140 meV below the conduction band were found and an electron effective mass of 0.39 m_e was found consistently in all of the analyses. Also, a technique for fabricating Schottky barriers on stannic oxide has been developed and these devices have been used extensively to measure the net donor concentration of samples. The close agreement between these and Hall measurements of the net donor concentration indicate that shallow traps are not important in these crystals; that is, that all carriers excited from donors actually contribute to conduction.

With the present study, then, the fundamental parameters influencing conduction in stannic oxide can be considered, and a more complete appraisal of its potential as a useful semiconductor obtained. Stannic oxide of carrier concentration and quality suitable for device application has been produced; Schottky barriers usable as gate electrodes in field effect devices have been developed; and the sophistication required to produce device geometries has been designed into the crystal growth system. In addition, a source of stannic oxide crystals of value for studies of basic physical parameters of this anisotropic semiconducting material is available, and a number of stannic oxide parameters have been considered here.

2 - Growth of Stannic Oxide Crystals

2.1 Material Requirements

The history of the study of semiconductors is a lesson to the point of obsession in the importance of crystal purity and perfection to the electronic, in fact to all, properties of these materials. It is a good lesson to learn as many studies of semiconductors have, in fact, been studies of impurities in those semiconductors. As the introduction pointed out, stannic oxide is no different in this respect although often researchers have realistically admitted the existence of this problem. It was one that had to be considered from the start when the present system to grow stannic oxide crystals for electronic study and for potential use in devices was selected and designed.

In addition to requiring that the crystals grown be of very high quality - meaning, simply, as stoichiometric and as free of any foreign atoms and crystal defects as practically possible - there were several other basic requirements of the system chosen. First, the introduction of electronically active dopants in controlled amounts had to be possible. The growth of layered geometries for field effect devices, for example, had to be feasible. And, crystals of a manageable size for electrical evaluation had to be obtainable. The potential for growth on seeds and substrates was also desirable.

2.2 Methods of Crystal Growth

The high melting point of stannic oxide, if in fact it even melts before simply decomposing, limits immediately the possible methods of crystal growth to two: growth from a solution in which stannic oxide is

dissolved and chemical vapor phase deposition in which gaseous reactants produce stannic oxide as a reactant product. Natural crystals of cassiterite grow hydrothermally from a water solution under great pressures and at high temperatures deep in the earth but these conditions are hard to duplicate in the laboratory and the resultant crystals contain water molecules.* Kohnke[23] reported growing small SnO_2 crystals from a solution using cuprous oxide as the flux, or solvent, but as one might anticipate, his crystals contained large amounts of copper, a very undesirable electronic dopant. All other laboratory grown stannic oxide crystals have been grown by chemical vapor deposition. On the basis of this fact and considering the success of this technique in growing high quality and very pure crystals of many other materials, it is an attractive choice as the general method of crystal growth to use.

Marley,[3] Reed,[10] and Wright[11] all used variations of the same reactions to produce their crystals:

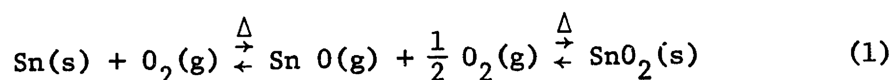

$$Sn(s) + O_2(g) \overset{\Delta}{\rightleftarrows} Sn\ O(g) + \frac{1}{2}\ O_2(g) \overset{\Delta}{\rightleftarrows} SnO_2(s) \qquad (1)$$

Marley started on the right and reduced stannic oxide to a lower oxide before reoxidizing it to deposit SnO_2 as crystals. The reaction was done at 1650°C which is one difficulty and control over crystal stoichiometry and purity appear to be other major problems with this system. Reed and Wright both started on the left and oxidized tin to the stannic oxide. Reed[12] placed tin in a quartz ampoule at 1350°C that was sealed except for a small "leak" through which air entered to slowly oxidize the tin to

*Probably the source of the large static dielectric constants measured earlier in stannic oxide.

stannic oxide. With this method one has no control over the reaction and the crystal purity is dependent on the purity of the tin initially. Somewhat more control is realized in a flowing system such as Wright[11] used although the reaction itself limits one's flexibility and purity is still directly related to - and limited by - the initial tin charge and the need to operate at such high temperatures, 1450°C in this case.

The more successful stannic oxide crystal growth methods have been based on reacting a stannic halide with water vapor. VanDaal[21] mentions using stannic bromide but more common is the use of stannic chloride:

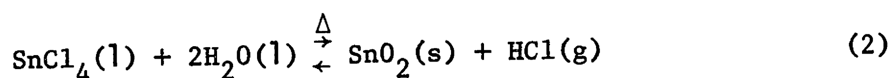

$$SnCl_4(l) + 2H_2O(l) \overset{\Delta}{\rightleftarrows} SnO_2(s) + HCl(g) \tag{2}$$

This is the reaction used to produce stannic oxide films on glass and was used by Nagasawa[15] and, recently, Wright[12] to grow single crystals. Two streams of a carrier gas, helium, for example, are saturated with the two reacting liquids and injected into a furnace hot zone, 1100°C - 1300°C, where the reaction occurs producing stannic oxide. An indirect control over the reaction is obtained by controlling the flows of the two carrier gases. Still, Nagasawa found that most growth occurred almost immediately where the gas streams entered the furnace resulting in a dense lump of growth which soon blocked the gas flows. Also, crystal purity still is a problem being tied closely to the starting materials.

In light of the difficulties and limitations of these methods, and with the guidance of Dr. A. Linz, it was decided that a still more sophisticated approach to the growth problem would be required. A technique he had been interested in and one which seemed ideally suited to producing stannic oxide crystals suitable for study and potential electronic

device application was the one which Schaffer[24] and Folweiler [25] had used to grow large, high quality ruby (chromium doped Al_2O_3) crystals. Their technique is a low pressure chemical vapor deposition technique using chlorine transport and involving no inert carrier gases. At the low pressure used the reactants are all gaseous, as are all but one of the products, i.e. the crystals grown, so that control of the reaction is direct through control of gas flows. The chloride of the metal, $AlCl_3$ in their case and $SnCl_4$ here, is produced by reacting chlorine with the metal, a reaction which itself is purifying in nature. Electronic doping is easily done by doping the metal charge. And, growth dynamics are simplified and enhanced by elimination of the inert carrier gas molecules; suitable dilution of the reactants is achieved by operating at reduced pressure. The extra difficulties of using low pressure and chlorine gas are not great and are more than compensated for by the sophisticated control realized over the growth process and, most importantly, by the high quality crystals produced.

2.3 Present Growth Method

As mentioned above, the crystal growth method developed is a low pressure, inert carrier-gas free chemical vapor deposition technique. The starting point in the system is tin metal and the gases chlorine, oxygen, and hydrogen. The chlorine and tin are reacted in a special reactor external to the main growth furnace to produce stannic chloride:

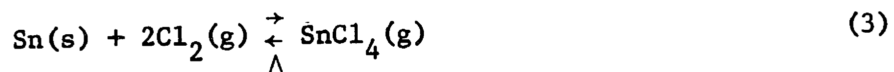

$$Sn(s) + 2Cl_2(g) \underset{\Delta}{\rightleftarrows} SnCl_4(g) \qquad (3)$$

The pressure in the reactor and the following portions of the system is

below 10 torr so that the stannic chloride is a gas also. It is injected into the growing furnace with the gases hydrogen and oxygen which react to form stannic oxide:

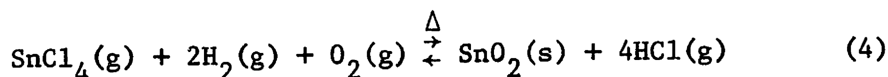

$$SnCl_4(g) + 2H_2(g) + O_2(g) \overset{\Delta}{\rightleftarrows} SnO_2(s) + 4HCl(g) \qquad (4)$$

Several points can be made immediately concerning features of this approach to growing stannic oxide. First, all of the reactants are gases so that control over the amount of reactants present is easily and directly maintained and monitored by controlling gas flows. Note that if care is taken to insure that reaction 3 is complete the flows of chlorine in and stannic chloride out of the reactor are directly proportional. Second, by combining unreacted chlorine with the gases put into the growing furnace one is essentially adding one of the reaction products, HCl, which means that one has control over the rate, and even the direction, of reaction 4. This allows direct control over the rate of growth and permits back etching of seeds and substrates. Third, the reaction of tin and chlorine, reaction 3, is purifying in the sense that any metallic ion transported into the growing furnace must first react with chlorine at a relatively low temperature and second must have a volatile chloride, requirements met by few common elements.

2.4 The Growth System

The actual growing system is illustrated in Figure 2. More detailed drawings and photographs can be found in Appendix B but all of the essential features of the system are present in this artist's rendering. The gas flow rates are monitored by flow meters just before the needle

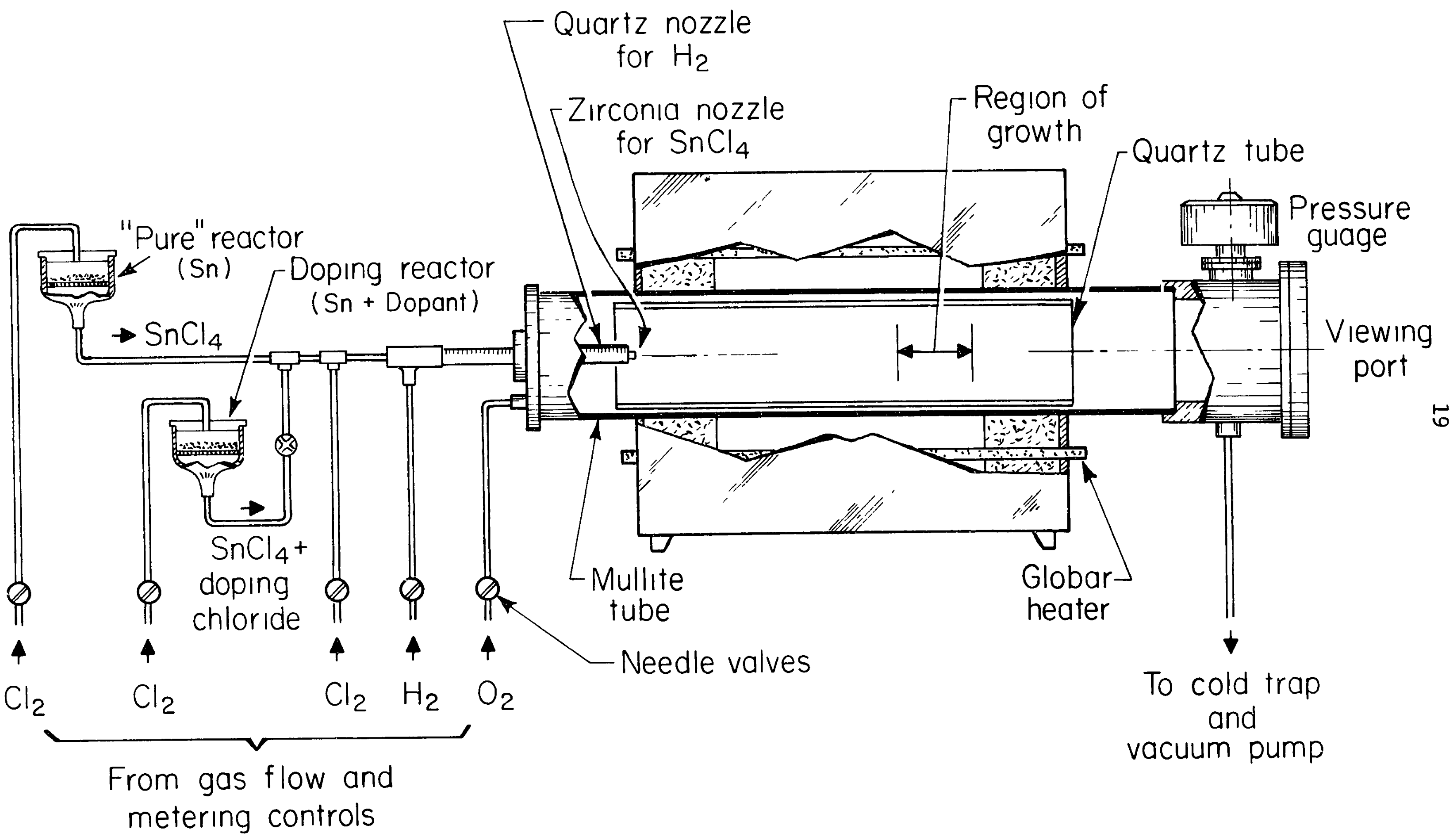

Figure 2 - Illustration of the stannic oxide crystal growing system.

valves in the lower left of Figure 2 and where the gas pressure is about 900 torr. After the needle valves and in the entire remaining portion of Figure 2 the pressure is maintained at approximately 10 torr. This is done by limiting the pumping efficiency of the vacuum pump through a controlled leak of nitrogen immediately before the pump - see Appendix B-4.

As shown in Figure 2, the reaction of tin and chlorine, Equation 3, occurs in a Pyrex Buchner type funnel with a coarse fritted disk on which the tin charge, in the form of 30 mesh powder, rests. This "$SnCl_4$ reactor" is wrapped with heater tape and heated to 100°C which was found to be sufficient to give a uniform and complete reaction. When the reactor was not heated slightly it was found that the reaction was dominated by the heating due to its exothermic nature and was impossible to control at low flow rates. Electrically active dopants are introduced into the crystals by using other $SnCl_4$ reactors in parallel with the "pure" $SnCl_4$ reactor and in which the tin charges contain small amounts of the desired dopant elements. In these reactors the dopant chloride is formed along with the stannic chloride and enters the gas stream with it. The chlorine flow to these reactors is turned on when doped material is desired and the flow to the reactor is adjusted to be the proper fraction of the total flow, or this fraction is changed as the material grows, to give the desired doping concentration profile. It should be noted that in selecting a dopant attention must be given to the vapor pressure of its chlorides to assure that it will indeed enter the gas flow and eventually the crystals. Antimony, an n-type dopant, works very well in this respect.

The furnace tube is a mullite tube of 15 cm inside diameter and

91.5 cm in length mounted in an eight element Globar furnace. It is sealed on either end with Inconel endcaps. As shown in Figure 2, the oxygen inlet and the hydrogen and chlorine-stannic chloride injector tubes are on the input endcap; while the output endcap provides a mount for a diaphragm pressure gauge, a quartz viewing window, and the connection to the cold traps and a vacuum pump. Not shown in the figure are a quartz window on the input endcap, and a coupling on the output endcap which allows for the insertion of a rod and seed into the growth region along the furnace tube axis (see Appendix B-2). A quartz tube closely fitting inside the mullite tube is used as the growing substrate. It is 72 cm long, long enough to cover the entire high-temperature region of the furnace to protect against contamination from the mullite and to preserve the mullite tube. A spiral of 20 mil platinum wire wrapped around the quartz liner keeps it from touching and possibly sticking to the mullite.

The method of introducing the reacting gases into the furnace was chosen to reduce the amount of deposition immediately where the gases enter and start to mix. A set of injector tubes, or nozzles, is used. Stannic chloride and chlorine enter through the center nozzle which is a 3/16" O.D., 3/32" I.D. zirconium oxide tube concentric with the furnace tube. Concentric with this center nozzle is a second nozzle, an 11 mm I.D. quartz tube, through which the hydroegn flows. The edges of the ends of the nozzles are ground to a 15°-20° taper to reduce turbulence at their ends so that the hydrogen gas enters the furnace as a sheath about the center stannic chloride flow separating it for a while from the oxygen which is flowing in the remaining portion of the tube, and preventing the immediate reaction of the gases. Some interdiffusion and deposit of stannic oxide on the inert

nozzle does occur anyway but the amount is relatively small and, if care has been taken in positioning the nozzles concentrically, does not interfere with the gas flows. The optimum relative placement of the nozzle ends appears to be with the inner nozzle extending slightly, on the order of 1 mm, past the outer nozzle end.

The cold traps on the output are glass, liquid nitrogen cooled traps designed to remove the water, hydrogen chloride, and chlorine from the flow before they can enter the vacuum pump, a Welch model 1402, and damage it. As is detailed in Appendix B-4, this is actually a system of two traps arranged in parallel so that one can be used while the accumulation in the other is cleared out without ever interrupting the gas flows and crystal growth.

Most of the valves, fittings, and tubing in the system are 316 stainless steel. Initially some fittings of Monel and pieces of Inconel tubing were used but showed no superiority to stainless steel in dry chlorine service, while being considerably more expensive and more difficult to work with. Any replacement parts and additions to the system have been made of stainless steel. Lengths of teflon tubing are used to connect the flow control panel to the gas pressure regulators and to the input endcap. Provision is made in the flow control panel to vent any or all of the gases to a chemical hood, and to flush all lines or individual lines with helium gas.

In all of the results reported in this work reagent grade tin and chlorine, and prepurified hydrogen were used in the system.

2.5 Conditions for Crystal Growth

The large number of variables in the present system - pressure,

total gas flow, individual gas flow ratios, temperature - give a great deal of control over the growth process but create a large optimization problem in finding the best grwoth conditions; that is, in making the most efficient use of the material available to produce the largest, best quality crystals most quickly. The adjustment of the variables presented below was arrived at by fixing certain parameters - the furnace peak temperature of 1300°C and the ratio of hydrogen to oxygen, 2:1 - and varying others over wide ranges in the course of several - 9 - growth runs during which careful and continuous observations of the results of each change were made. Analyzing the record of each run to narrow in on an optimum selection of variables in successive runs, the set of conditions discussed below were finally discovered to give very good results. It is not implied that they are anything more than a local maximum, or "optimum", and that another completely different choice for the variables might not give even better results. They work well which is sufficient justification for their use in this study.

As was mentioned above, the peak furnace temperature was 1300°C as measured by a thermocouple just touching the outside of the mullite tube at its center. Also, the ratio of flow of hydrogen to the flow of oxygen was 2:1 or the ratio found in water, while the flow of chlorine into the $SnCl_4$ reactor was about one fifth the hydrogen flow. Relying on the calibration curves supplied with the flow meter tubes, and correcting for the gas densities and the pressure to units at standard temperature and pressure, one finds the flows to be about 18 cc/min chlorine into the reactor, 100 cc/min hydrogen, and 50 cc/min oxygen. With these gas flows on, the pressure in the system adjusted to about 9.5 torr, the furnace hot,

and the $SnCl_4$ reactor heated to $100^{o}C$ to insure the complete reaction of the tin and chlorine, the flow of extra chlorine is varied to control the rate of Reaction 4, of nucleation, and of growth. Above a flow of 7 cc/min no growth occurs. At lower rates growth starts near the output end of the liner and occurs deeper into the furnace as the excess chlorine is reduced. The optimum growth occurs in the region on the output side of furnace center where the temperature gradient is about $10^{o}C/cm$ and the temperature is between $1250^{o}C$ and $1175^{o}C$, as measured with an optical pyrometer. If the nozzles extend into the furnace so that the end of the inner nozzle is flush with the start of the insulated furnace enclosure as shown in Figure 2, little deposition occurs before this optimum growth region even as the extra chlorine flow is reduced to zero. The deposition of stannic oxide that does occur elsewhere is predominantly polycrystalline whether the deposit is dense or sparse.

Most of the growth that has been done with this system has relied on spontaneous nucleation on the walls of the quartz liner to start the growth of crystals. Knowing where the best growth occurs, particular attention is given to this region. The run progress is easily observed through the viewing port and the flow of extra chlorine is adjusted often during the initial stages of a growth run to first create conditions for nucleation and growth, and then to reverse the growth reaction just long enough to remove all but the largest crystallites that have started to grow. The best results are obtained by going through this cycle several times and then growing slowly until a good growth has been established. If too many crystallites nucleate, growth at any one site is slow and the yield of large crystals is small. A large amount of nucleation upstream

from the optimum growth region is also avoided as this depletes the gas stream quickly and slows growth.

The reactions, Reaction 3 and 4, used to describe the crystal growth system are probably only approximate models of a more complex series of reactions. By measuring the weight loss of the tin charge in the $SnCl_4$ reactor during a run and calculating the total chlorine flow into the reactor during the same runs, it has been found that the equivalent chloride produced was more nearly $SnCl_x$ with $2.7 < x < 3.0$. With more accurate calibrations of the flow meters this figure could change slightly but the indication is clearly that more tin is transported into the furnace than Reaction 3 indicates. It is also obvious that the situation inside the furnace is more involved than simply shown by Reaction 4. First the ratios of the reactants present is different than needed to balance the reaction. When the oxygen and hydrogen are reduced towards the balanced proportions large amounts of white compounds - undoubtedly chlorine compounds - form and deposit in and near the output endcap soon blocking the flows. Second, there is evidence that there are intermediate reactions and/or mixings involved in moving from the left-hand to the right-hand side of Reaction 4. There is a region about and before the center of the furnace where minor deposition occurs if the injector nozzles are positioned as discussed earlier and shown in the figure. When the nozzles are moved back as little as one half an inch deposition is increased markedly in these regions, with a corresponding decrease in the rate of growth in the optimum growth region which is downstream from this. Also, there is evidence that some of the deposited stannic oxide reenters the gas stream for when the extra chlorine flow is adjusted to give a slow growth rate the larger crystals are found

to grow while small nucleations decrease in size, a useful fact when starting a run where it is desirable to favor the larger crystals so the depositing stannic oxide will be concentrated there. That the actual growth system is more complicated than the two reaction equations, Reactions 3 and 4, would imply is not surprising nor is it a problem. This fact must be realized, though, and remembered when an attempt is made at more carefully exploring the growth dynamics or even when changing the growth conditions or the physical system.

2.6 Crystals Grown - General

The stannic oxide crystals grown are clear and transparent - water-white in color. They show no optical distortion in untwinned portions, have no visible voids or inclusions, and only occasionally show milkiness as a faint localized veil. The dominant crystal habit is illustrated in Figure 3. Typical dimensions for crystals grown 40 hours are A = 2.5 mm, and B = C = 5 mm. A photograph of several antimony doped crystals is shown in Figure 4. All of the large single crystals that grow, usually in what has been referred to above as the optimum growth region, grow as these diamond cross-sectioned prisms. They are attached at their base to the quartz liner and stick out into the tube with a slight upstream tilt. Note that the larger surfaces are well formed 111 faces and that all of the crystals are actually twins. The twin plane is the (011) plane (the conventions (a, a, c) is being used) and is indicated in Figure 3. In some crystals (100) and (122) faces of small area are evident, dulling the points of the diamond slightly, and in some small crystals found growing on the upstream side of the furnace center large parallel (011)

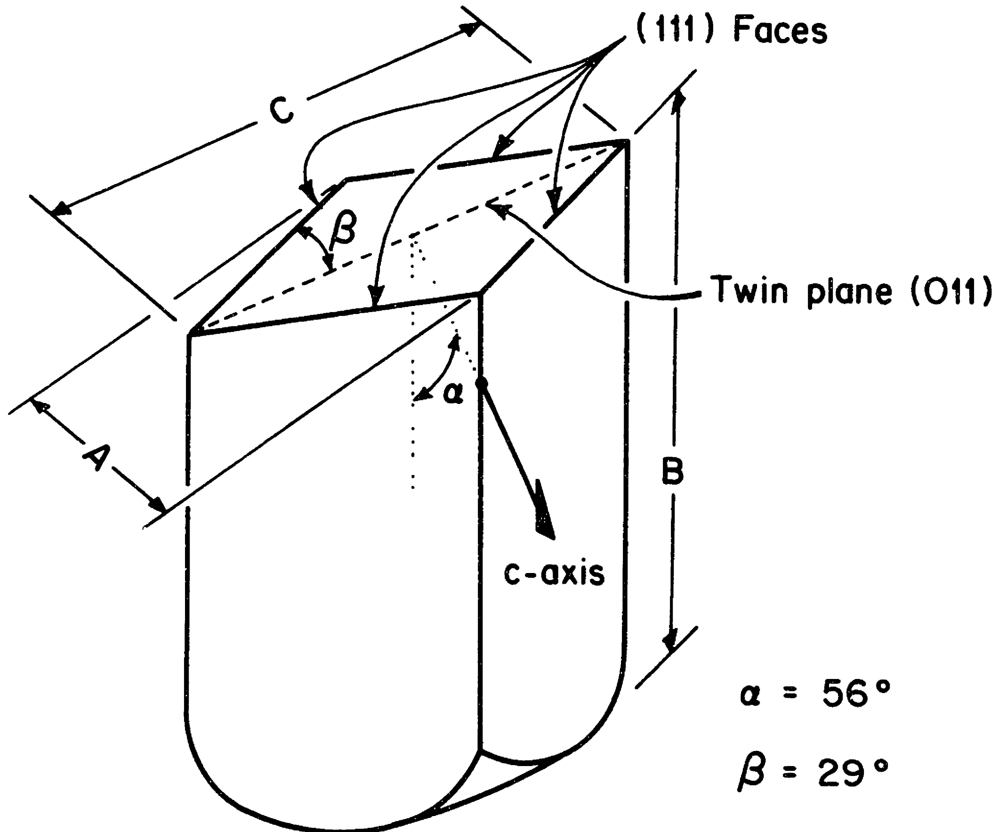

Figure 3 - Artist's sketch of a stannic oxide crystal illustrating the most common growth habit. Note the (011) twin plane bisecting the crystal along the long diamond diagonal, and the position of the c-axis. The large side faces are (111) faces.

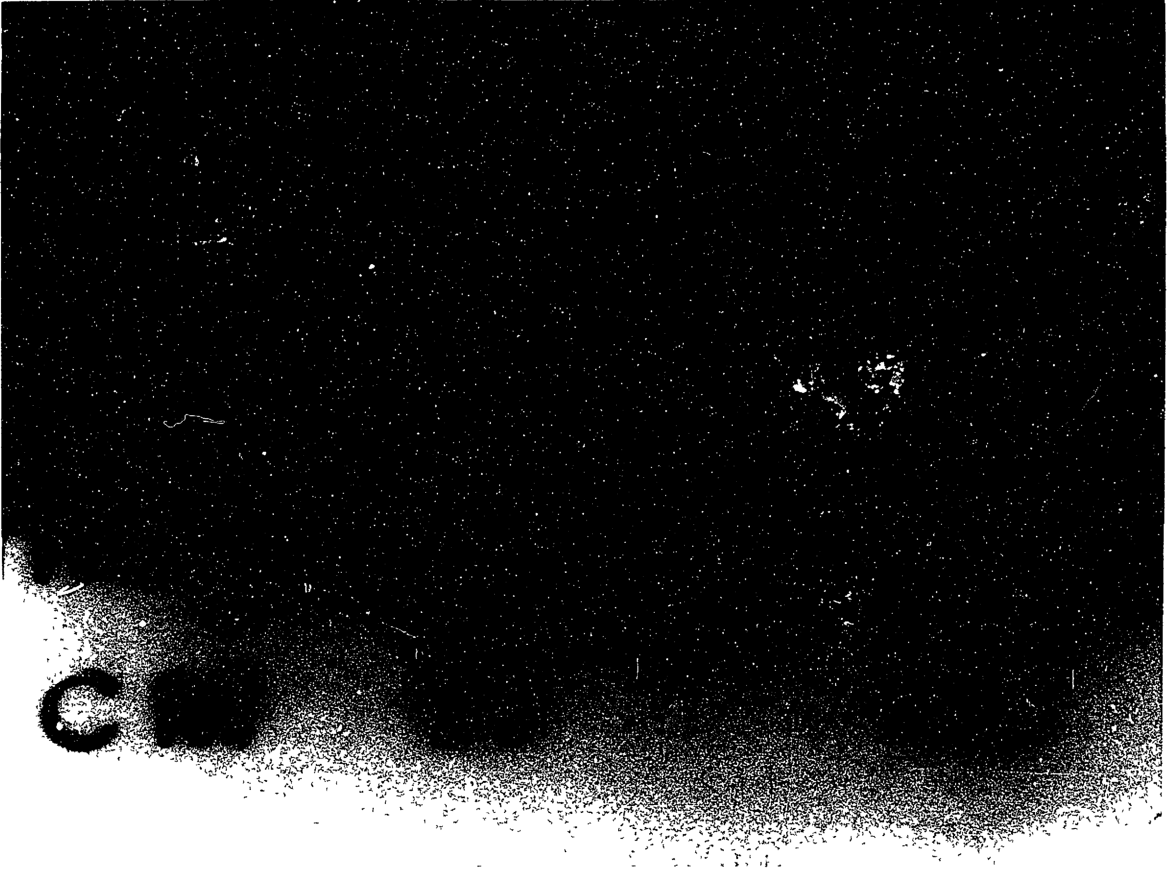

Figure 4 - Photograph of two typical stannic oxide crystals grown with the present system in 40 hours. These crystals are undoped but there is no difference in the appearance of antimony doped crystals.

faces are present. No change in the growth habit has been noted when antimony is introduced as a dopant.

Laue x-ray photographs of crystals taken primarily to orient them and to identify the growth habit, show a large number of sharp spots indicating good crystalline quality. For example, moving between the (100) and (001) directions twenty sponts were identified.

Spectrochemical analyses were performed on crystals from most runs to determine what impurities were present in them. An analysis was also made for comparison of a stannic oxide crystal obtained from Marley.[4] The analyses were all done by the Center for Materials Science and Engineering Analytical Laboratory. The most abundant impurity reported in our crystals other than intentional dopants was silicon which was present in less than 10 ppm. As expected, the silicon concentration was much higher in pieces cut from the bases of crystals where they were attached to the quartz liner. Less than 1 ppm of Ca, Fe, and Mg were also regularly reported in the crystals. Several other elements - Ag, Al, Cr, Cu, Ni, Pb, and Ti - were reported sporadically, i.e., once or twice, as being present but their actual existence in the crystals is doubted. In the crystal grown by Marley less than 1 ppm Ca, 1 to 10 ppm Fe and Mg, 10 to 100 ppm Si and Ti, and more than 100 ppm Al were found. It should be pointed out that the analysis technique used cannot detect the element chlorine so its presence in the crystals cannot be discounted. Also, Ca, Fe, and Mg are common carbon electrode impurities and are common contaminants in this type of an analysis.[26] Accepting the analysis though, a comparison of the results found for our crystals with the analysis of the Marley sample and with the

analyses published for stannic oxide crystals grown by other groups[10,12,15] shows that our crystals contain significantly fewer impurities. This in spite of the fact that no special effort was made to use high purity starting materials. The purity of the crystals may be due to several occurrences. The first, mentioned previously, is the purification of the tin source by the chlorine reaction. Impurities in the crystals must either be inside the furnace initially, or enter the furnace as a gas, most likely as a compound with chlorine. If the impurities in the tin do not react with chlorine producing volatile chlorides they will remain in the reactor. This same type of situation could also reduce contamination from the injector nozzles and the quartz liner although this obviously not completely true for silicon. The second occurrence is a purification by rejection of foreign atoms by the crystal lattice as it forms. While segregation coefficients for impurities are not known for SnO_2 so that this is speculation, such rejection is very common - zone-refining of ingots is perhaps the best known example - and could contribute importantly to the purity of the crystals. A third possibility, of course, is that impurity atoms which can enter the gas flow never reach the crystal lattice either because they are oxidized and removed before they reach it or because they never react and remain in the gas stream.

2.7 Specific Growth Runs

Before discussing crystals produced in specific growth runs the run numbering system used should be mentioned. Three digits are used to denote a crystal harvest: the last two digits are used to number the runs in sequence and the first digit is non-zero only if harvests of crystals

or changes in the liner were made during a run.

The first successful run, that is, the first yielding crystals like those in Figure 4, was Run 207 and this run produced undoped, high resistivity crystals. The next run, Run 008, was a growth of 45 hours with antimony doping during the final 15 hours; this run had the largest crystal yield of any run made. A net donor profile make using 2 mil diameter Schottky barriers on a slice cut perpendicular to the long prism axis of a crystal showed that the donor concentration was about 1.3×10^{18} cm^{-3} in the outer 5 mils of the crystal and then dropped to 4×10^{16} cm^{-3} by a depth of 10 mils, being uniformly this concentration inside this depth.

Run 009 was an attempt to dope with thallium, a possible p-type dopant, but the yield was poor and spectrochemical analysis showed no trace of thallium in the crystals. Runs 010 and 011 were growth runs to dope with antimony in a lower concentration than 008. Difficulties with the growing system during these runs limited their lengths and yields.

The output endcap was modified after Run 011 to allow for the insertion of a seed rod as described earlier and Run 012 was the first attempt at growing on a seed. After the run the input endcap was redesigned to include a window which was found desirable to have for observing the seed and this new piece was used for the first time in Runs 013 and 113, also seeded growth runs. The work on seeding will be discussed more below.

Runs 014 and 015 were growths, like 010 and 011, to grow crystals with lower antimony concentrations than Run 008; they were successful but had low yields. Runs 016 and 017 were attempts to dope with gallium, another possible p-type dopant. Again spectrochemical analysis showed no trace of gallium in the crystals but the yield of Run 017 was very good.

A common difficulty encountered during the course of some runs, and a direct contributor to low yields, has been an increase of the pressure inside the system because of the partial blocking of the output lines or cold traps by deposits or the development of a leak, usually where the output endcap seals to the mullite tube. If the problem occurs while the system is being watched corrective measures can easily be taken. The difficulty arises because growth runs are long duration and watching the system continuously is impractical. As a solution a feedback pressure controlling system utilizing a diaphragm pressure transducer and a servo-motor geared to the nitrogen bleed-in valve used to limit the pumping efficiency of the vacuum pump has been constructed and installed on the system. This unit is patterned after one designed by Folweiler[27] and is discussed in Appendix B.4. It will maintain the pressure in the system at the desired value automatically and will be available for use in future runs made with the system. By automatically compensating for most of the leakage and other pressure problems that arise, the growth will not be irreparably disturbed and corrective measures can be taken when the next regular check on the run's progress is made.

Another major reason for poor yields of some of the growth runs was that too much nucleation occurred either too soon in the liner in front of the optimum growth region because the nozzle placement was wrong (too shallow), or too thickly in the optimum growth region because not enough care was taken during the early stages of the run to limit the number of nucleation sites through growth-etch cycles and slow initial growth. A substantial amount of artistry and feel is involved in obtaining a good yield. A much more efficient way of growing large crystals, a necessity

for studies requiring oriented samples, and/or a collection of variously doped crystals would be by seeding the growth. Modifications were made in the output endcap to permit the insertion of a rod, to which a seed rod can be attached, into the growth region along the furnace tube axis and this was in fact done during Runs 012, 013, and 113. The seeds were crystals selected from previous growths and attached to the end of an 1/8" O.D. zirconia rod by a 10 mil platimum wire threaded through a small hole sandblasted in the base of the seed. The seed for Run 012 is shown in Figure 5a. The seeds were cleaned, but not etched, before being placed into the furnace; etching was done with the seed in position in the optimum growth region by increasing the extra chlorine flow sufficiently to reverse Reaction 4. Then growth was started. As the result of Run 012 in Figure 5b illustrates, substantial growth does occur - this sample was grown in 26 hours - but although the growth is single crystal, the crystal surfaces show many re-entrant faces indicating that there is turbulence in the gas flow near the seed. The result of Run 013 was similar and the seed for Run 113 was lost because of too much initial etching. The difficulty, then, is not getting growth on stannic oxide seeds as the feasibility of this has been demonstrated but rather getting conditions adjusted for smooth growth. This is essential if layers are to be grown for device application and can perhaps be achieved if the seed is carefully shaped initially. Similar considerations are important for the growth of epitaxial stannic oxide layers on other substrates also. Numerous options to vary the placement and temperature of the seed and the growth rate exist in the system and can be employed to perfect seeding and epitaxial growth. While the feasibility

(a) Seed prior to the run attached to a Zirconia rod with Pt wire.

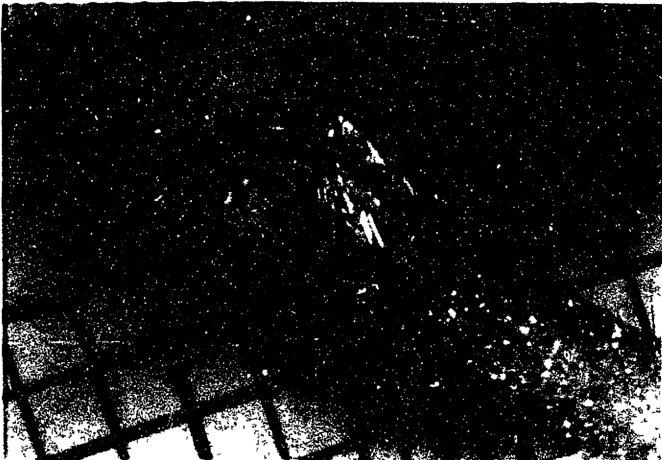

(b) Growth on seed after 26 hours total time in furnace. Note the appearance of the crystal faces and the thick polycrystalline deposit on the supporting rod.

Figure 5 - Seed growth from Run 012.

of growth on seeds was demonstrated, the optimization required to produce device quality material was not undertaken in this work and no electrical evaluation of seed grown material was made.

The lack of success in doping crystals with thallium, Run 009, and gallium, Runs 016 and 017, could be due to any of the factors contributing to sample purity discussed in Section 2.6. The dopants are, after all, impurities. It is suspected that the dopant atoms were not even transported into the growing furnace because of the insufficient volatility of the relevant chloride. To overcome this may require an alteration of the growth system to allow the doping reactor and the lines from it to the furnace to be heated to a higher temperature. This would not be a major difficulty.

Another modification in the growing system which would be advantageous to make is to change from a simple physical mixture of the dopant and tin as a doping reactor charge to an alloy of the dopant and tin. With a simple mixture one can easily see that if the dopant reacts more readily with chlorine than the tin, the doping can be very nonuniform, particularly since very small amounts of dopants are involved. This difficulty would be largely overcome if an alloy was used as a charge and the additional advantage is gained that the preparation of dilute doping charges is easier. The main problem with the use of alloy charges appears to be in their fabrication in a small mesh pellet or shot form.

2.8 Summary of Growth Technique

The technique of growing crystals of stannic oxide described above was developed to obtain high quality crystals for a study of the

electrical properties of this anisotropic wide bandgap semiconductor. This objective was met very successfully. The crystals that have been produced have been shown to have fewer impurities and higher electron mobilities than any previously available stannic oxide crystals. More importantly, their electrical properties appear to reflect intrinsic stannic oxide processes rather than solely the influence of impurities. Further, it is expected that the technique and system developed have much more potential value than has been exploited here both for the study of stannic oxide and for the growth and study of other materials.

The possibilities for seeded growth and epitaxial growth on prepared substrates have been discussed, as have the possibilities of introducing various other electronically active dopants - ideally p-type - into the crystals. The system allows a great deal of control over the growth reaction which should make the achievement of these goals far easier here than in more conventional systems.

To the author's knowledge this is the only other material to which Schaffer's technique for growing Al_2O_3, i.e., low pressure, inert carrier-gas free chemical vapor deposition, has been successfully applied. At present it is being applied to the growth of several other oxides in other laboratories, and in light of its success in producing high quality stannic oxide crystals it looks very attractive for application in the growth of many crystalline materials. It is, of course, ideal for materials that can only be grown from the vapor phase because it has advantages over the usual vapor phase systems. The most important advantages are the ease with which the quantities of reactants in the system are monitored and controlled,

the control realized over the growth reactions, the purification through the chlorine reaction and the gaseous transport, and the ease with which electronically active dopants can be introduced into the crystals.

3 - Electrical Studies

3.1 Schottky Barrier Program

Schottky barriers - rectifying metal-semiconductor contacts - are of interst in the study of stannic oxide both because of what can be learned from them about SnO_2 and because of their importance to device applications of this material. This latter factor was the main motivation for studying Schottky barriers here and barriers suitable for application in field-effect devices have been developed. Using the resulting barriers to study parameters of stannic oxide has also been very valuable and this work, too, is discussed.

3.1.1 Nature of Program

The objective of the Schottky barrier program was to consider the behavior of metal areas on stannic oxide surfaces prepared in various ways with the aim of developing a technique of fabricating metal-semiconductor devices useful for future application in field effect transistor geometries. The primary criterion for evaluating the product of a particular set of fabrication steps, then, was the current-voltage characteristics of the device. For early attempts, the reverse characteristics were used as a quick check on the device; as the reverse resistance increased in the devices produced, the nearness of the forward characteristics to a theoretical device was also considered. Except where noted below in the calculation of ε_r, no particular attention was paid to the crystal orientation in the Schottky barrier program.

By way of standardizing the study a fixed geometry and contacting scheme were used for all of the devices. All of the other fabrication and

evaluation steps were, of course, also rigorously controlled and were varied only as consistent with the overall development. The metal barriers were formed by evaporating the metal in a bell jar through a mask placed over the stannic oxide surface. At first the mask was simply a piece of aluminum foil with small pin holes in it; this was soon changed to a stainless steel mask with 20 mil diameter holes. Contact was made to the evaporated barrier with a 2 mil diameter platinum or gold wire on the end of a probe mounted on an x-y micromanipulator stage.

Ohmic contact was made to the stannic oxide with indium metal, or with Wetalloy-232 (Victor King Laboratory, Los Altos, Calif.), an alloy of mercury, indium and thallium which is liquid at room temperature. The latter was a quickly made contact (the sample was simply set on a drop of the liquid alloy) that was good for a short term measurement. A large area low resistance contact was obtained and it was unnecessary to heat the sample to make it. For a more solid contact indium could be used. Brief attempts at alloying indium dots to samples were unsuccessful, and the best method for applying indium contacts was found to be by taking a small amount of indium on the tip of a pencil soldering iron heated to 200 - 225°C, dipping this briefly in a flux such as Superior No. 30 (Superior Flux and Mfg. Co., Cleveland), and then dabbing this indium quickly against the sample. Indium would stick although it would not wet the surface. It could be shaved off cleanly, at least to the eye, with a sharp blade and would also loosen if heated too much when attaching wires. Still the contact had a small amount of physical strength, and it was of low resistance and ohmic. Evaporated indium contacts behaved similarly. It should also be noted that none of the other common solders tried nor an alloy of 99%In- 1 %Sn that was

available wet better or formed any stronger a contact than did indium.

To observe and study the voltage-current characteristics of the barriers a Tektronix model 576 curve tracer was used. No special guard-ring device geometries were used nor was any special effort made to separate parallel and series resistance from the observed characteristics. For the measurements of barrier small-signal capacitance as a function of bias voltage a Boonton model 75C capacitance bridge was used at 1MHz, and a Boonton model 75B-58 was used from 5 to 500 KHz. The bias voltage was obtained from the bridge or from a Hewlett-Packard model 6205B d.c. voltage source and was measured on a Hewlett-Packard model 3440A digital voltmeter. More specific details of the measurements will be found in section 3.1.3.

3.1.2 Fabrication Procedure

The procedure developed to fabricate Schottky barriers on stannic oxide crystals will be presented first; a detailed discussion of the function of each step and of some of the alternatives considered before arriving at that step will follow. Some of the steps, of course, would be used on any material and are simply common-sense; other steps are peculiar to stannic oxide and it is these which will be of most interest to consider here. The procedure is:

1. Cut a sample from a crystal and shape it using a wire saw. A slurry of 600 grit silicon carbide in light oil works well. Use a low temperature wax to hold the sample and do not heat it excessively ($<150^{\circ}C$).
2. Mount the sample on a polishing block with the face of interest up. Again avoiding excessively heating the sample.

3. Gently lap the face flat using 600 grit paper and water on a polishing flat. Clean the sample and block after this in a mild soap solution taking care to remove all traces of grit. (Do this after each polish step also).
4. Polish the surface with 15μ diamond paste and oil on AB Metcloth (Bueler Ltd., Evanston, Illinois) until only polish scratches are visible (usually 5-10 min.). Use a polishing wheel set at low speed to do the polishing and keep the sample always at the same orientation relative to a wheel diameter moving it back and forth along a radius while polishing. The 15μ polish scratches will then all run in the same direction and if the sample is rotated 90° for the next polish size the scratches from that polish will be perpendicular to the scratches being removed and can easily be distinguished.
5. Polish the surface for 5 to 6 minutes on 6μ diamond paste and oil on Metcloth.
6. Polish the surface for 15 to 16 minutes on 1μ diamond paste and oil on felt.
7. Remove the sample from the polishing block by soaking it in a solvent of the mounting wax (usually acetone) and clean all traces of the wax from the sample. Rinse it in methyl alcohol and blow it dry with dry nitrogen. A fine tipped stainless steel tweezers can be used to handle the sample but avoid touching the polished surface.
8. Etch the sample 15 minutes in a hot hydriodic acid solution. (Prepare this solution by pouring a 1/2" depth of 57% HI into a

small petrie dish and heating on a hot plate heated to 280°C. Remove any free iodine from the solution by adding hypophosphorous acid, H_3PO_2, to it drop by drop until it clears to a pale yellow color but do not add too much as the etch then becomes ineffective). The solution should be stirred constantly with a small teflon covered magnetic stirring bar. Remove the sample directly to a deionized water rinse. Rinse it a second time, rinse it in methyl alcohol, and blow it dry with dry nitrogen.

9. Repeat the above step using a fresh etch solution.
10. Etch the sample 10 minutes in a 0.1 M NaOH solution heated to about 90°C in a double boiler. Again, stir the solution constantly with a magnetic stirrer. Remove the sample to a deionized water rinse, rinse it again, rinse it in methyl alcohol, and blow it dry with dry nitrogen.
11. Place the sample under the desired mask and place it in an evaporator bell jar. Evacuate the jar to under 5×10^{-7} torr before evaporating the barrier metal. The evaporator source should be placed far from the sample (7-8 inches) and the evaporation should be done very slowly (a deposition rate of 100 Å/min and a total thickness of 700° Å is typical).
12. Remove the sample; contact and measure as desired.

Considering now these steps in detail with particular attention to their significance to stannic oxide, the first item is cutting the samples. Stannic oxide is listed on the Mohs' hardness scale as 6-7 or similar to silicon (7.0). The crystals could be cut on a wire saw if care was taken to cut slowly and guard against wandering of the blade. Using this saw

has the big advantage of wasting very little material both because of the small saw width and the shallow surface damage.

The polishing steps were developed using silicon as a guide in as much as in that material the surface damage due to a polish is found to extend much deeper in than grit size (about 10 times as deep). Thus a polish must remove much more than the scratches of the previous grit polish and the above series of polishes, each smaller for a longer time, was directed towards doing this. Still, as the next paragraph will vividly demonstrate, the surface remains damaged and it seems heavily n-type. Barriers evaporated on such a surface are invariably ohmic; in fact, the only way found to contact high resistivity samples was by first abrading the surface. Using finer polishes such as Linde A (0.3μ alumina) and/or Linde B (0.05μ alumina) was of no value.

To remove the surface damage the hydriodic acid etches were used. HI is not polishing etch but attacks damaged areas most strongly. It was first used by Koffyberg[9] to produce etch pits for a study of dislocations in stannic oxide crystals, and the effect of this etch is quite dramatic. After five minutes of etching many fine, sharply distinct scratches appear on a sample surface which had initially been polished "scratch free" on 1μ diamond. These scratches run in all directions showing that some damage still remains from the coarser grits. As the surface is etched more these scratches start to become less sharp; they broaden as well as deepen and, in fact, it soon seems that they are etching no more quickly than the rest of the surface area. The damaged regions have evidently been removed and the entire surface is eroding (etching away) uniformly. The thirty minutes of etching used is more than sufficient time for this to occur.

The stannic oxide surface is still not suitably prepared for making Schottky barriers and gold areas evaporated on such a surface generally show poor rectification. Several treatments of the etched surfaces were tried to correct this and it appears that the etched surface is oxygen poor. This would make it strongly n-type and is consistent with hydriodic acid's strongly reducing nature. Samples etched in hydriodic acid were left in air for 24 to 48 hours prior to evaporating the barrier, others were placed in an oxygen atmosphere at 400°C for hours prior to evaporating the barrier, some were etched in hydrogen peroxide, and others were boiled in de-ionized water for 90 minutes. All of these processes gave some improvement but results were sporadic. The only treatment giving consistently good barriers was the sodium hydrozide etch, step 10, that is suggested by the work of Surhigh and Mead.[28] They did some work on Schottky barriers on SnO_2 studying the barrier height as a function of the barrier metal work function and concluded that there was a one-to-one relationship. Their only reference to sample preparation is that the surface was "prepared by etching in a dilute solution of NaOH followed by a distilled water rinse". Many etch techniques and solution strengths could fit this description, but no success was had using an NaOH etch as the sole surface treatment of either a polished or natural surface. Used as outlined in the barrier fabrication procedure, though, it is very successful.

The evaporation of the barrier metal has also been found to be a critical step. The barrier metal used most in the present work was gold and if the evaporation was done quickly or from a close source the barriers showed poor rectification characteristics that changed (improved

somewhat) over a period of days. Moving the source as far from the sample as possible in the available evaporator, and using the slowest evaporation rate that could be set (a Sloan Omni II was available to monitor the deposition rate although the evaporation was controlled manually) eliminated this problem and improved the device characteristics.

The fabrication procedure developed has worked well on all the crystallographic faces it has been used on (these have been the (100), (011), and (111) surfaces and the surface perpendicular to these three) and gives consistently good results. To summarize this procedure, the sample is first cut and the surface carefully polished. Any surface damage present (which is strongly n-type) is then etched off with hydriodic acid, a strong reducing agent which appears to still leave an n-type surface on the SnO_2. To finally prepare the surface it is etched in a sodium hydroxide solution (an oxidizing agent) before slowly evaporating the barrier metal through a suitable mask from a distant source.

3.1.3 Electrical Characteristics

The devices that will be discussed here are all gold Schottky barriers fabricated on stannic oxide crystals following the above procedure. At the end of this section barriers made with several other metals will also be mentioned but they were of lesser interest. The first electrical characteristics discussed are the current-voltage characteristics. This is followed by a presentation of measurements of the small signal device capacitance as a function of bias voltage and their application to the study of stannic oxide.

A photograph taken of a curve tracer display of the current-voltage characteristics of a typical Schottky barrier device is shown in Figure 6.

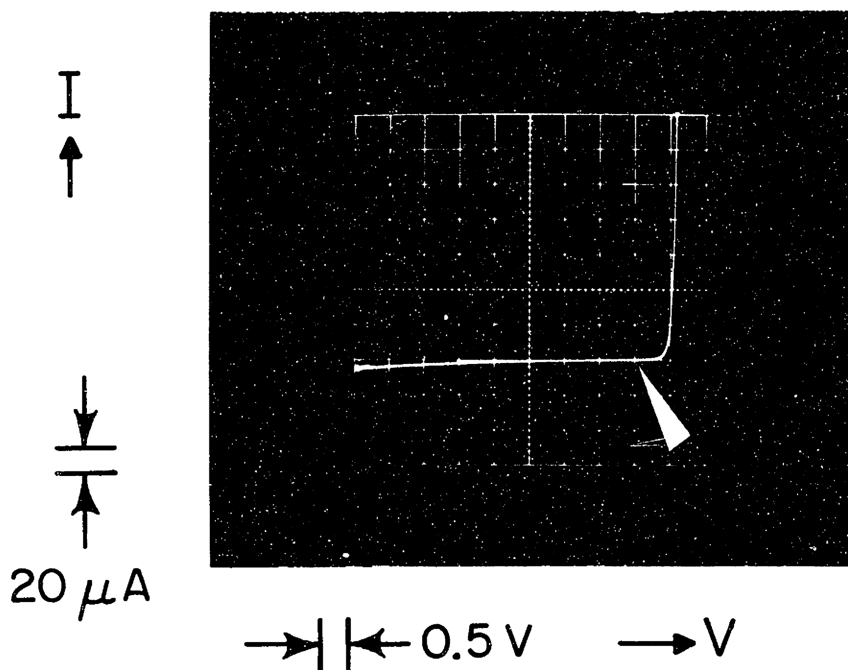

Figure 6 - Photograph of a curve-tracer display showing the current-voltage characteristics of a gold Schottky barrier diode 20 mils in diameter on stannic oxide. The zero point is indicated by the white arrow point in the lower right of the photograph.

The vertical scale is 20 μA per large division; the horizontal scale is 0.5 V/div. Note that in the photograph the zero point is shifted down to the right of the center and is indicated by the small arrow. This particular device is a gold barrier 20 mil in diameter on a stannic oxide crystal doped with 8×10^{16} cm^{-3} antimony atoms. As described earlier the gold is contacted by a fine wire probe and the ohmic contact is made to the stannic oxide using indium. The trace was made with room lights on, and no other lighting, but no change was noted when all the lights were turned off.

In the forward direction the current is expected to have an exponential dependence on voltage if the series resistance and any shunting resistance are neglected:[29]

$$I \propto (\exp eV/nkT - 1) \simeq \exp eV/nkT \qquad (5)$$

Here e is the electronic charge, k is the Boltzmann constant, T the device temperature, V the externally applied voltage, and I the current through the device. The parameter n is expected to be 1 from the simple theory. A change in V of ΔV will cause an increase in I to mI with

$$m = \exp q\Delta V/nkT \qquad (6)$$

At room temperature m is 4 for $\Delta V/n = 35$ mV which offers a crude method of comparing a given device's characteristics with an ideal device. One simply measures ΔV for several four-fold increases in I on a device and considers the n's indicated. Early devices produced showed soft forward characteristics with n between 3 and 4 clearly indicating improvement could be made in the fabrication technique. (There were of course usually other indications such as in the reverse characteristics of something

wrong too.) Devices produced with the final fabrication procedure developed show n's under 1.5. It is important to again point out that no attempts to correct for series or parallel resistances were made nor were any guard-ring geometries employed. Without doing these things any more rigorous analysis of forward I-V is not justified.

In the reverse direction the features of interest are the current level and the breakdown voltage. As the reverse voltage was increased no sharp break-down was observed but rather a soft knee was seen in the curves. At still higher voltages a downward shift (increase in current) of the entire curve occurred much like a heating effect. Too much voltage would destroy the device. For the device pictured in Fig. 6 the knee occurs at minus 5-10 volts and the current is about 10μA at -5 volts. Generally speaking the magnitude of the reverse current increases and the knee voltage decreases as the donor concentration of the stannic oxide increases. It is worthwhile noting that devices prepared before the fabrication technique discussed earlier was perfected had, in addition to more reverse current and softer forward characteristics, a substantial amount of hysteresis in their characteristics. Devices formed simultaneously on the sample often also differed greatly and they, further, would age (surprisingly enough, improving with time). Properly fabricated devices were, of course, sensitive to mishandling, but showed none of these random idiosyncrasies. The predominant form of device failure is shorting out of the barrier, an occurrence evidencing itself as a resistance in parallel with the device.

The small signal impedance - capacitance and resistance - of a Schottky barrier measured as a function of a D.C. bias voltage and at different frequencies can yield information on the donor concentrations,

on the nature of the donor levels, and on the barrier height. Such measurements were made on the devices produced on stannic oxide in this study using the electronics described earlier, section 3.1.1. In making the measurements care was taken to have the bridge oscillator signal level low enough that the capacitance and resistance measured were, within the measurement accuracy, independent of that level; that is, to assure a "small-signal" measurement. Also, since the bridge registers the device impedance it sees as a parallel RC it must be determined that the resistance (due to the semiconductor bulk) in series with the Schottky barrier is not important or, if it is, is corrected for. This is done, if it necessary, by converting to a series equivalent, subtracting the fixed series resistance, and then converting back to a parallel equivalent. Such a correction was only required on the lowest concentration samples studied, and then only if the ohmic contact was not near the barrier. For example, measurements were made on one sample which had two ohmic contacts, one near the barrier and the other far enough away to have an appreciable series resistance; after correcting for this series resistance the results using either ohmic contact were identical.

The graph in Figure 7 shows the small signal capacitance of a 20 mil diameter gold barrier on stannic oxide plotted versus the applied DC bias voltage in the manner allowing the easiest comparison with Schottky barrier theory.[29] The inverse square of the capacitance is plotted and, following the theory for a uniformly doped semiconductor, should be related to the bias voltage by:

$$1/C^2 = 2(V_b - V)/eN_d A^2 \varepsilon \qquad (7)$$

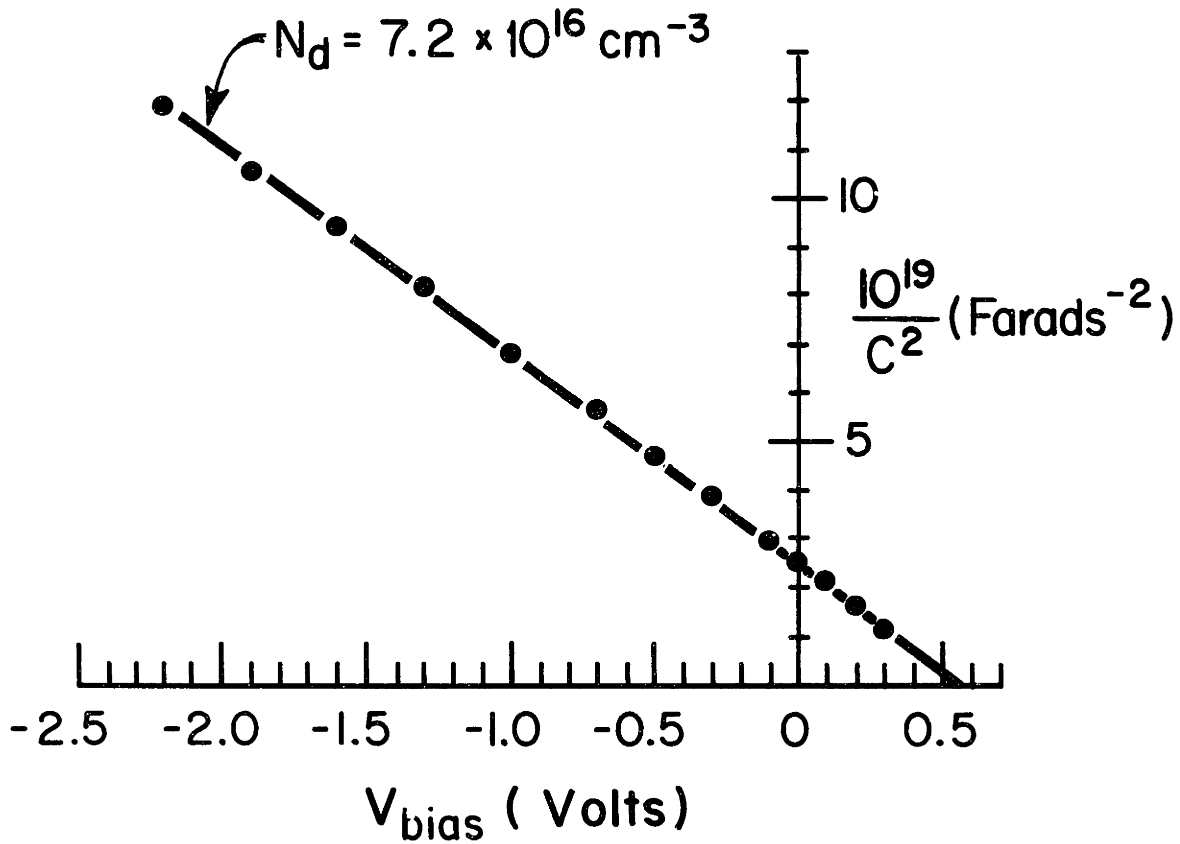

Figure 7 - Inverse squared small signal capacitance of a 20 mil diameter gold Schottky barrier diode on stannic oxide plotted as a function of the applied DC bias voltage. The slope of the curve is proportional to the net donor concentration of the sample.

Here ε is the static dielectric constant of the semiconductor, N_d the net donor concentration, A the area of the barrier, V_b the apparent barrier height, and e the electronic charge. The plot of $1/C^2$ vs. V should be then a straight line with slope proportional to the net donor concentration:

$$-\frac{d(1/C^2)}{dV} = \frac{2}{eN_dA^2\varepsilon} \qquad (8)$$

and whose voltage axis intercept is the apparent barrier height

$$1/C^2 = 0 \ @ \ V = V_b$$

If the semiconductor is not uniformly doped the slope of the curve at a given bias voltage is proportional (equation 8) to the net donor concentration at the corresponding depletion depth:

$$d = [2\varepsilon(V_b - V)eN_d]^{1/2} \qquad (9)$$

If several donor levels are present, one being deep enough that it is not ionized with 0 bias, the plot of $1/C^2$ vs V may show two straight line regions of different slopes, the first corresponding to the concentration of the shallower donor, and the second corresponding to the total donor concentration and starting when sufficient bias is applied to ionize the deeper doncrs.[30]

As Figure 7 illustrates, the data measured for gold Schottky barriers on stannic oxide could be fit to equation 7, and a net donor concentration and a barrier height determined. This was done for Schottky barriers fabricated on all of the samples whose bulk properties are considered in the following section, 3.2, and the net donor concentrations calculated are further discussed in section 3.3. In some barriers on other samples a deviation from linearity was seen as a decrease in the slope of the

curve at high reverse bias. This was not large - under 20% change in slope - but might indicate the presence of some deep levels that are ionized only at large biases. It was also noted in the same samples that after making measurements at reverse bias the zero bias capacitance was lower than initially and slowly drifted (with time constants apparently minutes long) towards its original value. This drift was accelerated by the application of light from the microscope lamp (incandescent). These observations also might indicate the presence of deep levels in the samples.

There was, on the other hand, no dependence of the zero bias capacitance on measurement frequency over the range considered, e.g. 5 kHz to 1 MHz.

Returning to the determination of a net donor concentration using equation 7, there are several items to be noted. The first is that for any calculation of an N_d it is necessary to know the barrier area. Since the barriers are circular the quantity actually measured is the diameter which then appears to the fourth power in equation 7. The estimated $\pm$ 2% uncertainty in determining this quantity contributes an uncertainty of $\pm$ 8% to N_d.

The second item is the need to know the value of ε to use in Equation 7; this is complicated by the fact that stannic oxide is an anisotropic material. The important observation is that the electric field is constrained by the barrier metal to be perpendicular to the surface so that the pertinent ε is the component of the static dielectric constant tensor in the direction perpendicular to the surface. Thus, if $u_\perp$ is a unit vector perpendicular to the surface, the desired ε_r ($\varepsilon = \varepsilon_r \varepsilon_o$) is simply:

$$\varepsilon_r = \left| \vec{u}_{\perp} \cdot \begin{pmatrix} 14 \pm 2 & 0 & 0 \\ 0 & 14 \pm 2 & 0 \\ 0 & 0 & 9.0 \pm 0.5 \end{pmatrix} \right| \qquad (10)$$

where Van Daal's values[22] of $\varepsilon_r = 14 \pm 2$ for $E \perp c$ and 9.0 ± 0.5 for $E \parallel c$ have been used with a rectangular coordinate system oriented with the z-axis parallel to the crystallographic c-axis and the x- and y- axes parallel to the a-axes (see Figure 1). As an example, if the surface is a (011) face, $u_{\perp} = (0, 0.56, 0.83)$ and $\varepsilon_r = 10.9 \pm 1.1$ or ε_r is $\simeq 11$ with a $\pm$ 10% uncertainty.

Additional uncertainty from determining the slope $1/C^2$ vs. V, combined with those already mentioned in determining d and in ε, makes the estimated overall uncertainty in $N_d \pm 15\%$.

A very useful application of the C-V determination of N_d has been to study sample donor concentration uniformity and/or profiles. To do this a mask producing 2 mil diameter barriers spaced in a square array on 5 mil centers is used. With this grid of measurement points the variation in the net donor concentration across a crystal slice can be determined to better than 5% (note that this is a comparative measurement so that with an accurate mask the major uncertainties in an absolute N_d calculation cancel out) and this information can be used when cutting samples for bulk property measurements. Several samples cut before this technique was developed were quite inhomogeneous and the bulk measurements made on them were erroneous. It is indeed an important tool and should be of value to anyone developing new materials. In such work the crystal growth or other material source is often not under complete control and material inhomogeneities should be anticipated and considered. With this technique

they can be easily and nondestructively tested. The information obtained can also be correlated with the growth run record of when doping was done to learn more about the growth process and the control realized over doping. One such study was briefly mentioned in section 2.7.

The other information obtained from C-V measurements is the barrier height, V_b. It was observed that V_b for gold Schottky barriers increased with the donor concentration. This was best seen using many 2 mil diameter barriers all fabricated simultaneously on an inhomogeneous sample so one is more certain that the change is not due to differences in the way the barriers were made, but the relationship between N_d and V_b is general and appears in all samples. For $N_d \simeq 10^{16}$ cm^{-3}, $V_b \simeq 0.6$ V and for $N_d \simeq 10^{18}$ cm^{-3}, $V_b \simeq 0.9$ V.

The work of Surheigh and Mead indicates that V_b should also depend directly on the work function of the barrier metal. No direct study of this was made in the present work but results observed with low work function metals were consistent with this finding. In particular, evaporated barriers of In and Ti showed very little rectification, that is, small barriers.

3.2 Bulk Electrical Properties

The measurement and analysis of the bulk electrical properties of stannic oxide crystals was a major part of the present study. Of interest were the carrier concentration, mobility, and resistivity, and the variation with temperature of these quantities between 20°K and 625°K. The experimental techniques used to make these measurements and the data obtained are presented in this section, while the analysis of this data and that from the previously discussed electrical measurements will be found in section 3.3.

3.2.1 Crystal Anisotropy and Experimental Considerations

The determination of mobility, resistivity, and carrier concentration from Hall effect and four-terminal resistivity measurements is a common procedure and was the approach chosen for this study. Before discussing these measurements, though, it is important to first consider the consequences of the anisotropy of stannic oxide on these phenomenon. Stannic oxide has the rutile structure - see figure 1, which means it has a tetragonal unit cell and D_{4h} symmetry (the unit cell dimensions are $a_o = 4.738$ Å and $c_o = 3.188$ Å). This fact has already been used when the anisotropy of the static dielectric constant was discussed in section 3.1.3. In that discussion the tensor form of ε was shown; similarly, tensors are required to represent the resistivity and the Hall effect coefficient here. If we write a general expression for the electric field in a crystal with an applied magnetic field and under isothermal conditions we have, to second order in the magnetic field[31]:

$$E_i = \rho_{ij} J_j + R_{ijk} J_j H_k + M_{ijkl} J_j H_k H_l \quad (12)$$

Einstein sum notation has been used; i, j, k, and l are direction subscripts, i.e., x, y, or z; J is the current density, H the applied magnetic field, and E the electric field. Using the rectangular coordinate system of 3.13 where $a_1 \parallel x$, $a_2 \parallel y$, $c \parallel z$, the resistivity tensor, ρ_{ij}, in the rutile structure is:

$$\overleftrightarrow{\rho} = \begin{pmatrix} \rho_a & 0 & 0 \\ 0 & \rho_a & 0 \\ 0 & 0 & \rho_c \end{pmatrix} \qquad (13)$$

That is, only diagonal elements are present, two being equal. The mobility tensor has the same form and the resistivity tensor components are related to the components of the mobility tensor through $\rho_i = (ne\mu_i)^{-1}$. The mobility reflects the anisotropy of the effective mass and of the mean scattering time, i.e., $\mu_i = e\langle\tau_i\rangle/m_i^*$.

The Hall coefficient tensor, R_{ijk}, is zero except for $R_{a1a2c} = -R_{a2a1c}$ and $R_{ca2a1} = -R_{a2ca1} = R_{a1ca2} = -R_{ca1a2}$. There is therefore only a transverse Hall effect and the voltage due to this term is always perpendicular to the current. There are also only two independent elements corresponding to when the magnetic field is applied parallel to the a-axis and when it is parallel to the c-axis. The first is $|R_a|$ ($=R_{ca2a1} = -R_{a2ca1} = R_{a1ca2} = -R_{ca1a2}$) and the second is $|R_c|$ ($=R_{a1a2c} = -R_{a2a1c}$). These factors are related to the carrier concentration through the relations:[32]

$$R_a = -r_a^H/ne$$

$$R_c = -r_c^H/ne \qquad (14)$$

where r_a^H and r_c^H are called the Hall scattering coefficients. In an isotropic material the Hall scattering coefficient, r^H, is isotropic and simply related to the energy dependent relaxation time, τ, through $r^H = \langle\tau^2\rangle / \langle\tau\rangle^2$. For cubic crystals this factor and its dependence on the various scattering mechanisms has been well studied, but much less attention has been given to it in non-cubic crystals. It is expected though that the ratio r_c^H / r_a^H is roughly constant with temperature and is approximately unity.[32]

Finally, the magnetoresistance tensor, M_{ijkl}, has only terms of the form M_{iijj}, M_{ijij}, and M_{ijji} ($=M_{ijij}$). In a Hall effect geometry the current and magnetic field are perpendicular so only the M_{iijj} terms appear meaning that there is no voltage induced from this effect perpendicular to the current flow.

Because the size and growth habit of the stannic oxide crystals grown made cutting bars for Hall effect measurements with the c-axis along their length impractical, no attempt at all was made to orient samples. As will be discussed more in section 3.2.2, though, the samples for which results are presented here were (except for one sample where such an orientation was impossible) oriented so that the current was in the a-direction. Thus the resistivity measured is ρ_a. The mobility is calculated from the experimentally determined resistivity, ρ_a, and carrier concentration, n. To the extent, then, that the experimentally measured carrier concentration is equal to the true concentration, which in actual fact is an isotropic scalar, the mobility determined is μ_a. With the magnetic field not applied and the Hall voltage not measured along principal crystal axes, the appropriate Hall scattering coefficient, r^H,

to use when calculating n from the measured R lies between r_c^H and r_a^H and depends on the actual orientation. The important point again is that the ratio, r_a^H/r_c^H is expected to be roughly one and temperature independent so that the appropriate r^H for the present off-axis situation is a temperature independent fraction of r_a^H. This fraction is further expected to be nearly one and could reasonably be taken as one in light of the experimental deviation from theory commonly found for r^H. That is, it is anticipated that the uncertainty in r^H will be so large as to make the anisotropy considerations in the Hall effect measurement unimportant.

The only direct experimental investigation made of the anisotropy in the stannic oxide crystals studied was a measurement of ρ_a and ρ_c on a small, cube-shaped sample oriented with its edges parallel to the principal crystal axes; this investigation is discussed fully in Appendix D. It was found that ρ_c/ρ_a $(=\sigma_a/\sigma_c = \mu_a/\mu_c) \leq 1.2$ at 77°K and at 300°K. The resistivity anisotropy in stannic oxide is thus small and results obtained for one tensor direction, a in our case, will be qualitatively, and in fact quantitatively, very similar to what would be found for the other direction.

3.2.2 Sample Preparation

The measurements made were of Hall effect and resistivity on bar shaped samples. These bars were cut from slices previously cut from crystals with a wire saw. Two mil diameter Schottky barriers were used as described previously to first select a homogeneously doped portion of the slice and then the sample was cut. If necessary the cut edges were lapped flat and parallel to give a nicely shaped bar. Each sample was etched with HI and NaOH using the steps outlined in section 3.1.2 and

cleaned before mounting for measurement.

The samples for which data will be presented were uniform in concentrations to less than $\pm$ 5% as determined from Schottky barriers and from Hall measurements along the bar. Additional information on the specific sample bars of interest is given in Section 3.2.4.

3.2.3 Measurement Technique

For all measurements below 325°K (52°C) the sample bar was mounted on a holder in contact, through heat sink compound, to a block of boron nitride, BN. The temperature was measured using a copper-constantan thermocouple fitted in a hole in the boron nitride and positioned so that the thermocouple junction was just under the sample. For measurements below 77°K a 51 ohm carbon resistor whose resistance as a function of temperature was known was mounted on the BN next to the sample and was also used. For measurements above 325°K the sample was supported only by its ends and a iron-constantan thermocouple just touching it was used to measure the temperature.

Ohmic contact for the current leads was made to the ends of the bar with indium, and gold wires (typically 5 mil. diameter) were, in turn, attached to these end contacts. The voltage probes were made by positioning the ends of 2 mil diameter gold wires against the sides of the bar and forming the contact so made with a capacitance discharge (stannic oxide negative). The capacitance and voltage used varied with the sample carrier concentration from 10 μf and 45 volts on high concentration material to 90 μf and 90 volts on low concentration material. Well formed contacts are long life (on the order of days), low resistance contacts with some physical strength indicating that an actual weld occurs. Four

voltage probes were used and these were placed as two opposing pairs at approximately a third the way down the bar from each end. This allows for making two resistivity and two Hall voltage measurements simultaneously on each sample as a further check on sample homogeneity and measurement consistency. The two Hall voltages measured on the samples for which data will be presented agreed within $\pm$ 5% and showed the same variations with temperature.

Only DC measurements were made; that is, a constant magnitude magnetic field was applied and a DC current was used. The usual procedure of measuring the Hall voltage for all the four possible combinations of field and current direction was followed, and the resistivity voltage was measured in zero magnetic field. The electronics used to make the bulk property measurements in the temperature region above 77°K were part of a Center for Materials Science and Engineering central facility assembled by Dr. M. Lichtenstieger. This includes a Varian 9-inch Fieldial Mark II magnet, a PAR Model TC-100.2 BR voltage-current reference source, and Keithley Model 150B microvolt-ammeters. Between 77°K and room temperature ($\sim 300^{o}$K) measurements were made as the samples warmed slowly (at well under 1°K/min) in a simple liquid nitrogen dewar. Above room temperature a special heating chamber was used and measurements were made after the sample temperature had reached an equilibrium. The portions of this chamber exposed to the sample and holder were all quartz and the chamber was sealed when assembled except for a gas inlet on the bottom and an outlet at the top so that the atmosphere about the sample was controllable.

Measurements to temperatures requiring the use of liquid helium, i.e. essentially below 77°K, were made with the sample mounted on a holder

as discussed above in a Janis Super Vari-Temp dewar. To accomodate this dewar it was necessary to use a larger Varian 12-inch Fieldial magnet. The current source used was a Keithley Model 225 current source, and the voltages were measured with a Keithley Model 602 electrometer. Measurements were made with the sample temperature monitored and controlled by a Cryogenic Research (Boulder, Colo.) Model TC-103 temperature controller using a carbon resistor sensor.

A sample holder for use above room temperature-up to 500°C, for example - must meet certain requirements and the design of such a holder involves unique considerations not encountered in the usual Hall and resistivity measurement situation; it is worthwhile mentioning some items here. The materials used must withstand the high temperatures while retaining their useful properties and remaining chemically inert. Fired lava or other ceramics are good base materials for the holder. In the sample holder used in this work the sample was held between two gold-plated stainless steel contacts one of which was pressed to the sample by a tungsten spring. Stainless steel was used because leads could be welded easily to it, but even with gold plating it corroded quickly and was not wholly satisfactory. The 2 mil diameter voltage probe wires were held by small screw terminals. Brass screws in stainless steel posts were used and again are not really satisfactory. The "welded" voltage probe contacts to the sample worked very well but the indium current contacts (which are molten above 157°C), while being good electrical contacts, are reactive and are not ideal. The difficulty is that while the atmosphere about the sample is controlled by controlling the gas in the sample holder heating chamber, contamination and alteration of the sample can

still occur from the reactive metals in the vicinity of the sample, i.e. copper, iron, indium. A holder designed - but not constructed pending the arrival at the central Hall facility of a commercial high temperature (up to 1000°C) chamber promising much better temperature control and a longer temperature "flat-zone" than the available homemade chmaber - would use only ceramic, platinum, and tungsten. All of the current and voltage leads would be fine platinum wires discharged welded to the sample and spot welded to platinum terminal posts (which would be welded, in turn, to platinum lead wires connecting to the measuring electronics). A tungsten spring would hold the sample in place on a ceramic holder base. Thus only high temperature materials are employed and one would be fairly confident that any change in the sample's properties at elevated temperatures was due to the atmosphere - importantly, to the known atmosphere - about it, rather than possibly due to contamination from the sample holder itself.

3.2.4 Experimental Results

Data measured on four specific sample bars - labeled 008-8-b1, 008-9-b, 008-9-c, and 016-1-b - will be presented here, and the results are typical of those measured on similarly doped crystals. These bars are unique only in that they were more uniform and were studied more thoroughly than others. Samples 008-9-b, 008-9-c, and 016-1-b were oriented so that the current flowed in the a-direction and the magnetic field was directed perpendicular to the 011 face. Sample 008-8-b1 was a very thin sample (~125μ) cut from the highly doped outer portion of a crystal from run 008. From figure 3 it can be seen that the crystal habit required that it be cut from a 111 face so in sample 008 the magnetic

field was $\perp$ to the 111 face and the current was in the (011) direction. All of the bars were about 4 mm long, less than 1 mm wide, and less than 0.75 mm thick. The distance between voltage probes was about 1 mm.

The experimental results are most conveniently considered in three groupings: first, measurements between $80^{o}K$ and $300^{o}K$; second, measurements below $80^{o}K$; and finally, measurements above $300^{o}K$. Figures 8, 9, and 10 are graphs of the conductivity, Hall mobility, and carrier concentration between $80^{o}K$ and $300^{o}K$ measured on samples 008-8-b1 (Figure 8), 008-9-b (Figure 9), and 016-1-b (Figure 10). Note that the horizontal scale is inverse temperature so that the lower temperatures are to the right. The conductivity, σ, was obtained directly from the measured resistivity voltage at zero magnetic field knowing the current (1mA DC) and the sample dimensions. Here and in all of these measurements the uncertainty is dominated by the uncertainty in measuring the dimensions which is estimated to be $\pm$ 3%. The carrier concentration, n, was calculated directly from the measured Hall voltage knowing the current, field, and dimensions and assuming $r^{H} = 1$. The Hall voltage was measured with a current of 1mA DC and a magnetic field of 10 kG. It was found to be linearly dependent on the magnetic field strength over the range considered, i.e. 2.5 to 12.5 kG. The Hall mobility, μ_{H}, was calculated from the conductivity and carrier concentration results; it is "Hall" mobility as opposed to "drift" mobility in as much as r^{H} was taken as 1 in calculating n.

Figure 11 is a graph of the same quantities - σ, n, and μ_{H} - measured and calculated in the same manner for sample 016-1-b (see also Figure 9) in the temperature range between $20^{o}K$ and $90^{o}K$. As was mentioned in section 3.2.3 somewhat different electronics and magnet than

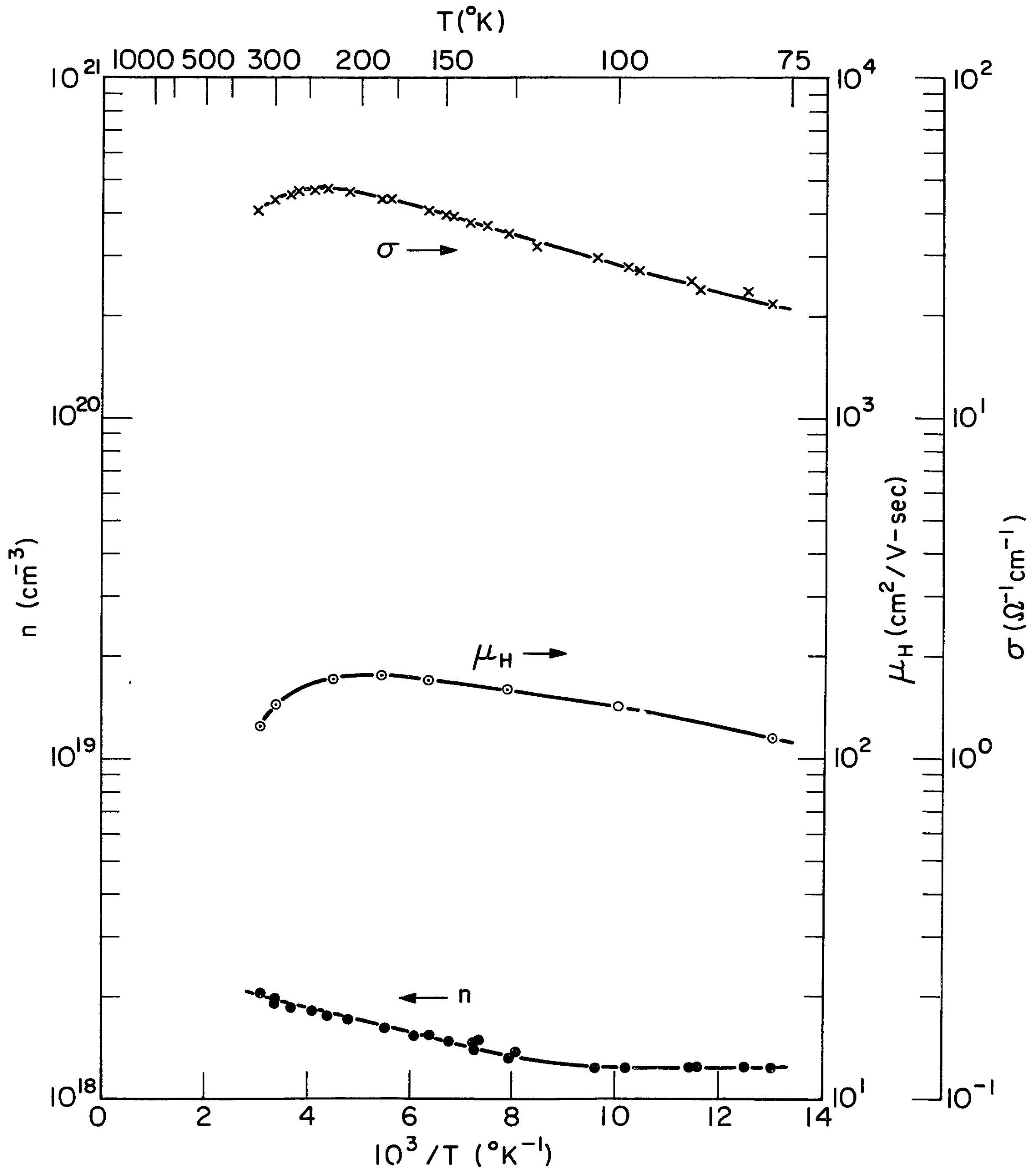

Figure 8 - n, μ_H, and σ for sample 008-8-b1 between 80°K and 300°K. n is 1.9 x 10^{18} cm^{-3} at 300°K; μ and σ are for the [011] direction.

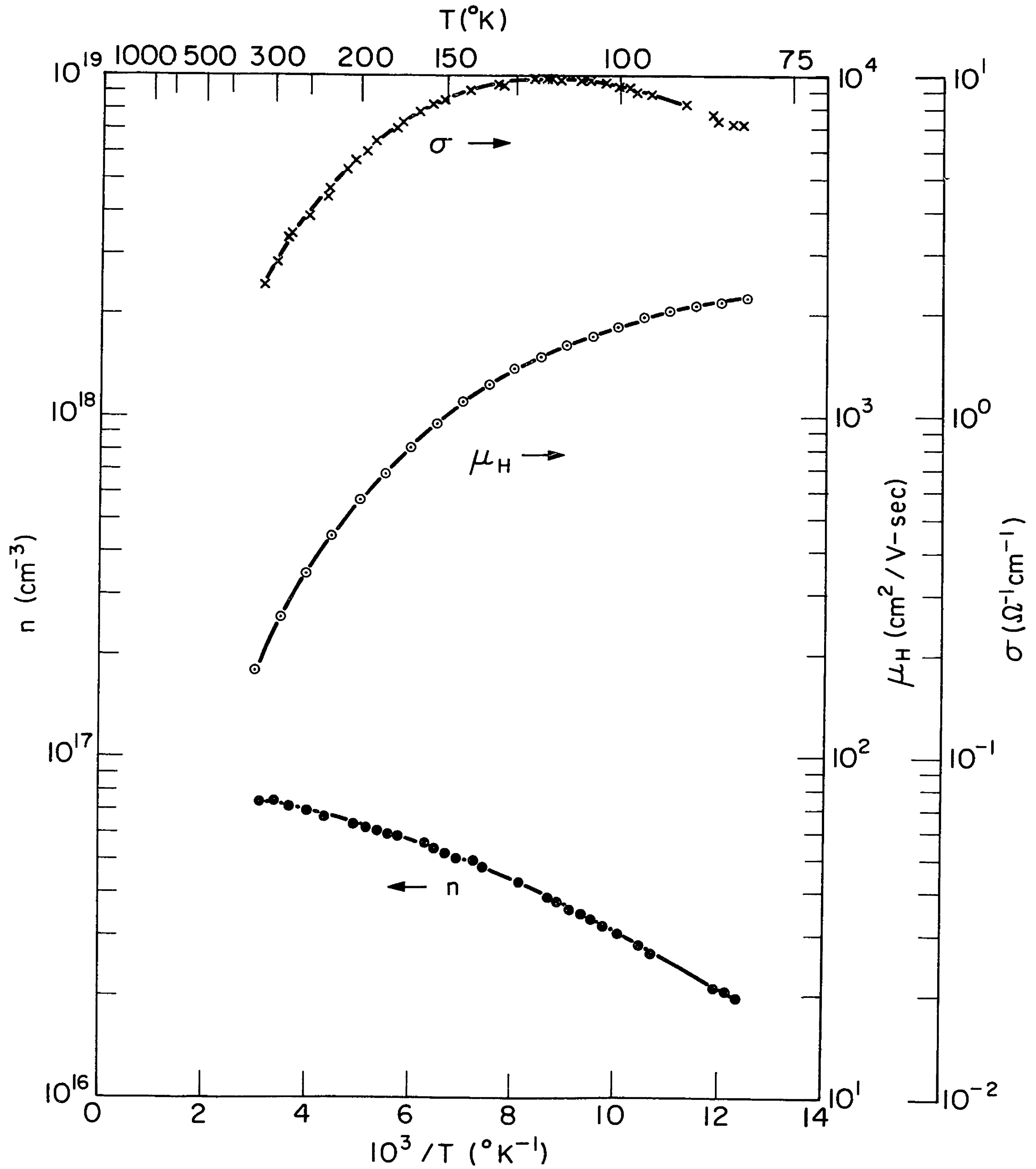

Figure 9 – n, μ_H, and σ for sample 008-9-b between 80°K and 300°K. n is 7.3×10^{16} cm^{-3} at 300°K; μ and σ are for the a-direction [100].

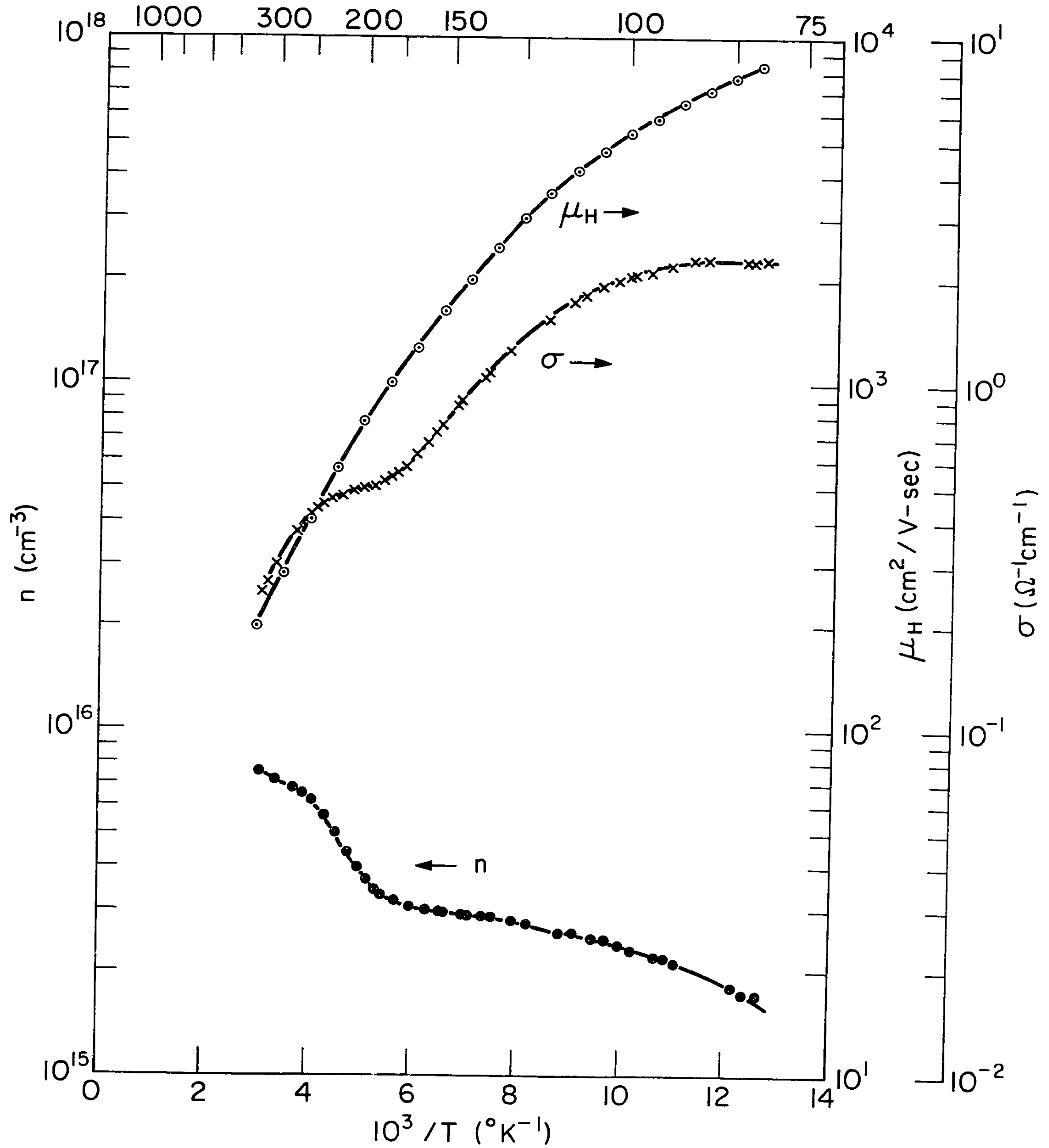

Figure 10 - n, μ_H, and σ for sample 016-1-b between 80°K and 300°K. n is 7.2×10^{15} cm^{-3} at 300°K; μ and σ are for the a-direction [100].

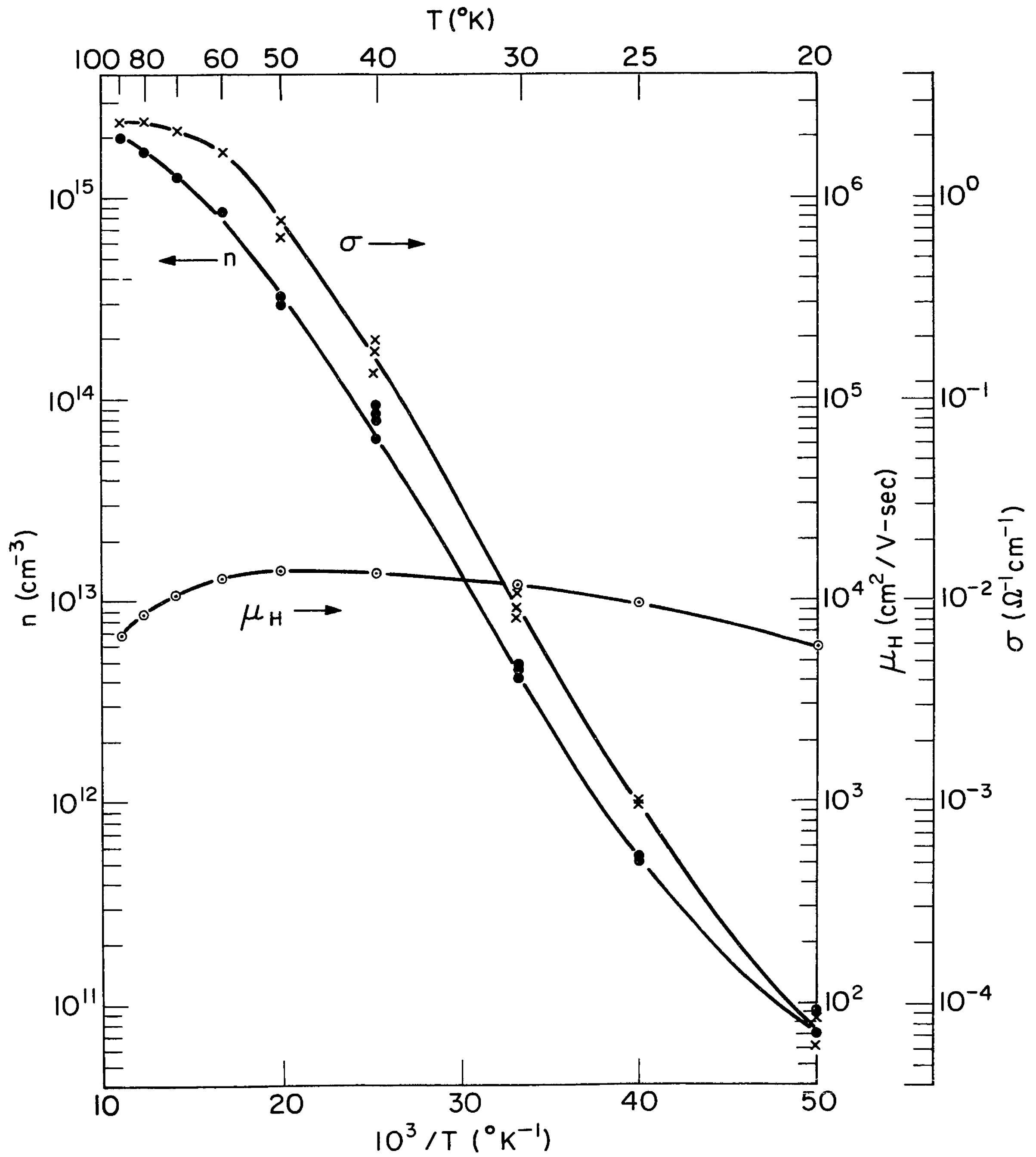

Figure 11 - n, μ_H, and σ for sample 016-1-b between 20°K and 80°K. See also Figure 10.

were used in the other measurements were used to measure below $80^{o}K$. Consequently, the magnetic field was only 5 kG and below $40^{o}K$ the current was less than 1mA because at these temperatures the sample resistance was so large that the source could not supply this current. The current was 10 μA at $20^{o}K$ and 100 μA at $25^{o}K$ and $35^{o}K$. Below $20^{o}K$ the sample resistance was so high that reliable measurements could not be made.

Sample 008-9-c was a bar cut from the same crystal slice as sample 008-9-b (in fact, from adjacent to it) and Figure 12 is a graph of σ, n, and μ_H found for this sample between $300^{o}K$ and $625^{o}K$. Also shown on the figure as dashed lines are the curves from sample 008-9-b taken from Figure 9. The same statements as made about the $80^{o}K$ to $300^{o}K$ measurements apply here with the additional observation that at room temperature the data from 008-9-b and 008-9-c agreed within the experimental uncertainty and that the data from 008-9-c has been adjusted so that they are in fact equal. This could be done, for example, by simply assuming that the actual resistivity probe spacing was ~10% larger than the measured separation.

It was observed in this and other samples studied that above $623^{o}K$ ($350^{o}C$) the sample carrier concentration, mobility, and resistivity changed irreversibly with time. Comparing room temperature measurements before and after making measurements above $623^{o}K$ ($350^{o}C$) to as high as $773^{o}K$ ($500^{o}C$) both in argon and in air the mobility was found to have decreased significantly. It is worthwhile noting that after growing, the crystals cool in air and are above $350^{o}C$ for several hours (see appendix C.3) before being harvested without apparently being adversely affected whereas in the samples studied here the resistivity change at $500^{o}C$, for

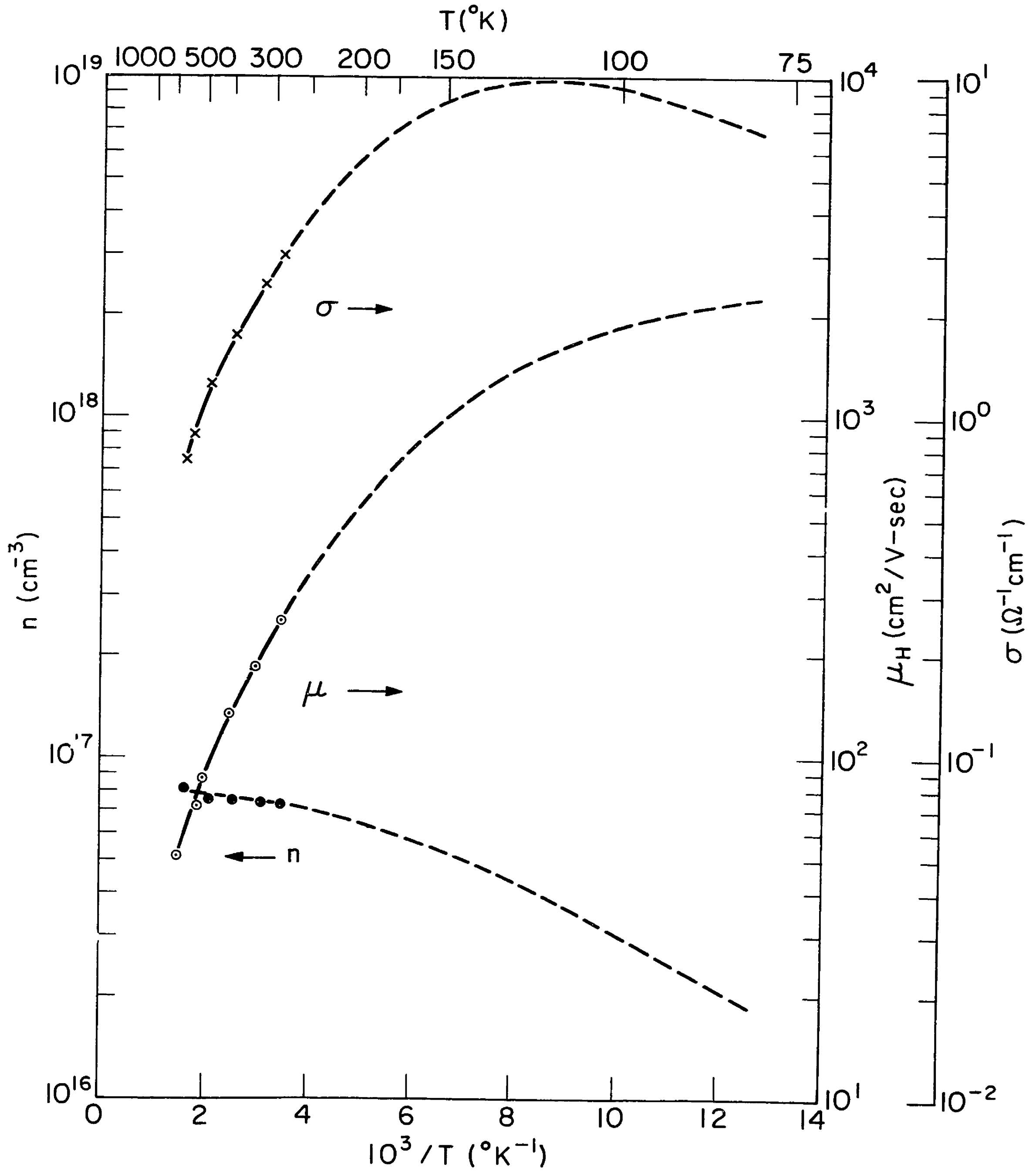

Figure 12 - n, μ_H, and σ for sample 008-9-c between 300°K and 625°K. The dashed lines are the curves for sample 008-9-b from Figure 9. Both samples were cut from the same crystal and the curves have been matched at 300°K.

example, was an observable drift occuring on a time scale of minutes. As was mentioned in section 3.2.3 a major problem with these measurements is the sample holder and insuring that it does not affect the sample. In light of this difficulty, the data which is discussed here is limited to 625°K at which temperature no change occurred and the data was reproducible. The other alternative of studying the high temperature electrical stability by making measurements only at room temperature and annealing the samples at 500°C, for example, in various atmospheres between measurements was not attempted. This would perhaps be the surest method of eliminating all but the influence of the surrounding atmosphere and once an "inert" atmosphere was found in this way a given holder could easily be considered by making measurements as a function of temperature using that sample holder in this atmosphere. The actual measurements are not so interesting, though, because the results can easily be anticipated by simply extending the curves of Figure 12; what is of more interest is learning the atmosphere and materials useful with stannic oxide at these elevated temperatures.

Before proceeding to the analysis of these experimental results in section 3.3 it is interesting to make some immediate observations about the data. The values of n, μ_H, and σ for these samples are summarized in Table 1. The room temperature carrier concentration is seen to span almost three orders of magnitude. Samples 008-8-b1, 008-9-b, and 008-9-c were cut from crystals intentionally doped with antimony; sample 016-1-6 was not intentionally doped although the possibility of doping from antimony remaining in the growing system exists. All of the samples were

Property / Sample	n (cm^{-3})		μ_H (cm^2/V-sec)		σ (Ω-cm)	
	80^oK	300^oK	80^oK	300^oK	80^oK	300^oK
008-8-b1	1.2×10^{18}	1.9×10^{18}	110	150	.047	.022
008-9-b,c	1.9×10^{16}	7.3×10^{16}	2200	240	0.17	0.36
016-1-b	1.6×10^{15}	7.2×10^{15}	8800	260	0.44	3.35

Table 1: Summary of n, μ_H, and σ at 80^oK and 300^oK for the samples of figures 8 thru 11.

---

n-type. The low temperature mobility increases dramatically as the crystal purity increases and the value of 8800 cm^2/V-sec at 80^oK in sample 016-1-b is the highest ever reported at this temperature for SnO_2 crystals. It is typical of crystals of this room temperature carrier concentration which is the lowest concentration material studied here.

To more readily consider the mobility results, the mobility data from all of the samples and temperatures presented in the previous figures has been combined on figure 13 in a log-log graph of Hall mobility versus temperature. Again the dependence on room temperature carrier concentration is evident. Having available only the results from sample 008-8-b1, which are typical of many of the stannic oxide mobility curves published in the literature, one would suspect that stannic oxide is a low-mobility semiconductor. That this is not true is clearly shown by samples 008-9-b and 016-1-b which both have much higher low temperature mobilities than any previously reported SnO_2. The mobility of the lowest concentration sample, 016-1-b, reaches a maximum, in fact, of 13,500 cm^2/V-sec at about 45^oK.

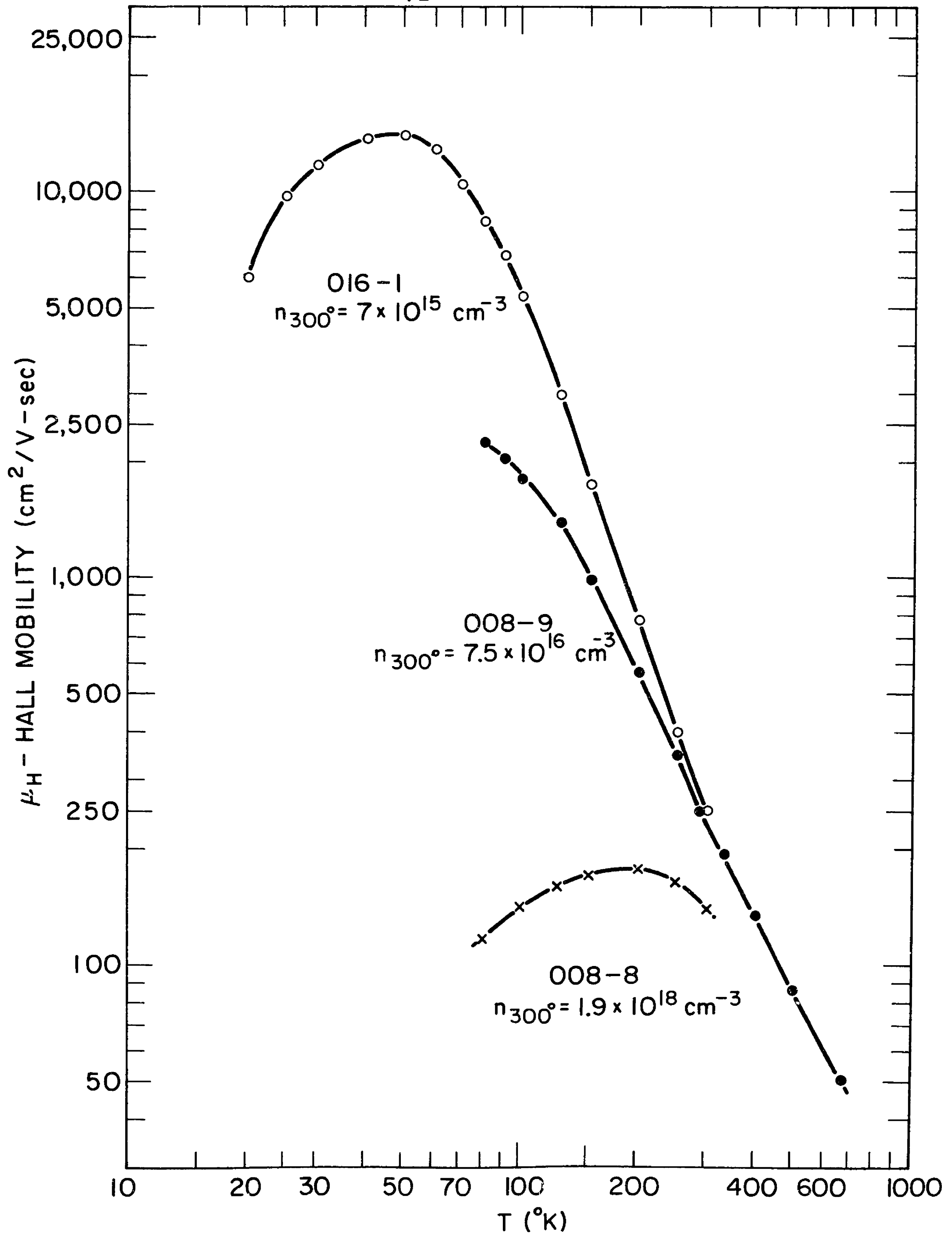

Figure 13 - Log-log composite of the Hall mobility curves from the previous figures. The temperature range of the data is from 20°K to 625°K and the peak mobility is 13,500 cm^2/V-sec. The quantity measured was the component of the mobility tensor in the a-direction.

It should be noted, finally, that all of the results that have been presented have been on low resistance samples. Crystals from Run 207 grown before any attempts were made to dope samples are, on the other hand, high resistance, undoped samples. Attempts at Hall measurements on these samples were unsuccessful, but a four terminal resistivity measurement was made on a sample from this run at 300°K. It was found that the resistivity was at least 6×10^{5} Ω-cm. No other electrical measurements were made on these crystals.

3.3 Analysis of Electrical Measurements Data

The analysis of the data from the Schottky barrier studies and the bulk property measurements will be presented here organized into four sub-sections. First, a quick review of the important points made and conclusions drawn thus far about the anisotropic nature of stannic oxide will be given in section 3.3.1. This will be followed in section 3.3.2 by the analysis of the carrier concentration as a function of temperature and in section 3.3.3 by a comparison of the net donor concentrations determined from Schottky barrier studies with those found from analyzing the measurements of the carrier concentration as a function of temperature. Finally, in section 3.3.4, the mobility versus temperature data will be analyzed. The implications of the conclusions reached in the analysis for electronic device applications of stannic oxide will be considered in section 3.4.

3.3.1 Review of Anisotropy Considerations

The anisotropy in the static dielectric constant has been taken into account in the Schottky barrier determinations of the net donor concentration by taking the tensor component perpendicular to the surface. In section 3.2.1 two anisotropies in the bulk electrical properties were considered: the anisotropy in the resistivity tensor, ρ_c/ρ_a, and the anisotropy in the Hall scattering coefficient, r_c^H/r_a^H. The latter anisotropy is expected to be small so that the approximation $r_a^H/r_c^H \simeq 1$ or $r_a^H \simeq r_c^H \triangleq r^H$ is justified in the present situation. The first anisotropy, i.e. in the resistivity, was found experimentally to be about 1.2 at 300°K, and at 77°K.

The samples for which data is presented - except for sample 008-8-[illegible] - were oriented with current along an a-axis so the conductivity measured, figure 8 thru 12, was ρ_a. Similarly, the mobility measured was the component of the Hall mobility tensor in the a-direction, μ_a^H. In sample 008-8 the current was in the (011) direction so the conductivity and mobility measured, figure 8, were the magnitudes of the projections of the corresponding tensors in that direction. At room temperature the experimentally measured conductivity in sample 008-8 is then

$$\sigma = \sqrt{(0.83\ \sigma_a)^2 + (0.56\ \sigma_c)^2}$$

$$= \sigma_a \sqrt{(0.83)^2 + (0.56/1.2)^2}$$

$$= 0.95\ \sigma_a$$

In the following analyses any additional consequences of the anisotropic structure of stannic oxide will be mentioned when they are pertinent.

3.3.2 Carrier Concentration vs. Temperature

As has been pointed out previously, when the carrier concentration was calculated from the Hall voltage a Hall scattering coefficient, r^H, of 1 has been used. Actually, r^H is not 1 and further may be a function of temperature so it is important to consider the consequences of assuming $r^H = 1$. It will be shown here that such an assumption is quite reasonable.

The coefficient r^H is determined primarily by the important conduction electron scattering mechanisms. It will be shown in section 3.3.4 where the mobility is discussed that three scattering mechanisms are important in stannic oxide: acoustic deformation potential scattering, polar optical

mode scattering, and ionized impurity scattering. For acoustic deformation potential scattering r^H is theoretically $3\pi/8$ (=1.18) at all temperatures while for polar optical mode scattering r^H is a function of temperature.[33,34] It is theoretically[33] about 1.07 at $\theta_D/T = 6$ ($\theta_D \simeq 1050^{\circ}K$ in stannic oxide, see section 3.3.4), increases with temperature to about 1.23 at $\theta_D/T \simeq 2$, and then drops again at still higher temperatures. In stannic oxide both acoustic deformation potential scattering and polar optical mode scattering are important in the range of $4.0 < \theta_D/T < 7$. Above this temperature range polar optical mode scattering dominates and here r^H for polar optical scattering lies within the limits[33] 1.18 ± 0.05. Below this range, and until impurity scattering becomes important, acoustic deformation potential scattering dominates and $r^H \simeq 1.18$. Where both polar optical and acoustic scattering are important, a detailed model of the scattering must be used to calculate r^H but it will lie between that for the two mechanisms and $r^H = 1.18 \pm 0.05$ is again a good approximation. Theoretically, a constant value for r^H at higher temperatures is then very reasonable within the experimentally required uncertainty. More care must be exercized at low temperatures where impurity scattering becomes important because here r^H is quite different from that for lattice scattering mechanisms. Theoretically for ionized impurity scattering[35] $r^H \lesssim 1.93$. The assumption of a constant r^H can thus be expected to breakdown when ionized impurity scattering becomes important and for that reason the analyses of n vs T are not extended to these temperatures.

Focusing now on the use of $r^H = 1$, two assumptions have been made. The first is that r^H is not a function of temperature; the second is that the magnitude of r^H is unity. We have shown that the first assumption

is reasonable within the experimental accuracy, and within the theoretical uncertainty in the description of the scattering mechanism in stannic oxide, i.e., in our analysis of μ. It is also well within accuracy of the theoretical fit of the data. To put this another way minor fluctuations in r^H as a function of temperature have automatically been corrected for by fitting a smooth curve to the measured data.

The second assumption, that $r^H = 1$, is justifiable because of the uncertainty introduced by the crystal anisotropy considerations discussed earlier and in light of the poor quantitative agreement found in experimental determinations[36] of r^H. For example, the predicted variation of r^H with temperature for polar optical scattering has been observed in GaAs experimentally[36] but with high and low extremes of 1.19 and 1.03 respectively so the agreement between theory and experiment is only qualitative. Lacking better experimental measurements of r^H any choice is a guess. The sole consequences of assuming that $r^H = 1$ are that the theoretically determined donor concentration, N_d, and the acceptor concentration, N_a, will be low by the factor $1/r_H$ and that the theoretically determined effective mass, m*, will be too low by a factor $(1/r_H)^{2/3}$. This last consequence arises because m* is calculated from the effective conduction band concentration, $N_c = (2\pi kTm^*/h^2)^{3/2}$, which like N_d and N_a is also low by a factor $1/r_H$.

The first samples considered were 008-9-b and 008-9-c because, looking at Figure 12, it appears that only one donor level is important in them (as opposed to two in sample 016-1-b, Figure 10) and the concentration is low enough so that the sample is not degenerate (as opposed to the situation in sample 008-8-1b, Figure 7). Under these conditions it

is possible to use a technique used by Hutson[37] to determine the conductivity effective mass, m^*; the donor ionization energy, E_d; the donor concentration, N_d; and the acceptor concentration, N_a. We start with the well-known equations[38] for n in a non-degenerate semiconductor with a single parabolic conduction band minimum and one donor level E_d below the conduction band edge, E_c, in the temperature region where the Fermi level, E_f, is such that $E_c - E_f >> kT$:

$$n = (2\pi kTm^*/h^2)^{3/2} \exp - (E_c - E_f)/kT \qquad (15a)$$

$$n = N_d/[1 + 2 \exp (E_d - E_f)/kT] - N_a \qquad (15b)$$

N_d and N_a are the donor and acceptor concentrations respectively and m^* is the conduction band effective mass. It has also been assumed that the valence band and the acceptor levels are so far removed from the conduction band that they are completely filled in the temperature range of interest. With an energy gap over 3.5 eV, this is a very good assumption.

If equation 15a is solved for $\exp E_f/kT$ and this expression is substituted in equation 15b one obtains, after a bit of algebraic manipulation, the following expression:

$$\frac{n\ (n + N_a)}{(N_d - N_a - n)T^{3/2}} = \left(\frac{2\pi km^*}{h^2}\right)^{3/2} \exp\ (-E_d/kT) \qquad (16)$$

To use this expression, values are chosen for N_d and N_a using the experimental curves as a guide to the first choices and the quantity on the left-hand side of the equation is evaluated for each experimentally measured n and T. The logarithm of this quantity is then plotted versus 1/T; a straight line should result. If it does not new choices of N_d

and N_a are made and the process is repeated until the plot is a straight line indicating that the proper values of N_d and N_a have been found. E_d is then determined from the slope of the line, and m* is calculated from the intercept at 1/T = 0.

The result of this type of an analysis for samples 008-9-b and 008-9-c yielded $E_d = 27.5 \pm 2.5$ meV, $m^* = 0.33 \pm 0.03\ m_e$, and $N_d - N_a = 8.0 \pm 0.2 \times 10^{16}$ cm^{-3}. If these values are now used to calculate n as a function of temperature directly the maximum difference between the theoretical and the experimental values of n is found to be < 10% giving an indication of the accuracy of the fit of the data.

In sample 016-1-b, see Figure 10, it appears that two donor levels are active and that the sample is not degenerate. For the analysis of n vs T here two donor levels were assumed - the deeper level taken to be a double donor - and the data was fit with the relations analogous to equations 15 when two donors are present:

$$n = (2\pi kTm^*/h^2)^{3/2} \exp - (E_c - E_f)/kT$$

$$n = N_{d_1}/[1 + g_1 \exp (E_{d_1} - E_f)kT]$$

$$+ N_{d_2}/[1 + g_2 \exp (E_{d_2} - E_f)/kT] - N_a \qquad (17)$$

The subscripts 1 and 2 refer to the shallower and deeper levels respectively. The shallow level was assumed again to be a single donor, $g_1 = 2$, while the best fit was obtained when the deeper level was assumed to be the first ionized state of a double donor, $g_2 = 1/2$. We first note that below 150°K only the shallow donor is important so the single donor analysis applied to sample 008-9 can also be used here to

determine N_{d1}, E_{d1}, N_a and m*. Using the data from 60°K to 150°K, it was found that $m^* = 0.35 \pm 0.03\ m_e$, $E_{d1} = 34 \pm 2$ meV, $N_{d1} = 3.05 \times 10^{15}\ cm^{-3}$, and $N_a \simeq 0$. With these values, trial-and-error selections of N_{d2} and E_{d2} were made until a close, < 10%, fit of the data was obtained over the entire temperature range, i.e. 60°K to 300°K. The final values obtained were $E_{d2} = 140$ meV and $N_{d2} = 4.8 \times 10^{15}\ cm^{-3}$.

The final sample, sample 008-8-b, is a much higher concentration sample than the others considered. It is, in fact, found to be degenerate below 150°K if m* is assumed to be $0.35\ m_e$. The picture is further complicated by the fact that ionized impurity scattering is important even at room temperature in this sample so the approximation $r^H \simeq 1$ is expected to break down. For the analyses here, the curve presented by Spenke[39] of $(E_c - E_f)/kT$ as a function of n/N_c, where $N_c = (2\pi kTm^*/h^2)^{3/2}$ is very useful. This curve applies to a semiconductor with a single parabolic conduction band minimum and covers the degenerate and non-degenerate regions. No satisfactory fit of the experimental data was found over the whole temperature range however; but it was possible to conclude from the slope of the curve near room temperature that the donor level lies 10 to 15 meV below the conduction band edge.

The shallower donor in the samples is probably due to the same impurity, antimony. The decrease of the shallow donor ionization energy, E_d, found as the donor concentration, N_d, increases in the samples, is anticipated and is similar to what is found in other semiconductors. In silicon[40] and also for a deep level in stannic oxide,[5] a function of the form $E_d = E_o - aN_d^{1/3}$ has been used to describe this dependence. Fitting the present rather limited data to such a function one finds $E_o = 37$ meV

and $a = 2 \times 10^{-5}$ cm meV. A measurement by Nagasawa, et al, of $E_d \simeq 24 \pm 4$ meV in an antimony doped sample with $N_d = 1.75 \pm 0.15 \times 10^{17}$ cm^{-3} is also consistent with this choice of parameters. It now is interesting to note that a simple hydrogenic model for the donor with an effective mass of $0.35\ m_e$ and $\varepsilon_s = 12.0$ yields an ionization energy of 33 meV in reasonable agreement with this E_o. With $m^* = 0.39\ m_e$, the calculated ionization energy is exactly 37 meV.

The deeper donor seen in 016-1 is perhaps due to oxygen vacancies; the ionization energy of 140 meV is consistent with Marley, et al's[5] findings on SnO_2 crystals annealed in an oxygen atmosphere. The fact that the best fit of the data was obtained when this level was assumed to be the first ionized state of a double donor further supports this identification.

The effective mass that has been found consistently in these analyses of n vs T is $0.35\ m_e$. As was noted previously if $r_H = 1.18$ instead of unity as assumed, this effective mass would be larger, $0.39\ m_e$; that is, $0.35 \times 1.18^{2/3} \simeq 0.39$. There are indications from the donor ionization energy, as mentioned, and in the analysis of mobility to follow, that this larger value is indeed more correct.

3.3.3 Net Donor Concentrations - Hall vs Schottky

Two independent determinations of the net donor concentrations in the samples have been made, the first from analysis of the capacitance-voltage characteristics of Schottky barriers and the second from the analysis of the carrier concentration as a function of temperature. The results of these two measurements on the samples reported are

summarized in Table 2 below.

Sample	Schottky Barriers	Hall Effect
008-8-b1	1.5×10^{18} cm^{-3}	> 1.9×10^{18} cm^{-3}
008-9-b,c	7.2×10^{16} cm^{-3}	8.0×10^{16} cm^{-3}
016-1-b	7.1×10^{15} cm^{-3}	7.8×10^{15} cm^{-3}

Table 2 - Net Donor Concentrations from Schottky barrier and Hall effect measurements

The agreement between the two determinations is found to be quite close and within the experimental uncertainties. It is thus concluded that the assumption made that r^H is of order one is justified and further that shallow trapping does not play a significant role in these crystals. That is, that all carriers excited to the conduction band from donors do indeed contribute to conduction.

3.3.4 Analysis of Hall Mobility Data

To analyze the Hall mobility data and to thus understand what the important carrier scattering mechanisms are we must first consider what scattering mechanisms are possible. These can then be individually evaluated and their role in the complete picture investigated.

Electrons can be scattered by displacements of the crystal lattice (phonons), by impurities, and by other electrons. Scattering due to the crystal lattice, i.e., due to phonons, takes four different forms: polar optical mode scattering, non-polar optical mode scattering, polar acoustic mode scattering, and non-polar acoustic mode scattering. The latter two

are also known as acoustic piezoelectric scattering and acoustic deformation potential scattering, respectively. Scattering due to defects must be qualified as that due to neutral defects and impurities, and that due to ionized impurities. We will consider these mechanisms in the order they have been listed after making several qualifying observations. First, electron-electron scattering will not be considered in this discussion. Second, it will be assumed that the conduction band of stannic oxide has a single parabolic minimum in the conduction band and, consequently, no inter-band or inter-valley scattering will be considered either. Finally, the mobility data being analyzed, Figure 13, is for the Hall mobility tensor component in the a-direction. From our measurements of the anisotropy at $77^{o}K$ and $300^{o}K$ we know that the tensor component in the c-direction will be very similar.

The rapid decrease of the mobility as the temperature increases above several hundred degrees Kelvin does not fit a simple power law dependence on temperature but it is more nearly exponential. This suggests that polar optical mode scattering is playing an important role in the conduction processes here. To quantitatively consider this possibility we must first look at how strongly the electrons are coupled to the polar optical phonon modes (note that it is the longitudinal modes which interact with the electrons here). Eagles[41] has discussed the extension of the normal isotropic polaron theory, the theory of coupled electrons and polar longitudinal optical phonons, to the anisotropic rutile crystal structure. This work will be used extensively in the following discussion along with the recent work by Van Daal[21-22] and Summitt[42] on the optical phonon modes in stannic oxide. We will follow Eagles' notation except that we

will use i (=a or c) for the direction index and γ (=1,2, or 3) for the mode index.

In stannic oxide there are three longitudinal polar optical modes with polarization perpendicular to the c-direction, and one such mode with polarization parallel to the c-direction. From Van Daal[22] the frequencies of these modes, $\omega_{\gamma i}$, are: $\omega_{a1} = 5.15 \times 10^{13}$ sec^{-1} (390^0K), $\omega_{a2} = 6.81 \times 10^{13}$ sec^{-1} (515^oK), $\omega_{a3} = 14.2 \times 10^{13}$ sec^{-1} (1080^oK), and $\omega_{c3} = 13.0 \times 10^{13}$ sec^{-1} (990^oK). The quantity in parenthesis is the characteristic temperature of the mode, θ, calculated from $\theta = \hbar\omega/k$. The general results of Eagles indicate that any polar optical mode scattering in stannic oxide can be expected to be dominated by the highest frequency modes as it is in rutile[41]. Thus Van Daal[21] and Wright[11] have both analyzed their mobility data assuming an iostropic theory with $\theta = 1050^o$K. It is possible though to use the recent results of Summitt[42] to actually evaluate the contribution to the mobility of each mode following Eagles; as will be shown, the lower frequency modes are more important in stannic oxide than they are in rutile and they do contribute moderately to the mobility particularly below room temperature.

The measure of the strength of the electron-phonon interaction for each mode is given by the polaron coupling constant, α, which is[41]

$$\alpha_\gamma = \left(\frac{m_b}{m_e}\right)^{1/2} \left(\frac{E_H}{\hbar\omega_\gamma}\right)^{1/2} \left\langle f_{\gamma i}^2 \left(\frac{1}{\varepsilon_{\infty i}} - \frac{1}{\varepsilon_{si}}\right)\right\rangle_{av} \qquad (18)$$

The average is a simple average over i, i.e., over the three axial directions. E_H is the Rydberg, 13.6 eV; m_b is the rigid-lattice or "bare" electron effective mass; $\varepsilon_{\infty i}$ and ε_{si} are the optical and static dielectric

constant, i-direction; and $f^2_{\gamma i}$ is a relative measure of how polar the modes are. In the c-direction there is only one mode so $f^2_{1c} = f^2_{2c} = 0$ and $f^2_{3c} = 1$. In the a-directions we can calculate $f^2_{\gamma i}$ from the polarization, $p_{\gamma i}$, and frequency, $\omega\gamma i$, of each of the three modes

$$f^2_{\gamma i} = (p^2_{\gamma i}/ \omega^2_{\gamma i}) / \sum_{\gamma=1}^{3} (p^2_{\gamma i}/ \omega^2_{\gamma i}) \tag{19}$$

using Summitt's values for $p^2_{\gamma i}$. We can then calculate $\alpha_\gamma(m_e/m_b)^{1/2}$ after first calculating the bracketed average term using $\varepsilon_{\infty a} = 3.785$ and $\varepsilon_{\infty c} = 4.175$,[14] and $\varepsilon_{sa} = 14$ and $\varepsilon_{sc} = 9$[22]. The results of these calculations are listed in Table 3 below.

γ	$f^2_{\gamma a}$	$\alpha_\gamma(m_e/m_b)^{1/2}$	α_γ
1	0.017	0.067	0.039
2	0.392	0.132	0.076
3	0.591	1.43	0.825

Table 3 - Summary of parameters in polar optical mode scattering theory.

The mass of interest in finally arriving at α is the effective mass the electrons would have if the lattice were rigid. It is a theoretical quantity only, because any low frequency experimental measurement is of the effective mass of the coupled electron and phonon, i.e., of the polaron, and this polaron effective mass, m_p, is related to the rigid lattice, or "bare", effective mass, m_b, through α_γ as[41]

$$m_p = m_b \{ 1 + (\sum_\gamma \alpha_\gamma)/6 \} \tag{20}$$

If we anticipate a $\sum_\gamma \alpha_\gamma \simeq 1$ and work backwards from our previously measured effective mass of 0.39 m_e, which is m_p, we find $m_b = 0.33\ m_e$. This

value has been used to calculate α_γ which is listed in the table. The anisotropy of the effective masses has not been considered in light of the little information available on this aspect of stannic oxide. We only know from our measurement of the anisotropy of the conductivity that it is not large and, from Eagles[41], should not be important here. The conduction band effective mass used above involves an average over directions that should be quite adequate for this discussion.

Looking at the values of α_γ found we see that indeed the strongest coupling is to the highest frequency mode, that is, α_3 is much larger than the others as anticpiated. The total mobility is now the sum of the contributions of each mode added as inverses in the normal way[41]

$$\mu = \left(\sum_\gamma 1/\mu_\gamma \right)^{-1} \qquad (21)$$

To calculate these mobilities we will use the intermediate coupling theory of Lee, Low, and Pines[43]. Their expression for the drift mobility due to polar optical mode scattering is, with a mode index added,

$$\mu^d_{IC_\gamma} = \frac{e}{2\alpha_\gamma \omega_\gamma m_b} \cdot \frac{f(\alpha_\gamma)}{\{1 + (\alpha_\gamma/6)\}^3} \left(e^{\hbar\omega_\gamma/kT} - 1 \right) \qquad (22)$$

The only new factor in this expression is $f(\alpha_\gamma)$, a function of α which is evaluated using the graph in reference 34. From that curve $f(\alpha_1) \simeq f(\alpha_2) \simeq 1$ and $f(\alpha_3) = 1.02$. The three mobility factors to be used in equation 21 to obtain the total polar optical mode mobility are then found to be:

$$\mu^d_{IC_1} = 1300(e^{390/T} - 1) \quad cm^2/V\text{-sec}$$

$$\mu^d_{IC_2} = 495(e^{515/T} - 1) \quad cm^2/V\text{-sec}$$

$$\mu^d_{IC_3} = 15.8(e^{1080/T} - 1) \quad cm^2/V\text{-sec}$$

Again it is evident that the highest frequency mode is dominant. If we evaluate these expressions and combine them using equation 21 we obtain the curve labeled μ_{IC} on figure 14. A value of $r^H = 1.18$ was used to convert from the theoretical drift mobility to the Hall mobility (which is higher). Also shown in this figure are the experimentally measured mobility curves from Figure 13. The qualitative agreement with the data at high temperatures is excellent and indicates that polar optical scattering is indeed the dominant scattering mechanism above 250°K in pure samples. The good quantitative agreement also indicates that the value of m_b used is reasonable. This is the only possibly adjustable quantity in the theoretical expressions as all other quantities have been measured by independent experiments and were found in the literature. It is important to note, though, that the calculation of α is sensitive to the dielectric constants and in light of the uncertainties in these quantities any attempt at further refining the value of m_b is not justified.

Looking at Figure 14 it is clear that even in the purest samples there is an additional contribution to the mobility from some mechanism besides polar optical mode scattering that is important particularly below 250°K. Recalling the discussion of possible scattering mechanisms given earlier we will first consider other lattice scattering mechanisms. One possibility is non-polar optical mode scattering. It is expected though that at all but very high electric fields this type of scattering is dominated by the polar optical mode scattering[44] and will not be important. We can also eliminate polar acoustic, or piezoelectric scattering, because stannic oxide crystallizes in a centrosymmetric

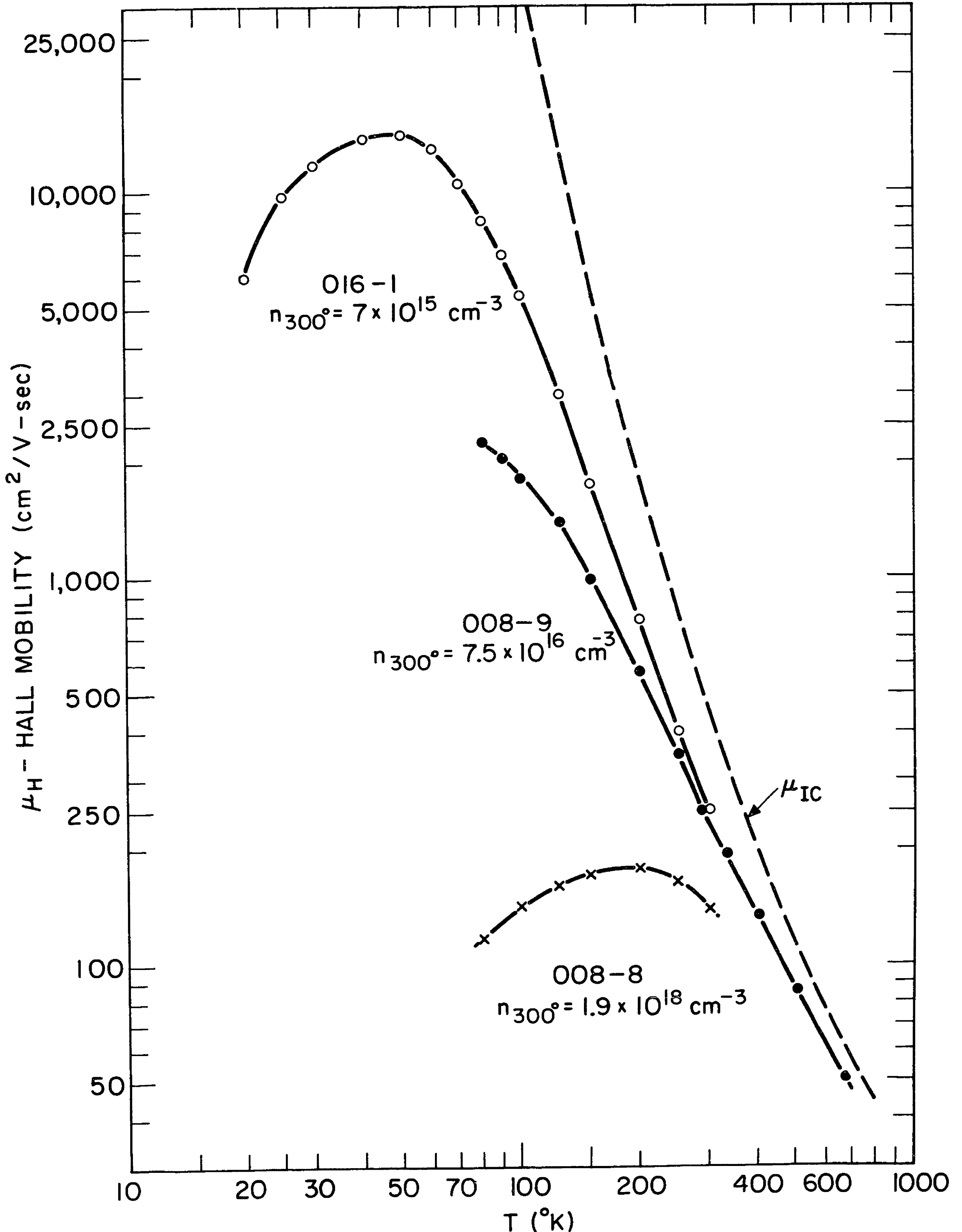

Figure 14 - Theoretical Hall mobility for polar optical mode scattering shown with the experimental curves. The characteristic temperature of the dominant LO mode is 1080°K.

structure, see Figure 1, and therefore shows no piezoelectric effect. The remaining possible mechanism is non-polar acoustic, or acoustic deformation potential, scattering. We will consider this now.

We will use the expression of Bardeen and Schokley[45] for acoustic deformation potential scattering

$$\mu_{AD}^{d} = \frac{2(2\pi)}{3} \cdot \frac{e\, d\, v_s^{2}\, \hbar^{4}}{E_{IC}^{2}\, (m_p)^{5/2}\, (kT)^{3/2}} \qquad (23)$$

In this expression d is the density; v_s the velocity of sound; and E_{IC} the deformation potential for dilating strain for the conduction band. There is enough uncertainty in these parameters to make anisotropy modifications unimportant. The main features of equation 23 would remain in an anisotropic theory; they are the $T^{-3/2}$ temperature dependence and the strong dependence on the effective mass (m_p is the pertinent mass here). We can anticipate a contribution from this type of scattering because stannic oxide has a rather large effective mass and, looking at Figure 14, the temperature dependence seems quite reasonable.

Using $m_p = 0.39\ m_e$, $d = 6.99 \times 10^{3}\ kg/m^{3}$, and $v_s = 4 \times 10^{3}$ m/sec, in equation 23, we find

$$\mu_{AD}^{d} = 4.8 \times 10^{8} / (E_{IC}^{2}\ T^{3/2})\ \ cm^{2}/V\text{-}sec$$

If E_{IC} is now assumed to equal 8.0 eV and $r^{H} = 1.18$ is used to convert to Hall mobility, we obtain the dashed curve labeled μ_{DA} in Figure 15. No measurement either direct or indirect[45] of E_{IC} is available for stannic oxide, but it is found to be several electron volts in common semiconductors,[45] so that this 8eV is not unreasonable.

The solid curve in Figure 15 labeled μ_T is the total Hall mobility

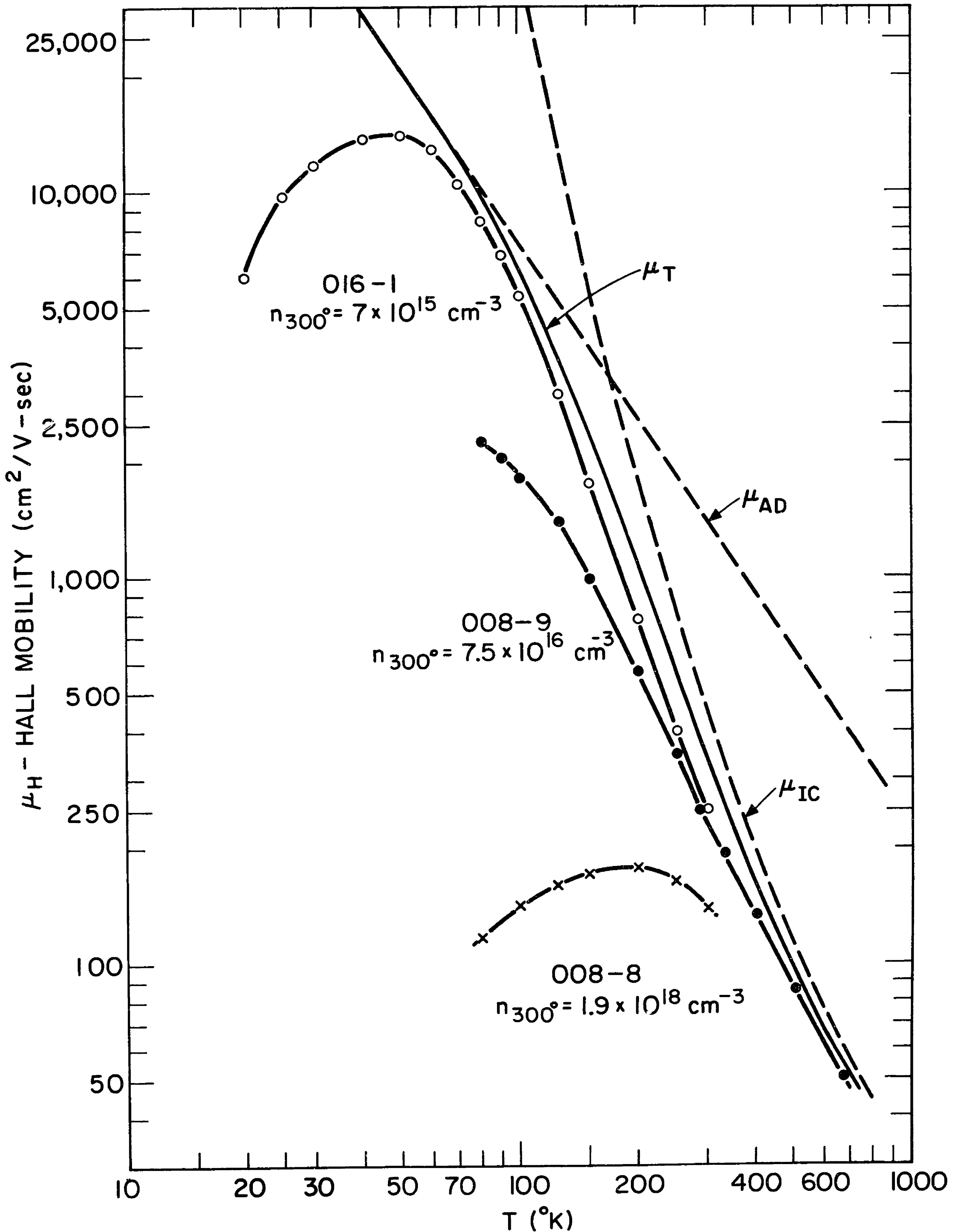

Figure 15 - Total combined Hall mobility for acoustic deformation potential scattering and polar optical mode scattering.

contribution of the two mechanisms discussed above calculated using simply:

$$\mu_T = (\mu_{IC}^{-1} + \mu_{AD}^{-1})^{-1} \tag{24}$$

The curve is in excellent qualitative agreement with the data from the lowest concentration sample and implies that the two scattering mechanisms together play an important role in conduction in stannic oxide. It would be very much of interest to have an independent measurement of E_{IC} for comparison with the value assumed here as this is the major unknown and the biggest limitation on a quantitative evaluation.

Having explained the Hall mobility in the purest sample as being due to polar optical mode scattering and acoustic deformation potential scattering we can now consider the lower mobilities in higher concentration samples. What is likely to be important here is ionized impurity scattering. The other possibility, scattering due to neutral impurities, is not a function of temperature[33] and does not appear to be the important mechanism in these samples. To investigate the contribution due to ionized impurity scattering we will use the Brooks-Herring[47] formula:

$$\mu_{I_d} = \frac{2^{7/2}}{\pi^{3/2}} \cdot \frac{(4\pi\varepsilon_o\varepsilon_s)^2 \, (kT)^{3/2}}{m_p^{1/2} \, e^3 \, N_I} \cdot \frac{1}{\ln (1 + b) - b/(1 + b)} \tag{25}$$

with

$$b = \frac{24\varepsilon_o\varepsilon_s \, m^* \, k^2T^2}{n\hbar^2 e^2}$$

In this expression N_I is the number of ionized impurities and n the density of free carriers. We will take account of the anisotropy of stannic oxide by using the dielectric constant in the a-direction; and we will use the

polaron effective mass, $m_p = 0.39\ m_e$.

We will also introduce the additional refinement of using Blatt's[35] expression for the Hall scattering coefficient, r^H, for ionized impurity scattering. This factor, often taken to be 1.93, is in fact a function of temperature and the carrier concentration; when it is greater than unity it is given by:

$$r_H = 1.93\ [\ln\ (b - 1)\ /\ \ln\ (3b/2 - 1)]^2 \qquad (26)$$

In sample 008-8 with $\varepsilon_s = 14$, $m_p = 0.39\ m_e$, and $n = N_I = 2 \times 10^{18}\ cm^{-3}$ at 300°K we calculate an ionized impurity drift mobility of 325 cm^2/V-sec. The parameter b is small so $r_H \simeq 1$ and the Hall mobility contribution is also 325 cm^2/V-sec. When combined with the polar optical mode scattering and acoustic deformation potential scattering total of 350 cm^2/V-sec, the total mobility is found to be 170 cm^2/V-sec in good agreement with the measured value of 150 cm^2/V-sec. Note that the mobilities have been added as inverses as in Equation 24, an approximation which is adequate for the present discussion.[35]

Sample 008-8-b1 is degenerate at lower temperatures so is hard to treat but the ionized impurity contribution at 80°K can be calculated for sample 008-9. Here, using $n = 1.9 \times 10^{16}\ cm^{-3}$ and $N_i = 2.3 \times 10^{16}\ cm^{-3}$ at 80°K, an ionized impurity drift mobility of 2,200 cm^2/V-sec is calculated. The Hall coefficient, r_H, is 1.68 (b = 230) so the impurity scattering Hall mobility contribution is 3,700 cm^2/V-sec which with the theoretical polar optical mode and deformation potential total of 10,000 cm^2/V-sec yields a total Hall mobility of 2,700 cm^2/V-sec again in good agreement with the measured value of 2,200 cm^2/V-sec. The ionized impurity Hall mobility contribution in sample 016-1 is found to be about 40,000 cm^2/V-sec

at 80°K which demonstrates that it is much less important in this sample as was suggested previously.

Summarizing the analysis of the Hall mobility data, it has been found that in the lowest concentration stannic oxide samples studied the mobility is dominated by acoustic deformation potential scattering below 250°K and above 250°K by polar optical mode scattering with a characteristic temperature in the a-direction of 1080°K. At very low temperatures the mobility is dominated by ionized impurity scattering in all of the samples. The quantitative and qualitative agreement between theory and experiment is excellent particularly when it is recalled that only one "adjustable" parameter was involved, that being E_{IC} for the calculation of the acoustic deformation potential scattering. The effective mass used, 0.39 m_e, was obtained from the analysis of the carrier concentration data and was used consistently in the calculations for each of the three scattering mechanisms considered.

3.4 Implications of Results for Device Applications of SnO_2

The motivation for studying stannic oxide, SnO_2, in the present work was obtaining a better understanding of this wide band-gap semiconductor and its potential for use in active electronic devices. Let us then summarize the results of the electrical studies in the context of stannic oxide's device potential.

Only n-type conduction has been observed to date in stannic oxide so one must think in terms of a field-effect device. Schottky barriers have been produced that would be suitable for use as the gate electrode in such a field effect transistor, in particular, an FET operating in the depletion mode. It has been further demonstrated through barrier capacitance measurements made as the bias voltage was varied that surface states and trapping do not interfere with the surface depletion. The net donor concentration is similar to the carrier concentration. With the low concentration crystals which have been produced in this study depletion layers several microns deep are obtained with a bias of 4 to 5 volts.

Because low carrier concentrations are necessary in these devices so that useful depletion depth, 1-10 microns, is obtained with reasonable gate voltages, 1-10 volts, the mobility findings are particularly significant as they indicate that at low concentrations stannic oxide will still have finite conductivities. Our measurement of mobilities over 8000 cm^2/V-sec at 80^oK dispells the belief that stannic oxide is a low mobility semiconductor. The limitation on the mobility at low temperature, below 250^oK, is acoustic deformation potential scattering which is important because of the large electron effective mass, 0.39 m_e. This mechanism was evaluated assuming a deformation potential, E_{IC}, of 8 eV. but until

an independent measure of this parameter is made a realistic estimate of the maximum low temperature mobility cannot be made. At high temperatures, above 250°K, the mobility is limited by polar optical mode scattering with a characteristic temperature of ~ 1050°K. The high characteristic temperature means that the mobility is a very strong function of temperature above 250°K as Figure 13 illustrates. Because the carrier concentration is not varying much with temperature in this region, the conductivity shows the same temperature dependence as the mobility; that is, it decreases exponentially. This fact is likely to be one source of difficulty in using stannic oxide at high temperatures as the conductivity both decreases at high temperatures and is a strong function of temperature thus being sensitive to the ambient. More important though will be the finding of materials and atmospheres for use with stannic oxide at elevated temperatures.

Electronic doping has been found to be readily achieved in this semiconductor. The shallow donor level, ~ 35 meV, due to antimony and a deeper donor level, ~ 140 meV, ascribed to oxygen vacancies, have both been observed.

In total, stannic oxide has been found to be a conventional semisonductor in the sense that all of the analysis has been adequately handled by assuming broad band conduction in a conduction band with a single parabolic minimum. It further has been shown to have high mobility inspite of its wide band-gap of over 3.5 eV. Finally, the effects of its anisotropic crystal structure on the conduction processes were found to be small.

4 Summary of Results ana Proposals for Future Work

In the present study high quality stannic oxide crystals have been grown and have been studied electrically. The primary result of this work is that stannic oxide no longer ranks as a poorly understood, low mobility material but instead must be considered as an exciting wide band-gap semiconductor - liquid nitrogen Hall mobilities over 8500 cm^2/V-sec - with excellent potential for active device applications.

A low pressure, inert carrier-gas free, chemical vapor deposition growth technique utilizing chlorine transport was used to grow the stannic oxide crystals. The system developed has advantages over conventional vapor growth methods in the degree of control realized over the growth reaction, in the ease with which the quantities of reactants are monitored and controlled, in the purifying nature of the chlorine transport process, in the elimination of the inert carrier gas, and in the ease with which electronic dopants are introduced. The crystals grown have had higher purity than any previously grown stannic oxide and show a high level of crystalline perfection. Undoped crystals, antimony doped crystals, and seeded crystals have been grown. Most importantly Hall mobilities over 8500 cm^2/V-sec at 80^oK have been measured in lightly doped crystals vividly demonstrating that stannic oxide is not a low mobility semiconductor.

A technique of fabricating good Schottky barriers on stannic oxide has been perfected and used to determine the net donor concentrations of samples. A very valuable tool developed for the study of new materials is the use of small area barriers to profile donor concentration variations in crystals. This must be done to select homogeneous samples for bulk

property measurements. The agreement between the net donor concentration measured with Schottky barriers and that determined from Hall measurements shows that shallow trapping is not important in these crystals.

Measurements of carrier concentration, Hall mobility, and conductivity were made between 20^oK and 625^oK, and it was found that conventional semiconductor statistics for a single parabolic minimum in the conduction band at $k = 0$, with $m_b = 0.33\ m_e$, could be used in the analyses of non-degenerate samples. The coupling to polar LO phonons, i.e. polarons, was included. The most important alteration of the theories necessary is the inclusion of the crystal anisotropy and these anisotropy effects were found to be small. A donor level due to antimony was found at ~35 meV below the conduction band; and another, ascribed to oxygen vacancies, was found ~140 meV below the band edge.

Polar optical mode scattering with a characteristic temperature of 1080^oK was found to dominate the mobility above 250^oK; acoustic deformation potential scattering with $E_{IC} = 8$ eV is dominant below 250^oK. In all samples ionized impurity scattering plays a role at low temperatures. The agreement found between the theoretically claculated Hall mobility and the experimental data was excellent.

With high quality, high purity crystals of stannic oxide to study, it has been possible to analyze processes fundamental to electron conduction in stannic oxide. Using samples doped from $8 \times 10^{15}\ cm^{-3}$ to $2 \times 10^{18}\ cm^{-3}$ it has been possible to observe various scattering mechanisms in stannic oxide and to determine a polaron effective mass which is consistent with all of the measurements made. As the sample quality improves as it has here, the analyses can become more sophisticated and it becomes possible,

with good crystals, to consider making realistic measurements of many material parameters which are at present not accurately known. It would be interesting, for example, to measure the effective mass more directly, perhaps by cyclotron resonance, for comparison with the value found here. Measurements at optical frequencies are expected to be able to distinguish between the bare and polaron effective masses and would also be most interesting to try on SnO_2. A measurement of E_{IC} would be valuable for estimating the real maximum low temperature mobility in stannic oxide. A more thorough study of the resistivity anisotropy ratio, and the Hall coefficient anisotropy ratio, as a function of temperature might be quite instructive.

The device potential of stannic oxide seems obvious. With suitable carrier concentration crystals and good Schottky barriers and low resistance contacts all available, a field effect transistor seems well within reason. Before a device can operate above $350^{o}K$, however, the proper materials and ambient atmosphere for use with stannic oxide at these temperatures must be found.

Work on the growth of crystals could receive still more attention. New dopants, better seeded growth, growth on substrates - all would be valuable additions to the system and interesting to consider. A growth with very high purity starting materials should be made.

The entire spectrum of optical properties and characteristics has hardly been considered. With a source of high quality crystals, such studies are an obvious endeavor. The results of an initial investigation of the optical absorption edge in some undoped crystals - T. Credelle's Masters Thesis, MIT, September, 1970 - indicate that there are very

interesting features of the shape and temperature dependence of the absorption edge which deserve more attention. Luminescence has also been seen in some samples under ultraviolet illumination and has not been explained or even characterized.

As a wide band-gap, now high mobility semiconductor available in single crystal form and about which much is still unknown, stannic oxide is an excellent material for continued study. It is a semiconductor with potential for device applications and it is an anisotropic material of interest for basic physics investigations. The present study has produced a source of quality crystals and demonstrated stannic oxide's exciting potentials; it should serve as a solid foundation for future studies.

Appendix A - Stannic Oxide Parameters

The following table has been copied directly from IV-VI Semiconducting Compounds Data Tables compiled by M. Neuberger and published by the Electronics Properties Information Center, Hughes Aircraft Company, Culver City, California, October, 1969. The values listed should be used with a degree of caution both because of errors in the table and because many have been measured only by one group and/or in poor quality material. In particular:

1. The colour is clear, water-white.
2. The melting point is much greater than 1127°C. It is likely that it is greater than 2000°C.
3. The electrical resistivity and temperature coefficient have little meaning. The footnote has even less.
4. The mobility values are low. We have measured 8800 cm^2/V-sec at 80°K and 250 cm^2/V-sec at 300°K.
5. The Debye temperature, which strictly is a misnomer in a rutile structure crystal, is more nearly 1050°K.
6. The nature of the energy gap is an open question. Nagasawa, et al.[17,19] indicate direct; others indirect.[3,13] Note also that Summitt and Borrelli measured single crystals.
7. The effective mass is also an open question (see text).
8. The phonon spectrum has been measured in more detail than is indicated here.[19,42]

TIN DIOXIDE

Property	Symbol	Value	Units	Notes	Temp. (°K)	References
Physical Properties						
Formula		SnO_2				
Molecular Weight		150.7				
Density		6.99	g/cm^3			Donnay
Mineral Name		Cassiterite				Dana
Colour		yellow-red to brown-black		transparent when light		
Hardness		6-7	Mohs	brittle		
Lustre		adamantine to metallic				
Symmetry		Tetragonal (C4)				Donnay
Space Group		P4/mnm Z2				
Lattice Parameters	a_o	4.738	Å			Clendenen and Drickamer
	c_o	3.188				
	O-O	2.54				Wyckoff p. 252
Melting Point		1127	°C			Hansen
Sublimation Point		1800-1900				
Specific Heat, molar		3.1	gr cal		72	Millar
	- -	11.1			115.5	
		12.4			289.4	
Debye Temperature		500	°K		>300	Marley and Dockerty, Wright

Property	Symbol	Value			Units	Notes	Temp. (°K)	References
Thermal Conductivity		0.239			W/cm °K		425	TPRC p. 441-2 v. 4 part 1
		0.314					315	
Thermal Coefficient of Expansion		⊥-c	∥-c					
		0.005	0.005		%		300	TPRC p. 443-4
		0.27	0.35				860	
		0.51	0.57				1273	
Shift in Volume with Pressure		V/V_o	a/a_o	c/c_o				
		0.995	0.9942	1.007		P = 34 kbars	300	Clendenen and Drickamer
		0.980	0.9848	1.011		= 83 (max)		
		0.930	0.9629	1.003		= 226		
Electrical Properties								
Dielectric Constant								
Static (transverse)	$\epsilon_{o\perp}$	13.5 ±1.5				10^4 - 10^{10} Hz	300	Van Daal
(longitudinal)	$\epsilon_{o\parallel}$	9.0 ±0.5						
Optic (transverse)	$\epsilon_{\infty\perp}$	3.785				λ = 5 - 100μ	300	Summitt
(longitudinal)	$\epsilon_{\infty\parallel}$	4.175						
Dissipation Factor	$\tan\delta$	0.01 - 0.001				10^4 - 10^{10} Hz	300	Van Daal

Property	Symbol	Value			Units	Notes and Sample	Temp. (°K)	References
Electrical Resistivity*		10^{-3}			Ω-cm	$n_n=10^{20}$ cm^{-3}	77-300	Morgan and Wright
		10^{-2}				$n_n=10^{19}$ cm^{-3}		
		0.1 - 0.003				film	300	Koch (A), Viscrian and Georgescu
		~500				maximum for single crystal	800	Mass. Inst. Tech.
		~10					1100	
Mobility, Electron	μ_n	90°K	300°K	500°K				
		2	25	20	cm^2/V	film		Van der Maesen and Witmer
			20	60		natural, single crys.		
		12	80	40		n-type, synthetic		
		100-200				pure, single crys.	300	Wright, Nagasawa et al.
		1000					77	Nagasawa and Shinoya
Temperature Coefficient		$T^{1.5}$					77	Morgan and Wright
		$T^{-0.5}$					400-1000	

*As-grown, undoped crystals will have a 25-50 micron thick surface with a resistivity of over 10^6 ohm-cm, whereas the bulk resistivity of the crystal will be of the order of 0.01 ohm-cm. (Marley and Dockerty)

Property	Symbol	Value		Units	Notes and Sample	Temp. (°K)	References
Effective Mass							
Transverse electron	$m_{n\perp}$	0.16		m_o	single crystal	300	Wright
Longitudinal electron	$m_{n\parallel}$	0.11					
electron	m_n	n-10^{19} cm^{-3}	$n=10^{20}$ cm^{-3}				
		-	0.17			100	Morgan and Wright
		0.11	0.17			300	
		0.10	0.10			1100	
	m_n	0.17 ±0.02			film	300	Koch (B)
hole	m_p	0.3			single crystal	300	Koch (C)
Electron density of states	m_d	0.22				300	Marley and Dockerty
Energy Gap							
direct		2.7		eV	film	300	Spence
indirect		4.3					
		E∥c-axis	E⊥c-axis				
direct		3.947	3.631	eV	film, T=20-1300°K optical absorption	0	Summitt and Borelli
direct		4.07 ±0.02	3.69 ±0.02		Single crystal, optical absorption	300	Reddaway and Wright
indirect		2.45 ±0.05	2.55 ±0.05				
Temperature Coefficient	dEg/dT	-12		10^{-4} eV/°K	E∥c-axis, natural	300	Summitt and Borelli
		-14.1			E⊥c-axis	700-1100	Kohnke (A)
		-6			natural crystal	80-415	Kohnke (B)

Property	Symbol	Value	Units	Notes	Temp. (°K)	References
Valence-band gap,	ΔE	0.3	eV		300	Summitt et al., Wright
Phonon Spectra						
Longitudinal optic	LO	85.5	meV	E ∥ c-axis	300	Van Daal
Transverse optic	TO	54.4				
Seebeck Coefficient		-500	$\mu V/^{o}K$	pure, single crystal	300-800	Mass. Inst. Tech.
		-875			950	
		-183		as-grown	303	Marley and Dockerty
		-263		annealed in O_2	328	
		+100		$10^{19} cm^{-3}$ Sb-doped	300	Morgan and Wright
		+ 50		$10^{20} cm^{-3}$ Sb-doped		
g-factor						
transverse	$g_{\perp}$	1.876		E ∥ c-axis		Hajimoto et al.
longitudinal	$g_{\parallel}$	1.905				
Optical Properties*						
Transmission		90	%	0.2 μ thick film, λ = 0.4 - 0.7 μ	300	Baillou et al.
		75-80		0.5 - 0.7 μ thick film, λ = 0.4 - 0.7 μ		Vaynshteyn

*Tin dioxide is uniaxial positive and dichroic. Birefringence increases with increasing wavelength and decreases with increasing temperature. The refractive index at a fixed wavelength increases with increasing temperature.

Property	Value		Wavelength (λ)	Notes and Sample	Temp (°K)	References
Refractive Index	1.96		0.5	polycrystalline film	300	Ishiguro et al
	1.85		0.7			
	n_o	n_e		natural crystals	294	Dana p 576 (V-1)
	2.0475	2.1397	0.440			
	2.0239	2.1188	0.496			
	2.006	2.0972	0.585			
	1.9899	2.0874	0.653			
	1.9836	2.0818	0.715			
	2.007	2.0980	0.578		289	
	2.0173	2.1135			594	
	2.0316	2.1275			806	
	2.0545	2.1489			1097	
	2.0702	2.1658			1287	

REFERENCES

BAILLOU, J., et al. Optical Transmission and Electrical Resistance of Thin Tin Oxide Films Prepared by Reactive Cathode Powdering (In Fr.). REVUE DE PHYSIQUE APPLIQUEE, v. 3, no. 1, Mar. 1968. p. 78-82.

CLENDENEN, R.L. and H.G. DRICKAMER. Lattice Parameters of Nine Oxides and Sulfides as a Function of Pressure. J. OF CHEM. PHYS., v. 44, no. 11, June 1, 1966. p. 4223-4228.

DANA'S SYSTEM OF MINERALOGY. V. 1, 7th Ed. N.Y., London, Wiley Inc., 1944.

DONALDSON, J.D., et al. Red Tin (II) Oxide. J. CHEM. SOC., no. 178, 1961. p. 839-841.

DONNAY, J.D.H. (Ed.) Crystal Data. Determinative Tables. 2nd Ed. AMERICAN CRYSTALLOGRAPHIC ASSOCIATION, Apr. 1, 1963. ACA Monograph no. 5.

HAJIMOTO, Y., et al. Electron Spin Resonance in Reduced Tin Oxide. PHYS. LETTERS, v. 23, no. 1, Oct. 3, 1966. p. 50-51.

HANDBOOK OF CHEMISTRY AND PHYSICS. Cleveland, Ohio, The Chemical Rubber Co., 49th Ed. 1968-1969.

HANSEN, M. and K. ANDERKO. Constitution of Binary Alloys. 2nd Ed. McGraw Hill, N.Y., 1958.

ISHIGURO, K., et al. Optical and Electrical Properties of Tin Oxide Films. PHYS. SOC. OF JAPAN, J., v. 13, no. 3, Mar. 1958. p. 296-304.

HIRAYAMA, C. Thermodynamic Properties of Solid Monoxides, Monosulfides, Monoselenides and Monotellurides of Ge, Sn and Pb. J. OF CHEMICAL AND ENGINEERING DATA, v. 9, no. 1, Jan. 1964. p. 65-68.

KOCH, H. Electrical Studies of Nonadditive Tin Oxide Layers of High Electron Concentration in the Temperature Range 90 Degrees to 290 Degrees K (In Ger.). PHYSICA STATUS SOLIDI, vol. 3, no. 6, 1963. p. 1059-1071. (A)

KOCH, H. Optical Natur of Semiconductor Tin Dioxide Layers in Near Infrared at 300 Degrees K (In Ger.). PHYSICA STA'US SOLIDI, vol. 3, no. 9, 1963. p. 1619-1628. (B)

KOCH, H Influence of Free Electrons on the Intrinsic Absorption Edge of Semiconducting Tin Dioxide Films (In Ger.). PHYS. STATUS SOLIDI, v. 7, no. 1, Oct. 1, 1964. p. 263-275. (C)

KOHNKE, E.E. Electrical and Optical Properties of Natural Stannic Oxide Crystals. PHYS. AND CHEM. OF SOLIDS, v. 23, Nov. 1962. p. 1557-1562. (B)

OKLAHOMA STATE UNIV., STILLWATER RES. FOUNDATION. Optical and Electrical Properties of Stannic Oxide Crystals. Fr, June 1958-Sept. 1967, by KOHNKE, E.E. Contract no. Nonr-2595-01. Nov. 1967. 24 p. AD 662 692. (A)

MARLEY, J.A. and R.C DOCKERTY. Electrical Properties of Stannic Oxide Single Crystals. PHYS. REV, v. 140, no. 1A, Oct. 4, 1965. p. A304-A310.

MASS. INST. OF TECH. LINCOLN LAB. Solid State Research. Rept. no. 1, 1962. Contract no. AF 19-604-7400. 1962. ASTIA AD-277 393.

MILLAR, R.W. The Heat Capacities at Low Temperatures of the Oxides of Tin and Lead. J. AM. CHEM. SOC., v. 51, no. 1, Jan. 1929. p. 207-214.

MORGAN, D.F. and D.A. WRIGHT. Electrical Properties of Single Crystals of Antimony-Doped Stannic Oxide. BRITISH J. OF APPLIED PHYS., v. 17, no. 3, Mar. 1966. p. 337-340.

NAGASAWA, M. and S SHIONOYA. Weak-Field Magnetoresistance in Tin Dioxide Single Crystals. J. OF PHYS. AND CHEM. OF SOLIDS, v. 29, no. 11, Nov. 1968. p. 1959-1972.

NAGASAWA, M., et al. Vapor Reaction Growth of Tin Oxide Single Crystals and Their Properties. JAPANESE J. OF APPLIED PHYS., v. 4, no. 3, Mar. 1965. p. 195-202.

PLATTEEUW, J.C and G. MEYER. The System Tin+Oxygen. FARADAY SOCIETY TRANSACTIONS, v. 52, (1956). p. 1066-1073.

REDDAWAY, S F. and D.A. WRIGHT. The Optical Properties of Tin Oxide Crystals. BRITISH J. OF APPLIED PHYS., v. 16, no. 2, Feb. 1965. p. 195-198.

SPENCE, W. The Ultraviolet Absorption Edge of Tin Oxide Thin Films. J. OF APPLIED PHYS. v. 38, no. 9, Aug. 1967. p. 3767-3770.

SUMMITT, R Infrared Absorption in Single-Crystal Stannic Oxide, Optical Lattice-Vibration Modes. J. OF APPLIED PHYS., v. 39, no. 8, July 1968. p. 3762-3767.

SUMMITT, R. and N.F. BORRELLI. Temperature Dependence of the Ultraviolet Absorption Edgés in Tin Oxide. J. OF APPLIED PHYS., v. 37, no. 5, Apr. 1966. p. 2200.

SUMMITT, R., et al. The Ultraviolet Absorption Edge of Stannic Oxide. J. OF PHYS AND CHEM. OF SOLIDS, v. 25, no. 12, Dec. 1964. p. 1465-1469.

TPRC, THERMOPHYSICAL PROPERTIES RESEARCH CENTER. Thermophysical Properties of High Temperature Solid Materials. Ed. by Y.S. TOULOUKIAN, v. 4, pt. 1. Simple Oxygen Compounds and Their Mixtures. 1967.

VAN DAAL, H.J. The Static Dielectric Constant of Tin Dioxide. J. OF APPLIED PHYS., v. 39, no. 9, Aug. 1968. p. 4467-4469.

VAN DER MAESEN, F. and C.H M. WITMER. Hall and Resistivity Measurements on Thin Films of Tin Oxide and Indium Oxide. In INT. CONF. ON SEMICONDUCTOR PHYS., PROC., 7th, Paris, 1964. v. 1. Ed. by HULIN, M. N.Y., Acad. Press, 1964. p. 1211-1215.

VAYNSHTEYN, V.M. Preparation and Properties of Stannic Oxide Films by Reactive Cathode Sputtering. SOVIET J. OF OPTICAL TECHNOLOGY, v. 34, no. 1, Jan-Feb. 1967. p. 45-47.

VISCRIAN, I. and V. GEORGESCU. Contributions to the Study of Tin Oxide Films. THIN SOLID FILMS, v. 3, no. 2, Feb. 1969. p. R17-R22.

WRIGHT, D.A. Electrical and Optical Properties of Tin Oxide Crystals. BRITISH CERAM. SOC., PROC., no. 10, Mar. 1968. p. 103-113.

WYCKOFF, R.W.G. Crystal Structures. 2nd Ed. v. 1, New York, Interscience, 1963.

Appendix B - Crystal Growth System Details, Drawings and Photographs

To supplement the description of the physical crystal growth system in the text and to present details of the various units of that system and their development, a discussion of specific pieces of the growth system accompanied by photographs and drawings of them is presented in this appendix.

B.1 Gas Flow and Metering Controls

The gas flow and metering controls referred to in the lower left of Figure 2 are the interface between the gas cylinders and the crystal growth furnace. Here the gas flows are controlled and measured. This portion of the system is illustrated skematically in Figure A-1, and shown in front and back view photographs in Figure A-2. The function is quite straight forward and only a few specifics need be dwelt on.

The lines from the helium regulator coupled into each of the other gas lines allow all of the lines or individual lines to be flushed with helium gas. They also allow for quickly relieving any pressure with the "vent" valve indicated. That is, by opening the "vent" valve and the flush valve of the desired gas, that gas line is vented.

The gas cylinders are all fitted with two stage regulators. The hydrogen and oxygen lines also have a low pressure single stage regulator set to give a pressure to the "shut-off" valves of 2.4 PSIG or 17 PSIA (900 torr). No such regulator was available for chlorine service so its stainless steel two-stage regulator is adjusted to give about the same pressure, though with less precision.

The flow meters are Brooks glass ball-float tubes, see Figure A-2.

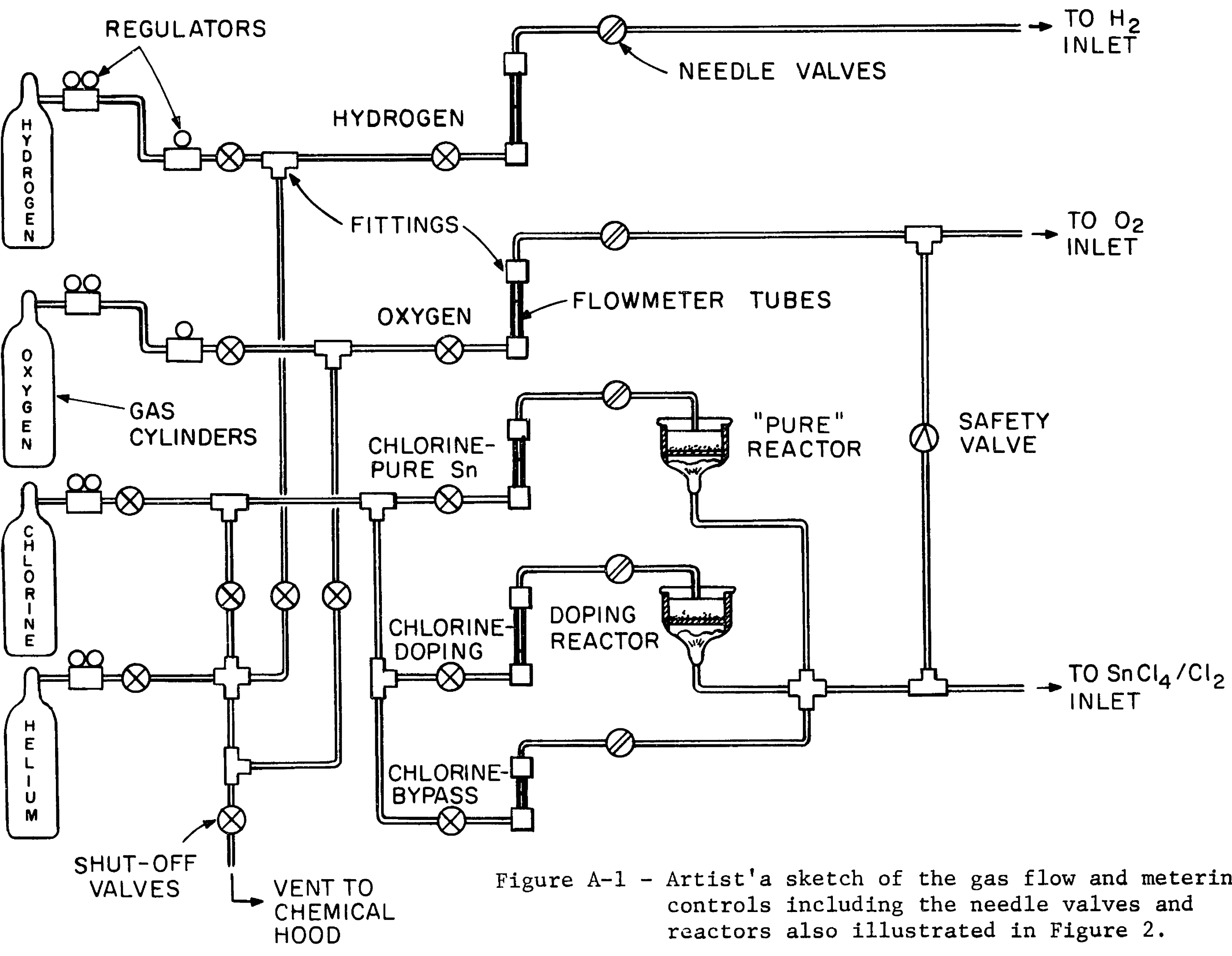

Figure A-1 - Artist'a sketch of the gas flow and metering controls including the needle valves and reactors also illustrated in Figure 2.

(a) Front view.

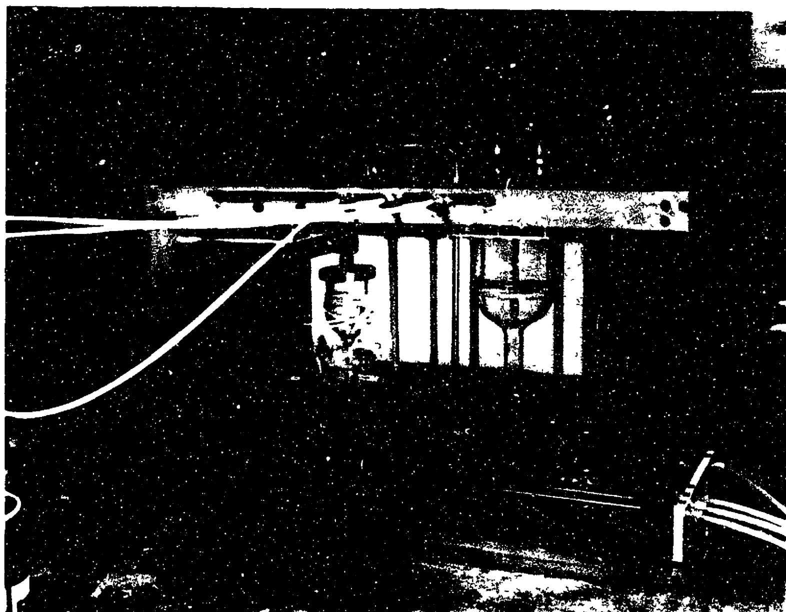

(b) Back view.

Figure A-2 - Photographs of the gas flow and metering controls.

The shut-off valves are Whitey toggle valves; the metering valves are Nupro very fine metering valves. All fittings, including those to the flow tubes, are Swagelok pipe fittings. To join to the glass flow tubes an oversized fitting with teflon ferrules is used. A teflon sleeve tightly fitting on the glass tube and the diameter of the fitting is machined for the ends of the tube where the fitting grips it. This makes a flexible enough union between the glass tube and metal fitting that breakage of the tubes is eliminated. Without such a construction, perhaps simply using a more closely fitting fitting and teflon ferrules, tubes are broken easily and it soon becomes more economical to purchase complete flowmeter units.

Visible in the photographs, Figure A-2, are the stannic chloride reactors and the heating controls for the heater tapes used to warm these reactors. The reactors are sealed at their tops to metal covers by rubber baskets and have o-ring glass joints coupling to metal fittings at their outputs. The heating controls are simply small variable transformers connected at their input through a switch and fuse to the line supply and at their output to the heater tape.

Also visible in the back view photograph, Figure A-2b, is a pressure release valve (not shown in Figure 2) joining the $SnCl_4$ and oxygen lines just before the furnace. This device is used to prevent the excessive accumulation of chlorine and stannic chloride in the reactors if the center injection nozzle becomes blocked. A pressure differential greater than 15 torr between the two lines opens the valve keeping pressure in the stannic chloride/chlorine line low. This is, of course, a temporary measure as the system cannot properly run with the nozzle blocked, but

it is a very necessary safeguard because the nozzle can easily become blocked creating a nasty disposal problem if there is a build-up in this line.

B.2. Furnace Tube Endcaps

Exploded cross-sectional views of the input and output furnace tube endcaps are shown in Figure A-3 and Figure A-4, respectively. Both units are constructed of stainless steel, except for the o-rings, gaskets, and other items indicated.

The gases enter the input endcap, Figure A-3, through the fittings shown via teflon tubing from the gas flow control panel shown in Figure A-2. The injector nozzles extend back into the two fittings on the left, the inner one reaching into the last fitting sufficiently to be sealed and held by the o-ring and the outer nozzle reaching into the second fitting enough to be gripped by the o-ring but not so much as to block the hydrogen inlet on the side. The window opening is donut shaped with three radial ribs crossing it which support the center unit. It has been found helpful to evaporate a semi-transparent coating of gold on the outside of the window to reflect heat back into the furnace while still transmitting visible light.

The output endcap, Figure A-4, has two possible windows. The normal window is simply a full disc opening. For seeded growth a window like that on the input endcap is used with a seed rod passed through the center. No coating has been used on the output windows.

Both of the endcaps are drawn to the mullite tube by three bolts attached to a collar which in turn is fastened to the mullite by special

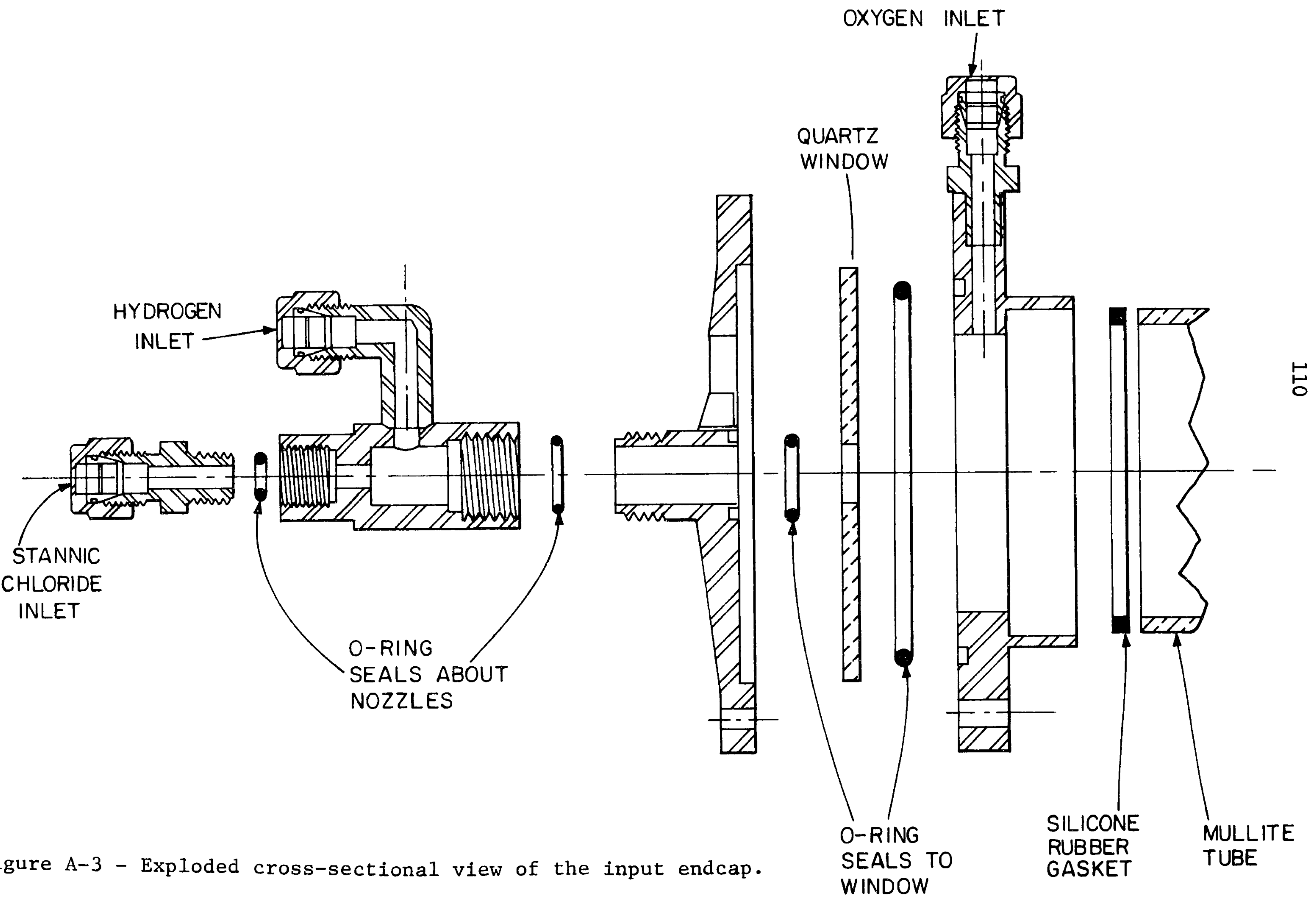

Figure A-3 - Exploded cross-sectional view of the input endcap.

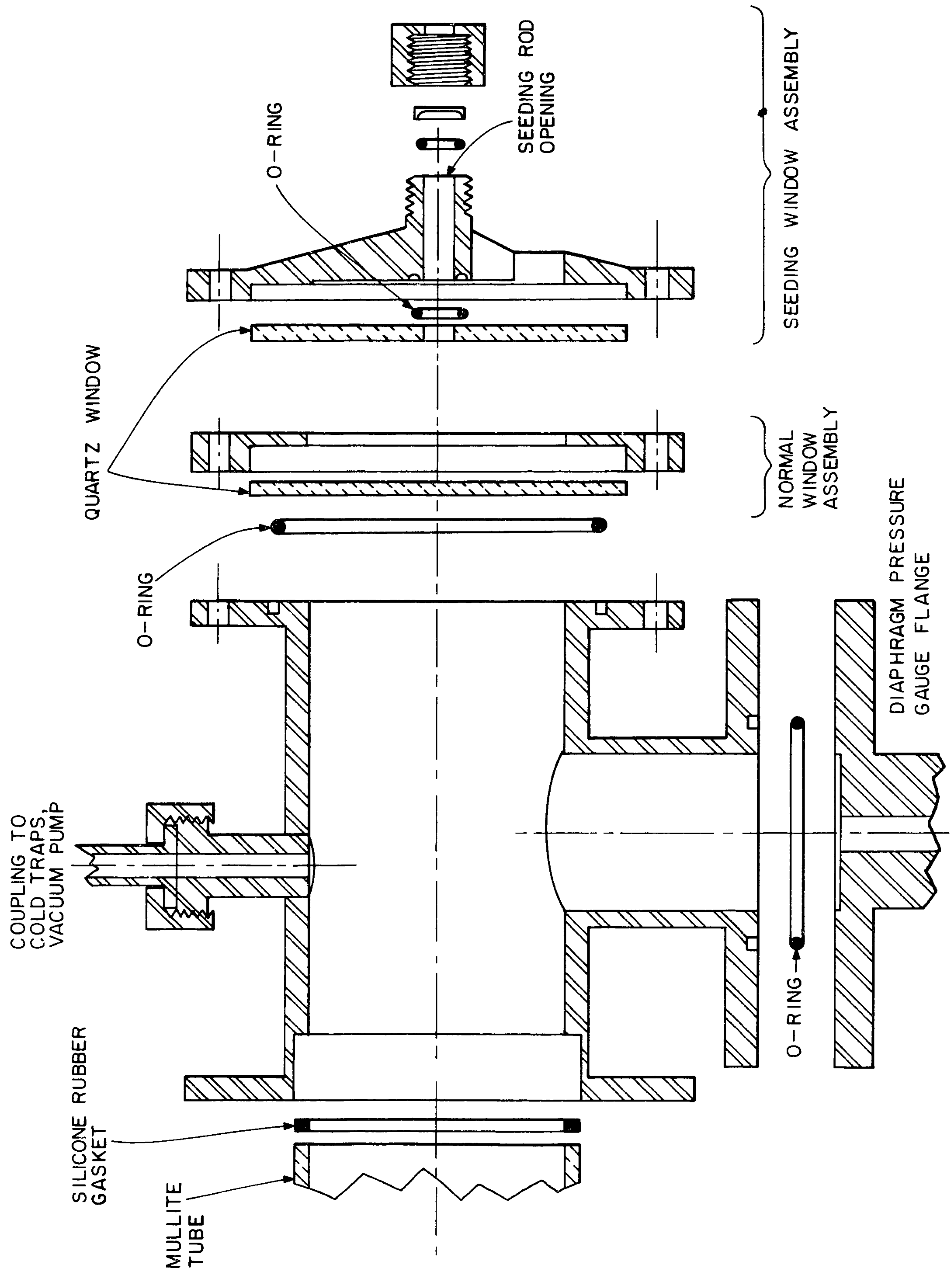

Figure A-4 - Exploded cross-sectional view of the output endcap with the normal window assembly and the seeding window assembly.

hardware on a large hose clamp. The basic materials are available from the mullite tube manufacturer, McDanel.

B.3. Injection Nozzles

The method of holding the injection nozzles was discussed in the previous section; of interest here are the nozzle diameters, the materials they are made of, and the shaping and positioning of their ends. Initially an inner nozzle of 1/16" I.D. and 1/8" O.D., and an outer nozzle of 1/4" I.D. was used. At first the nozzles were also made of a metal. Stainless steel, nickel and Inconel were tried but the change was made to quartz for both nozzles after the Run 001. The inner nozzle still reacted with the stannic chloride so it was changed to zirconium oxide. About the same time the size of the outer nozzle was increased to 11 mm I.D. to eliminate blocking of it by the slow deposit that still occurs on the nozzle ends. To further reduce blocking problems the size of the inner nozzle was increased to its present 3/32" I.D. and 3/16" O.D. after Run 013. Changing the nozzle diameters, of course, changes the velocities of the gases as they enter the furnace and could thereby change the growtn dynamics. The effect on the present system, however, has appeared to be minor.

The ends of a typical set of nozzle is shown in Figure A-5. The ends of the two nozzle tubes were ground to shape by hand with a diamond wheel. The bevel is intended to reduce turbulence at the tube ends and judging from the smoothness of any deposit at the ends, it is successful. The best relative placement of the tubes is with the inner nozzle extended out slightly, about 1 mm.

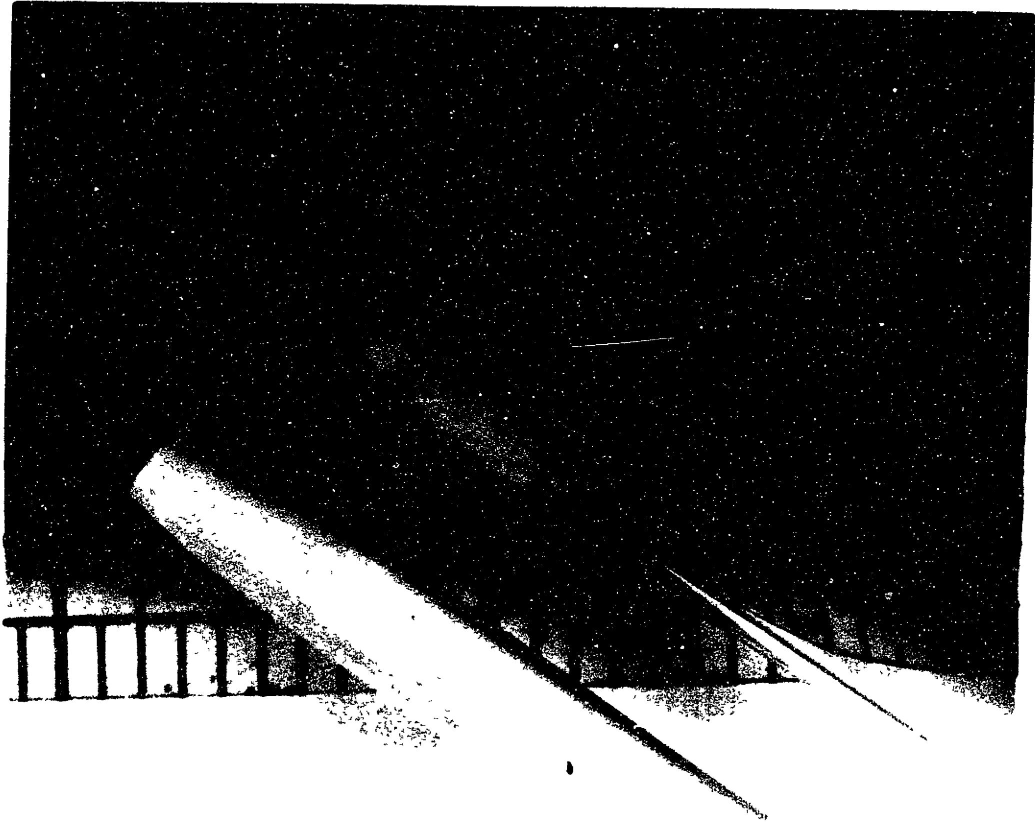

Figure A-5 - Photograph of a typical set of injector nozzles. Note the shaping of the ends.

B.4. Cold Traps, P-control, and Vacuum Pump

The "exhaust" gases leaving the portion of the system illustrated in Figure 1 pass through a cold trap before entering a vacuum pump along with an additional nitrogen flow controlled by the pressure controller. These units are all illustrated in Figure A-6, and photographed in Figure A-7.

The cold trap unit is actually two large glass, liquid nitrogen cooled cold traps and a series of shut-off valves designed so that either trap can be used to remove a portion, hopefully high, of the chlorine, water, and hydrogen chloride from the gas stream before it can enter the vacuum pump. When one trap has been filled with trapped material it can be isolated from the main flow stream and the second trap put into use. The first trap can then be warmed and the deposited gases and liquids drawn away as they thaw by a water-jet aspirator connected via another valve to the cold trap.

The traps are not 100% efficient so the vacuum pump oil must be changed regularly, but they do remove a great deal of material and with the initial size cold traps (on the right in Figure A-7) they had to be switched and cleaned every three hours. To extend the periods between changes, the larger trap which is visible as the left trap in Figure A-7 was designed. It has an inner tube diameter (which is where blockage usually first occurs) of 3 cm and an outer diameter of 8 cm. It requires cleaning only every 11 hours.

After the cold traps the remaining gases enter the vacuum pump. A Welch Duo-Seal 1402 pump is used and appears to operate well in spite of its use in chlorine service. The oil is attacked readily by the gases

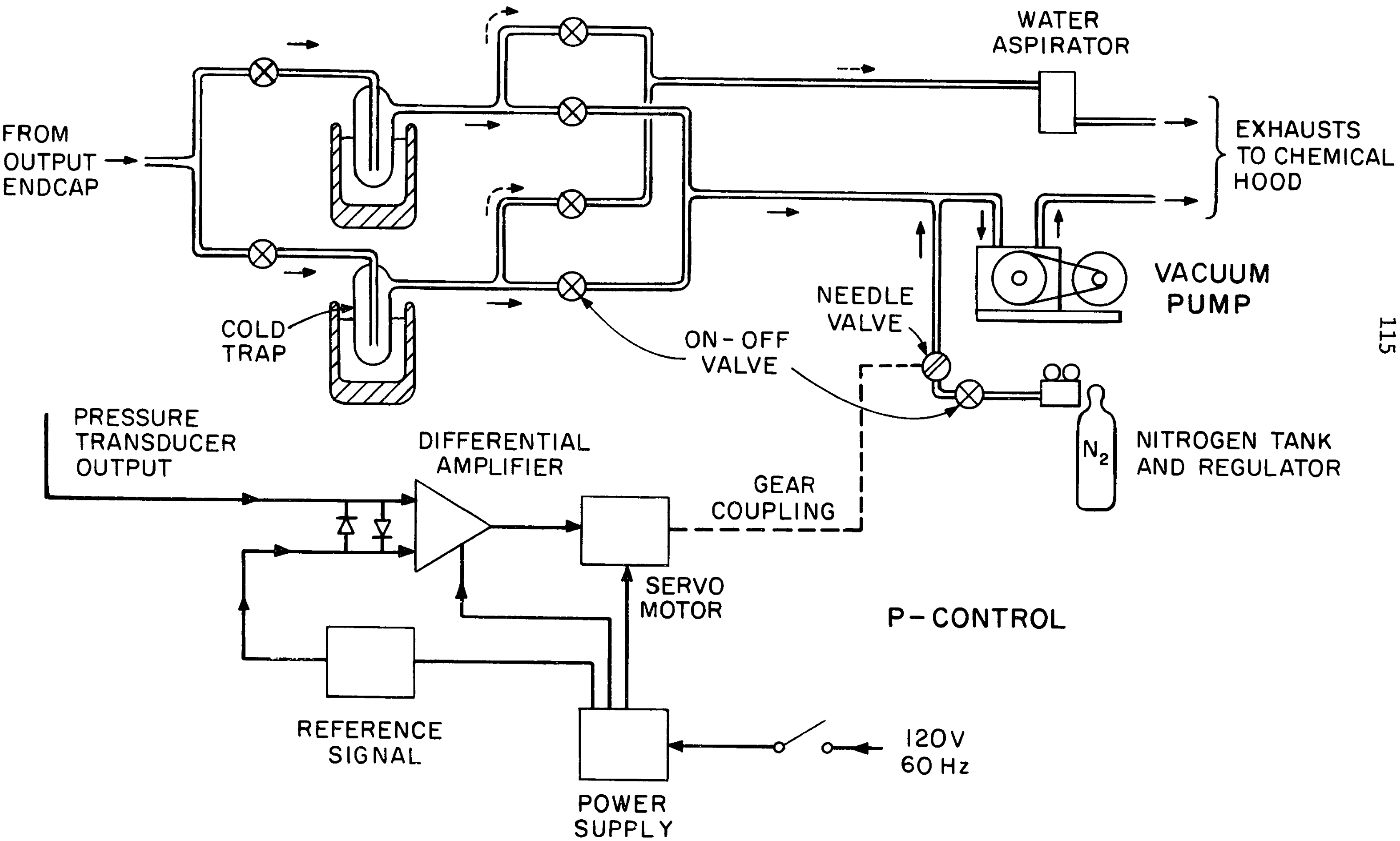

Figure A-6 - Artist's sketch of the output gas handling system showing the cold traps, pressure control system, vacuum pump, and cold trap cleaning provision.

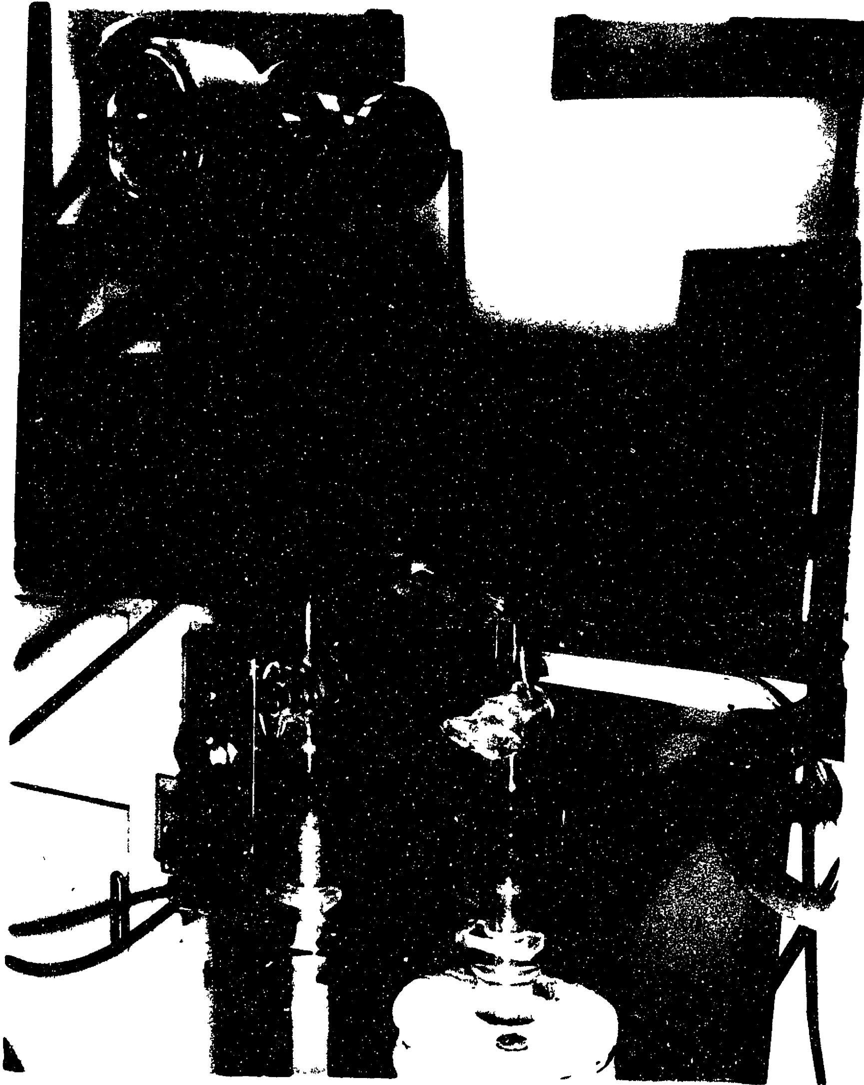

Figure A-7 - Photograph of the output gas handling system. The seeding window assembly is in position on the output endcap and the normal window assembly is seen on the table.

getting past the cold trap, and blackens, so it must be changed after every several growth runs. The exhaust of the pump goes to a chemical hood.

The vacuum pump can, of course, draw a much lower pressure in the system than the 10 torr required during a growth run. It thus must be throttled in some way. A technique used in early runs was to simply open only partially the shut-off valve between the cold trap and the pump. After careful and often frustratingly sensitive adjustment of this valve the pressure could be set at the desired level and would stay there as long as nothing changed elsewhere in the system. A readjustment was required each time a gas flow was changed or a cold trap cleaned. A much better technique is that illustrated in Figure A-6. That is, the pump is partially loaded by a controlled "leak" of nitrogen. This gas is introduced right before the pump and it is felt that a negligible amount diffuses back past the cold traps and into the growth region. It turns out that controlling the pressure in the system with this technique is much easier because the pressure is less sensitive to the needle valve control. This is not surprising. When a shut-off valve was partially closed to control the pressure, less than a 90° turn went from full "off" to full "on" so that finding the "10 torr angle" was difficult; with the needle valve, a full turn of the valve changes the pressure only 1 or 2 torr and adjustment to a desired setting is easy.

This adjustment of the needle valve can even be done automatically by a servo-system such as that illustrated in Figure A-6. The device that makes this possible is a diaphram pressure transducer (visible under the output endcap in Figure A-7 but not shown in the other figures) made by Rosemount Engineering. It monitors the pressure through a connection

near the diaphram pressure gauge on the output endcap and puts out a D.C. voltage proportional to the pressure (0-5 volts for 0-76 torr). This voltage and an adjustable reference voltage are compared by a differential amplifier and the difference signal is used to drive a servo motor geared to the needle valve so as to change the pressure in the system until the transducer output equals the set reference. This pressure control will then compensate automatically for any input gas flow changes, for load changes when cold traps are switched, and for all increased loading due to minor leaks developing during a run. Such a control unit has been built for the stannic oxide growth system using a basic design of Folweiler and works very well. As was discussed in the text, it is expected to be a valuable addition to the system and to help improve run yields.

B.5. Furnace Construction Controls and Characteristics

The cut-away view of the furnace presented in Figure 1 is quite illustrative of the actual physical situation. The mullite furnace tube is mounted in a fire brick enclosure which is in turn surrounded by 1/2" asbestos sheet and supported in an angle-iron frame. The fire brick insulation is 5" thick and consists of an inner layer of high temperature K-30 fire bricks with a layer of the more insulating K-20 brick on the outside. Eight globar heater elements are symmetrically mounted around the furnace tube through holes in the fire brick. The bricks are shaped so as to form an inner chamber about the elements and the furnace tube; this is the hot zone of the furnace and it is 13" long.

The globars are connected in parallel and through two large rotary switches to the secondary taps of a 5 kVA transformer. The peak voltage

to the globars is selected with the rotary switches and can be, for 130 V input, chosen in one volt steps from 25 to 60 volts. The actual transformer input is not line voltage but rather from a Barber Colman 621 Series Power Controller. This is an SCR supply unit whose output to the transformer primary is controlled by a D.C. level input to it. This D.C. signal is obtained, when initially heating the furnace, from a battery and potentiometer varied manually, and after the furnace is hot, from a Barber Colman Model 477P Capacitrol which maintains the furnace temperature at the desired value. It ultiizes a platinum-platinum rhodium thermocouple touching the furnace tube outside at its center to sense the temperature.

A second thermocouple near the first is used to monitor the furnace temperature continuously on a Barber Colman Series R strip chart recorder.

Being a simple single-zone furnace, the furnace has a temperature profile with no flat zone but with instead a long region of slowly varying temperature in the center and sharp temperature gradients on the sides as the furnace tube passes through the fire brick. The exact details vary with the peak temperature but can be roughly characterized as follows: The temperature drop passing through the 5 inches of insulation is about 600°C, while inside this region a total drop of about 100°C occurs (peak to either side) with 75°C of this drop occurring in the outer 2 inches. This leaves a 9 inch region in the center with a total temperature variation of 25°C. The best growth region is near the downstream edge of this region where temperature gradient is increasing. The temperature controller maintains the peak temperature of the furnace at a constant temperature during the normal course of a run within the sensitivity of the chart recorder (on the order of 2°C).

Appendic C - Detailed Procedures for Growth Runs

In addition to the usual common sense reasons for their use in a system intended to produce high quality crystals controllably, the presence of chlorine and chlorine compounds in this stannic oxide growth system makes the use of carefully developed operating procedures, particularly when preparing, starting, and finishing a run, very important. The steps outlined in the following sections have been found to be quite satisfactory for use with this system.

C.1. Pre-Run Preparations

Prior to a run, straight forward clean-up, check-out, and preparatory steps are followed. The reactors and flow-meter tubes are cleaned, new gaskets are installed and o-rings are inspected, and the tubing and valves are checked for deposits or corrosion. The endcaps are put on the furnace tube and a vacuum is drawn to check for leaks (short lengths of nozzle stock are used to seal where the nozzles ordinarily go). Any leaks are corrected so that the vacuum obtained is below the diaphragm gauge's limit.

With all of the system cleaned and functioning properly the quartz linear, the nozzles, and the tin charges are prepared for use. The liner must be cleaned and fitted with platinum wire spacers; the nozzles are ground and cut to length; and the tin charges are weighed and dopants are added. As these items are being readied the furnace is brought to temperature. The gas cylinder pressures are checked also.

The vacuum pump is left on all of the time once the system has been checked so the system is at low pressure. It is kept that way until just prior to the run. Then, with the furnace hot and all of the various items

prepared, the flow of helium gas is turned on, the vacuum pump inlet is closed, and the pressure inside the system is increased to atmospheric pressure. The tin charges are then placed in the reactors and the heater tapes are wrapped around them and are connected to their supplies. Next the input endcap is removed and the injection nozzles are inserted and carefully checked for concentricness and positioning along the furnace tube axis. With these ready the liner is slid into place, the endcap is replaced, and a vacuum is drawn again. A slight flow of helium is left flowing in all lines. It is turned off only briefly to check the ultimate vacuum pulled by the pump as a final test for leaks and is then turned on again. The system is ready for the start of the grow run proper.

C.2. Start-up Procedure

With the system prepared as described above, Section C.1. the start-up procedures for a growth run can be started. This is a more formally followed series of steps, unlike the above, and is the same in all runs.

The furnace is hot, a vacuum is being drawn, and a slight helium flow is in all lines; the nozzle, liner, and tin charges are in place; there are no leaks and all components are functioning properly. To start the run, the doping reactor is sealed off from the system by closing the shut-off valves before and after it, as well as the shut-off valve just before the flowmeter in this line. The pure tin reactor heater tape is turned on and the reactor is heated to about 100°C. While this is warming, the liquid nitrogen reservoirs of the cold traps are filled. Also the input to the cold trap not being used, usually the smaller one, is closed so that it can

be used later when the first trap is full. Finally, the gas cylinders are opened and the regulator pressures checked.

The helium flow is then turned off to the oxygen and hydroegn lines and these gases are put on and adjusted to the proper flows. The pressure control shut-off valve is opened and the nitrogen bleed-in needle valve adjusted so the pressure is 7-8 torr. When it is determined that everything is functioning properly the helium flow in the chlorine lines is turned off and the chlorine flow is started. The bypass flow is set high enough to prevent growth while the chlorine to the tin reactor is set at its proper level. The pressure is also adjusted to about 9.8 torr at this time. If all is still well, the bypass chlorine flow is lowered until nucleation and growth starts. The pressure control, if not operating automatically, must usually be readjusted as the flow is changed to maintain a constant pressure.

As growth starts the progress is watched continuously and adjustments made in the rate of growth so as to obtain a good growth. Several cycles of growing and etching back are normal, and for the first 12 to 18 hours growth is done quite slowly. The object is to have a limited number of nucleations start in the optimum growth region, and to let the larger crystals grow initially at the expense of smaller neighboring crystallites. Once growth is well established the remaining chlorine bypass flow is reduced to zero and doping can be started as desired. A continuous diary is kept during a run of all conditions (gas flows, temperatures, pressures) in the system and all of these adjustments and observations.

C.3. Shut-Down Procedures for Runs

The procedure followed to shut-down the growth system after a run

may be modified slightly if difficulties with the system force a premature shut-down, but it is still followed as closely as is possible. This procedure is intended to reduce the difficulty of clearing out any chlorine and chlorine compounds in the system, to minimize the effort necessary to prepare for the next run, and to expedite the harvesting of any crystals produced. A second procedure has been developed to be followed for temporary shut-downs of the system during a run when changes in the nozzles, liner, seeds, or any other portion must be made. Both of these procedures will be discussed here.

During a temporary shut-down it is normally the case that the furnace tube must be opened to make some modification such as changing the nozzles before continuing the run. When it is decided to do this, the gas flows are turned off at the regulator valves and helium put on in all lines. The tin reactor heaters are turned off and the pressure controller nitrogen flow is cut off, also. After letting the pump draw the other gases off and helium bleed into the system for a few minutes the cold trap inlet is closed and the pressure inside the system is increased with helium gas. When room pressure is reached the system can be opened and any necessary work is done as quickly as possible. When it is completed a vacuum is again drawn and the tin reactor heaters switched on. The same procedure used when starting up is used now except that the bypass chlorine is adjusted, after the chlorine to the reactors has been adjusted, from the high level to its level before the shut-down rather than to give slow growth, etc.

It should be noted that the seed rod, if used, can usually be moved in and out along the furnace axis without affecting the system pressure.

The shut-down procedure must, of course, be followed when it is to be removed.

The procedure for the final shut-down is similar to the above procedure. To terminate a run the gas shut-off valves just prior to the flow tubes are closed and the pressure controller flow shut off. The pressure in the system then drops and all of the gases (most importantly in the chlorine lines) are drawn off of the system. While this is being done the oxygen, hydroegn, and chlorine cylinders are closed and the pressure in their regulators is relieved by venting the gases. At the same time the tin reactor heaters are turned off. The furnace power is also turned off at this time. This is best done by changing the Capacitrol to a lower setting, say 1000°C, which causes the furnace controller to reduce the power to the furnace to zero and allows the transformer to be disconnected with no worry about interrupting large currents.

With these items taken care of (after about 5 min.) the helium flow is turned on to the oxygen and hydrogen lines. The cold trap input is then closed and the pressure in the system is increased to room pressure. After the pressure has risen, the helium flows are shut off and the chlorine-stannic chloride line is disconnected from the input endcap. It is reconnected instead to a special bypass line connected on its other end to the cold trap input in place of the line normally going there from the output endcap and which is removed at this time. A vacuum is then drawn in the chlorine-stannic chloride line and the helium is turned on in the chlorine lines. These steps are taken to flush as much chlorine as possible from the system.

After connecting this bypass, the output and input endcaps are disconnected and removed. Any deposit near the output end of the mullite tube is scraped out but the tube is otherwise not disturbed. The output endcap, the diaphragm pressure gauge, and the line from the endcap to the cold traps are all then thoroughly cleaned with water, rinsed with methyl alcohol, and dried. The input endcap requires little attention but the nozzles are removed and saved for the "post-mortem" analysis.

By this time most of the chlorine has been flushed from the chlorine lines and the reactors so the cold traps can be cleaned one at a time by removing them and rinsing them out with water. The chlorine lines are still flushed with helium and connected to the vacuum pump to remove all traces of chlorine though, of course, this chlorine is not now trapped before entering the pump. So little is left that this is of no importance.

The quartz liner and the crystals are not disturbed until the furnace has completely cooled. As an indication of how quickly this occurs the thermocouple indicates that starting from 1300°C, the temperature is 1200°C 10 minutes after the power is turned off, 1000°C after 30 minutes, 800°C after 80 minutes, 600°C after 170 minutes or about 3 hours, 400°C after 5 hours, and 200°C after 10 hours. The crystals inside the tube start out cooler and probably reach the lower temperatures somewhat sooner.

Attempts at removing crystals sooner to "quench" them, for instance, are not usually not successful. The liner cannot easily be removed because as it is moved the thick deposits of stannic oxide on its ends (where

the liner extends past the hot zone to cool regions of the furnace) contract breaking the liner up. The smaller fragments of the tube then keep the liner from sliding out. Furthermore, the crystals are too tightly attached to the liner when hot to be knocked off and onto a boat, for example, for quick removal. Once the tube and crystals have cooled, the liner is removed - the ends piece by piece - and the crystals are detached and stored. The liner and pieces, like the nozzles, are saved for later analysis.

At this time the mullite tube is cleaned usually by removing it and rinsing it with water. It is then replaced and the glass wool packing between it and the fire brick repaired. The chlorine line is disconnected from the pump after being brought to atmospheric pressure with helium, and the tin charges are removed from the reactors for weighing. The vacuum pump can then be turned off and the oil changed if desired.

A postmortem analysis of each run is written evaluating the yield of the run in light of important occurrences during the run; comparing the deposits observed, the condition of the nozzles, and the growth to those of other runs; and considering the success of any modifications made for the run and specific run objectives. Those analyses have proven invaluable to the success of the system.

Appendix D - Measurement of Resistivity Anisotropy

The size of the crystals grown and the most typical crystal habit, see Figure 3, made the cutting of all but very small oriented samples difficult. Specifically, bars with the a-direction along their length could be cut while homogeneous bars oriented along the c-direction could not be readily cut. To determine, then, what was missed by measuring only σ_a and μ_a a measurement of ρ_a/ρ_c was made on a small oriented cube at 77^oK and 300^oK. The sample was cut from a crystal from Run 017 (crystals from this run have high mobility similar to sample 016-1) and oriented with its edges parallel to the principal crystal axes, see Figure 1. The orientation was done with a polarizing microscope and checked with x-rays. It was within $\pm 1^o$ in all directions. The sample dimensions were 0.57 mm (a) by 0.73 mm (a) by 1.0 mm (c).

Because of the small sample size a two terminal resistivity measurement was made at room temperature. To reduce the possibility of errors due to contact resistance (note that ohmic contacts are easily made on SnO_2 but "ohmic" is not automatically "zero-resistance") the contacts were made, removed, and remade several times for each direction and the minimum sample resistance was observed in each direction and was reproduced. The sample was held between two thin indium coated phosphor bronze leaves and Wetalloy-232 was used on lapped faces for the contacts. The resistance was measured both from a Tektronix Model 576 curve tracer and on a General Radio Model 1650A impedance bridge. The most significant source of possible error besides the contact resistance is in the measurement of the sample dimensions.

The resistivities measured were $\rho_a = 3.0 \pm 0.1$ Ω-cm and $\rho_c = 3.5 \pm 0.15$ Ω-cm at 300°K. Thus $\rho_c/\rho_a = 1.2$ which is not a large anisotropy.

The two terminal technique did not work at liquid nitrogen temperature, 77°K, where the sample resistance was much lower , because the contacts hardened and had appreciable resistance. For the measurement at 77°K a four terminal measurement was made to indirectly measure ρ_c/ρ_a. With the sample in the above holder two 2 mil diameter gold wire voltage probes were positioned on the top surface of the sample and the contacts were formed by capacitive discharge. To obtain ρ_c/ρ_a at 77°K the ratios of the sample resistance between the voltage probes at 77°K and at 300°K in the a- and c-directions were used to obtain $\rho_a(300^\circ\text{K})/\rho_a(77^\circ\text{K}) = 11 \pm 2$ and $\rho_c(300^\circ\text{K})/\rho_c(77^\circ\text{K}) = 13 \pm 2$ from which $\rho_c/\rho_a \simeq 1$ at 77°K was calculated knowing ρ_c/ρ_a at 300°K. For the measurement a Hewlett-Packard Model 6205B DC power supply and a Simpson 260 Multimeter were used as the current source and ammeter with a Keithley Model 602 Electrometer to measure the voltage. The resistivity itself could be measured in this four terminal geometry also and the room temperature resistivity measured agreed with the two terminal measurement. There is more uncertainty here, though, due mainly to uncertainty in measuring the small distances involved.

The uncertainty in the present anisotropy measurement is still large and it is unlikely that it can be significantly improved without larger samples or a measurement technique not relying on contacts to the sample. The results are sufficient however to conclude that the resistivity anisotropy in stannic oxide is of order unity, i.e., $\rho_c/\rho_a \leq 1.2$ at 77°K and 300°K.

REFERENCES

1. W. H. Baur, Acta Crystallographica 9, 515 (1956).

2. E. E. Kohnke, J. Phys. Chem. Solids 23, 1557 (1962).

3. W. Spence, J. of Appl. Phys. 38, 3767 (1967). See reference 1 of this article for references to earlier work.

4. J. A. Marley and T. C. MacAvoy, J. Appl. Phys. 32, 2504 (1961).

5. J. A. Marley and R. C. Dockerty, Phys. Rev. 140, A304 (1965).

6. R. Summitt, J. A. Marley and N. F. Borrelli, J. Phys. Chem. Solids 25, 1465 (1964).

7. R. Summitt and N. F. Borrelli, J. Phys. Chem. Solids 26, 921 (1965).

8. R. Summitt and N. F. Borrelli, J. Appl. Phys. 37, 2200 (1966).

9. F. P. Koffyberg, J. Appl. Phys. 36, 844 (1965).

10. T. B. Reed, J. T. Roddy, and A. N. Mariano, J. Appl. Phys. 33, 1014 (1962).

11. D. F. Morgan and D. A. Wright, Brit. J. Appl. Phys. 17, 337 (1966).

12. D. F. Crabtree, R. N. S. M. Mehdi, and D. A. Wright, Brit. J. Appl. Phys. 2, 1503 (1969).

13. S. F. Reddaway and D. A. Wright, Brit. J. Appl. Phys. 16, 195 (1965).

14. S. R. Reddaway, Brit. J. Appl. Phys. 17, 697 (1966).

15. M. Nagasawa, S. Shionoya, and S. Makishima, Jap. J. Appl. Phys. 4, 195 (1965).

16. M. Nagasawa, S. Shionoya, and S. Makishima, J. Phys. Soc. Japan 20, 1093 (1965).

17. M. Nagasawa and S. Shionoya, J. Phys. Chem. Solids 29, 1959 (1968).

18. M. Nagasawa and S. Shionoya, Phys. Letters 22, 409 (1966).

19. M. Nagasawa and S. Shionoya, Phys Rev. Letters 21, 1070 (1968).

20. M. Nagasawa and S. Shionoya, Sol. St. Comm. 7, 1731 (1969).

21. H. J. vanDaal, Solid St. Comm. 6, 5 (1968).

22. H. J. vanDaal, J. Appl. Phys. 39, 4467 (1968).

23. H. F. Kunkle and E. E. Kohnke, J. Appl. Phys. 36, 1489 (1965).

24. P. S. Schaffer, J. Amer. Ceramic Soc. 48, 508 (1965).

25. R. C. Folweiler , Technical Report No. RADC-TR-67-575, Final Report, November, 1967.

26. D. Gabbe, private communication.

27. R. C. Folweiler , private communication.

28. J. W. Surhigh and C. A. Mead, Phys. Letters 20, 367 (1966).

29. C. A. Mead, Solid-State Electron. 9, 1023 (1966).

30. E. D. Hinkley and R. H. Rediker, Solid-State Electron. 10, 671 (1967).

31. A. C. Smith, J. F. Janak, and R. B. Adler, Electronic Conduction in Solids, McGraw-Hill (New York, 1967) p. 251.

32. J. H. Becker and W. R. Hosler, Phys. Rev. 137, A 1872 (1965).

33. S. S. Devlin in Physics and Chemistry of II-VI Compounds edited by M. Aven and J. S. Prener, North-Holland Publishing (Amsterdam, 1967).

34. R. A. Smith, Semiconductors, Cambridge University Press (London, 1961).

35. F. J. Blatt in Solid State Physics edited by F. Seitz and D. Turnbull, Academic Press (New York, 1957), p. 343 ff.

36. G. E. Stillman, C. M. Wolfe, and J. O. Dimmock, J. Phys. Chem.Solids 31, 1199 (1970).

37. A. R. Hutson in Semiconductors edited by N. B. Hannay, Reinhold Publishing (New York, 1959).

38. S. M. Sze, Physics of Semiconductor Devices, Wiley-Interscience (New York, 1969), p. 34.

39. E. Spenke, Electronic Semiconductors, McGraw-Hill (New York, 1958), p. 385.

40. G. L. Pearson snd J. Bardeen, Phys. Rev. 75, 865 (1949).

41. D. M. Eagles, J. Phys. Chem. Solids 25, 1243 (1964).

42. R. Summitt, J. Appl. Phys. 39, 3762 (1968).

43. F. E. Low and D. Pines, Phys. Rev. 98, 414 (1955). Also of interest is T. D. Lee, F. E. Low, and D. Pines, Phys. Rev. 90, 297 (1953).

44. E. M. Conwell, High Field Transport in Semiconductors, Solid State Physics, Suppl. 9, Academic Press (New York, 1967), p. 155.

45. J. Bardeen and W. Shockley, Phys. Rev. 80, 72 (1950).

46. See reference 45 for a discussion of several methods of measuring E_{IC}.

47. P. P. Debye and E. M. Conwell, Phys. Rev. 93, 693 (1954).

BIOGRAPHICAL NOTE

Clifton G. Fonstad, Jr. was born in Madison, Wisconsin, on August 28, 1943. He entered the University of Wisconsin, Madison, where he received the B.S. degree in Electrical Engineering in June, 1965. He continued his studies as a National Science Foundation Graduate Fellow at the Massachusetts Institute of Technology. There he received the S.M. degree in Electrical Engineering in September, 1966.

He has worked several summers in industrial research laboratories, most recently at the Corning Glass Works Research Laboratory, Corning, New York in 1967. He has coauthored several publications: C. G. Fonstad, A. Linz, and R. H. Rediker, "Vapor Phase Growth of Stannic Oxide Single Crystals," J. Electrochem. Soc. 116 (1969) 1269 and C. G. Fonstad and R. H. Rediker, "Electrical Properties of Single Crystal SnO_2," Bull. Amer. Phys. Soc., 15 (1970) 316. In addition to papers presented to the above organizations, he presented a paper entitled "Vapor Phase Growth of Stannic Oxide Single Crystals" to the ACCG Conference on Crystal Growth, NBS, Gaithersberg, Maryland, in August 1969.

He is a member of Phi Eta Sigma, Eta Kappa Nu, Tau Beta Pi, Phi Kappa Phi, and Sigma Xi.

He and his wife, Carmenza, have one child, a son, Nils.